GEOPHYSICAL INTERPRETATIONS OF BRISTLECONE PINE RADIOCARBON MEASUREMENTS USING A METHOD OF FOURIER ANALYSIS OF UNEQUALLY SPACED DATA

INAUGURALDISSERTATION
der
philosophisch-naturwissenschaftlichen Fakultät
der
Universität Bern
zur Erlangung der Doktorwürde
vorgelegt von
JAN CORNELIUS HOUTERMANS
aus New York

Von der philosophisch-naturwissenschaftlichen Fakultät auf Grund des Gutachtens und auf Antrag von Herrn Prof. Dr. H. Oeschger angenommen

Bern, den 6. Mai 1971

Der Dekan:

K. Meyer

Professor Dr. K. Meyer

Graphics and Reproduction Services
University of California, San Diego
La Jolla, California
1971

UNIV.
LEIDEN
BIBL.

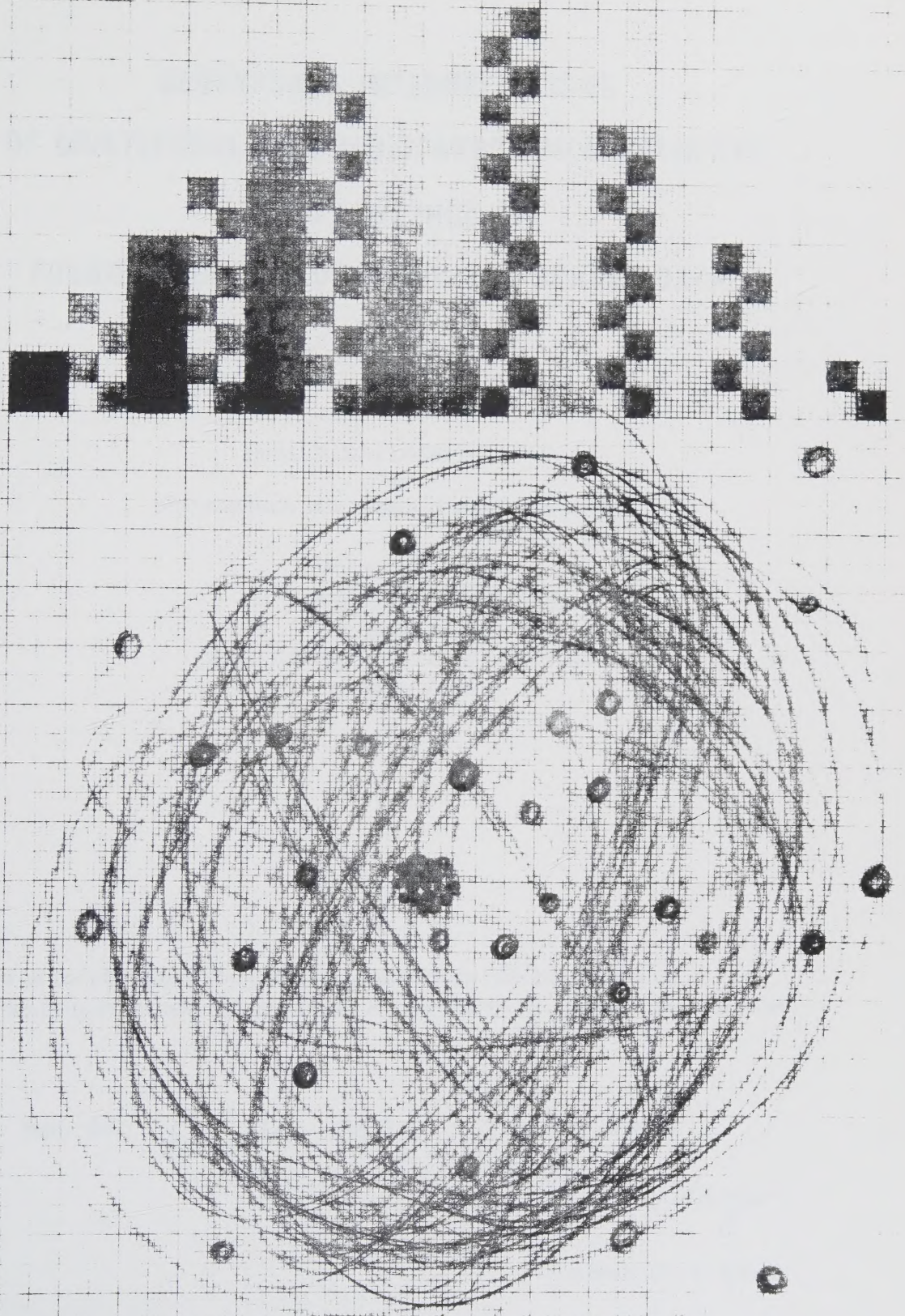

C 14 OR

IS THERE A PAST ?

by Ian Boulton

GEOPHYSICAL INTERPRETATIONS OF BRISTLECONE PINE RADIOCARBON MEASUREMENTS USING A METHOD OF FOURIER ANALYSIS OF UNEQUALLY SPACED DATA

INAUGURALDISSERTATION
der
philosophisch-naturwissenschaftlichen Fakultät
der
Universität Bern
zur Erlangung der Doktorwürde
vorgelegt von
JAN CORNELIUS HOUTERMANS
aus New York

Von der philosophisch-naturwissenschaftlichen Fakultät auf Grund des Gutachtens und auf Antrag von Herrn Prof. Dr. H. Oeschger angenommen

Bern, den 6. Mai 1971

Der Dekan:

K. Meyer

Professor Dr. K. Meyer

Graphics and Reproduction Services
University of California, San Diego
La Jolla, California
1971

Digitized by the Internet Archive
in 2026

https://archive.org/details/IA41547616_0021

TABLE OF CONTENTS

	page
List of figures	v
List of tables	vii
ABSTRACT	1
INTRODUCTION	2
CHAPTER I: THE RADIOCARBON MEASUREMENTS AND THEIR LARGE-SCALE TRENDS	
Introduction	7
C^{14} variations and measurement techniques	8
The ΔC^{14} data	10
Large-scale trends	12
CHAPTER II: FOURIER ANALYSIS OF UNEQUALLY SPACED DATA	
Introduction	22
Fourier analysis	25
Orthogonal basis	27
The "gower spectrum"	29
Alternative normalizations	31
Program of calculation and criteria for cut-off	32
Calculation	33
Criteria for the choice of N	35
A. The total square deviation and related functions	35
B. The Nyquist frequency and the total power	37
C. The power of the gower	39

page

CHAPTER III: FOURIER ANALYSIS OF RADIOCARBON CONCENTRATIONS IN BRISTLECONE PINE

Introduction 42
Data preparation 42
Choice of cut-off frequency 45
Analytical ΔC^{14} approximation functions 61
Periodicities in the ΔC^{14} data 68

CHAPTER IV: THE PRODUCTION RATE OF RADIOCARBON

Introduction 77
2- and 3-reservoir models 80
Finding production rates 93
Large-scale trends in Q 94
Residual Q 97

APPENDIX A: Recursive Fourier Analysis of Unequally Spaced Data 103

APPENDIX B: Two- and Three-reservoir Models of the Atmosphere and Ocean 112

APPENDIX C: Tables 11, 12 and 13 126

BIBLIOGRAPHY 131

LEBENSLAUF 135

ACKNOWLEDGMENTS 137

LIST OF FIGURES

		figure page	caption page
1	Interval Distribution	11	11
2	ΔC^{14} Data	16/17	15
3	Residual ΔC^{14} Data	16	15
4	Residuals from the Exponential Fit	17	15
5	Calibration of Radiocarbon Dates	19	18
6	Criteria Functions Run II	49	47
7	Run III	52	47
8	Run IV	55	47
9	Gower Spectrum Run II	50	48
10	Run III	53	48
11	Run IV	56	48
12	Power Spectrum Run II	51	48
13	Run III	54	48
14	Run IV	54	48
15	Fourier-Smoothed ΔC^{14}	64	63
16	Residual Fourier Fits	64	63
17	Fourier-Smoothed ΔC^{14} (2)	65	63
18	Residual Fourier Fits (2)	65	63
19	Power Spectra Runs II, III and IV, and overlay: Integral Transform Power	71	70

		figure page	caption page
20	Model Relations	89	87
21	Production Rate Power Spectra	90	87
22	Comparison of Models	91	88
23	Large-scale Production Rate Trends	92	88
24	Total Production Rates (1)	99	98
25	Residual Production Rates (1)	100	98
26	Residual Production Rates (2)	100	98
27	Total Production Rates (2)	101	98

Plate 1	Calibration of Radiocarbon Dates	at the end	18

LIST OF TABLES

		page
1	Data Series Parameters	45
2	Initially Chosen Degrees, N	46
3	Standard Error of Estimate	57
4	Maximum (rms) Cut-offs	58
5	Representative Cut-off Frequencies	59
6	Run Parameters	69
7	Major Frequencies	72
8	Weak Peaks	75
9	Parameter Values	85
10	Parameters of Reservoir Models and of Production Rate Sine Waves	94
11	Data List	126
12	Fourier Coefficients	129
13	Fourier Power	130

ABSTRACT

An analysis is made of 331 measurements of the C^{14} content of bristlecone pine wood, which were carried out in La Jolla, California by H.E. Suess. The dendrochronologically determined ages of the samples are irregularly distributed over the past 7000 years. The mean of the ΔC^{14} values is 26.4 ‰, the standard deviation from the mean is 33.0 ‰, and the statistical counting errors are about ±5 ‰. The large-scale trend of the data can be represented to within a standard error of estimate of about ±10 ‰ either by a sine wave with a 10400 y period, or by a linear term with a slope of -15.5 ‰/10^3y plus a 6080 y period sine wave. (The linear term is almost equivalent over the data range to an exponentially falling activity with a mean life of 67000 y.) The residual ΔC^{14} values after removal of the 10400 y period sine wave are Fourier analysed to investigate periodicities and find smooth curves approximating the data. For this purpose a method of efficiently Fourier analysing unequally spaced data is developed, and criteria are found for choosing an optimal cut-off frequency for such data. Power spectra found both from the Fourier series expansion and from the Fourier transform have strong peaks for periods of about 400 y and 2000 y, although these periodicities are not present throughout the whole 7000 y data span. Smooth interpolation functions representing the data to various degrees of fidelity are found, and presented graphically, both in the form (ΔC^{14}vs. time), and (C^{14}age vs. true age) for the calibration of radiocarbon dates. The time dependence of the production rate of C^{14} is calculated under the assumption that production rate variations are the sole cause of the C^{14} variations. This is done both for the large scale trends and for the detailed variations. The results are compared with the measurements by Bucha (Suess, 1970b) and others (Cox, 1969) of the earth's magnetic dipole moment. A two-reservoir model of the atmosphere-ocean system is sufficient for this purpose. The essential equivalence of this model with more complicated three-reservoir models is shown, together with relationships between the parameters of the various models. A two-reservoir atmospheric residence time of 50 y is adopted, corresponding to a three-reservoir atmospheric residence time of 7 y, and a deep-sea residence time between 500 y and 2000 y, depending on which three-box model is chosen. A production rate amplitude of about 20 ‰ would be needed to explain the large-scale ΔC^{14} behaviour, and an amplitude of about 10 ‰ would be needed to explain the behaviour of the residual data.

INTRODUCTION

The radiocarbon dating method consists in the determination of the time during which the radiocarbon concentration in a sample of carbon-containing material has decreased from its initial to its present value. It therefore depends on the knowledge of these concentrations and on the rate of decay. The initial concentration of a sample is its concentration when it ceases to assimilate carbon from, and to be in equilibrium with its environment (for example atmosphere or ocean). Except for the small fractionation effect due to the difference in mass between C^{12} and C^{14}, this assimilation results in the equality of the environmental concentration and the initial concentration of the sample. (The fractionation correction is proportional to and may be found from the sample's C^{13} concentration.) After the discovery by Libby of the existence of naturally occuring radiocarbon (Anderson et al., 1947), the basic assumption that the radiocarbon concentrations of the various carbon-containing reservoirs of the earth have remained constant and equal to their present concentrations was proposed and confirmed, to the extent then possible, by Libby and his co-workers (Anderson and Libby, 1951). Since then, this has made possible the widespread and fruitful use of the radiocarbon dating method.

Radiocarbon is produced in the atmosphere by the interaction of cosmic-ray neutrons with nitrogen, $N^{14}(n, p)C^{14}$, and beta-decays into N^{14} with the half-life $T_{1/2}$= 5730 ±40 y (Godwin, 1962). (Conventional radiocarbon dates are reported using the half-life 5568 y, according to the agreement confirmed at Pullman, Washington, in 1965 (Olsson, 1968).) After its production in the upper atmosphere, the radiocarbon is distributed among the various carbon-containing reservoirs: the carbon dioxide of the atmosphere, the terrestial biosphere, and the bicarbonates dissolved in the oceans. Most of the radiocarbon decay takes place in the oceans which constitute by far the largest of these reservoirs.

Thus the basic assumption of constant radiocarbon concentrations in the environment, primarily in the atmosphere, entails the following three assumptions (Suess, 1965):

1. The cosmic-ray flux incident on the atmosphere, and hence the production rate of radiocarbon in the atmosphere, has remained constant for several half-lives;

2. the stable-carbon contents of the various reservoirs containing cosmic-ray-produced C^{14} have remained constant over such a period of time;

3. the rates of C^{14} transfer between the reservoirs, in particular from the atmosphere into the oceans, have also remained constant over this length of time.

The intensive investigation of radiocarbon concentrations in many materials over the last twenty years has confirmed the general validity of these assumptions, but has simultaneously shown the existence of small variations with time in the atmospheric C^{14}/C^{12} ratio, indicating the slight failure of one or more of these assumptions. The discovery of these variations has led both to a refinement in the accuracy of radiocarbon dating (and a better assessment of its errors), and also to an increased knowledge in such diverse areas of geophysics as isotope production by cosmic-rays in the atmosphere, and mechanisms and rates of exchange of carbon dioxide between the atmosphere and oceans. (Information about such exchange has been derived also from the distribution of artificially produced radiocarbon and other isotopes from hydrogen bomb testing, after this contamination of the natural level began in 1953.)

The status of the present knowledge about radiocarbon variations was the subject of the Twelfth Nobel Symposium on Radiocarbon Variations and Absolute Chronology held at the University of Uppsala, Sweden, in 1969 (I. Olsson, editor, 1970). The pre-symposium status has been reviewed by Olsson (1968). A history of the radiocarbon dating method has been written by Libby (1967). In the following a brief and non-comprehensive description is given of the discovery of the variations with time of the atmospheric radiocarbon concentration, as has been found from the measurements of samples whose age is known independently.

Suess (1954) has shown the existence of a small decrease of about 2 % in the atmospheric C^{14} concentration during the last 100 years, due to the dilution of the atmospheric radiocarbon with stable carbon from the burning of fossil fuels since the beginning of the industrial revolution ("Suess effect").

De Vries (1958) found the existence of a positive anomaly in the atmospheric C^{14} concentration for the years around A.D. 1700, also of about 2 %, relative to the nineteenth century ("de Vries effect"). He suggested a causal connection between this anomaly and world-wide climatic conditions, through variations in the rates of transfer of carbon between the various carbon reservoirs.

Measurements of the C^{14} activity in tree-rings of known age brought to light increasingly more information about irregularities in the atmospheric radiocarbon concentration, showing variations of 2 or 3 % over the past 2 or 3 thousand years, and in particular a general decrease over the past 6 or 7 thousand years from a level which had been at least 10 % higher than the present one (see for example: Willis et al., 1960; Stuiver, 1961; Suess, 1960, 1965, 1967 and 1970a; Ralph, 1967; Damon, 1968; Damon et al., 1970; Ralph and Michael, 1970; and Lerman et al., 1970). These measurements of tree-ring samples were made possible by the development of tree-ring chronologies, on such trees as the bristlecone pine from the White Mountains in California, which allowed the extremely accurate dating of wood even when individual tree-rings or whole sections of wood were missing (Ferguson, 1968 and 1970). Calibration curves for correcting conventional radiocarbon dates have been calculated on the basis of the true initial radiocarbon concentrations of the atmosphere as found from the tree-ring activities (Suess, 1965, 1967 and 1970a; Stuiver and Suess, 1966).

The causes of these observed variations in radiocarbon concentration have been attributed variously to the failure of one or more of the three assumptions given above. They may be classified as being due either to climatic changes which may influence the distribution of carbon in the various reservoirs, or to changes in the cosmic-ray flux in the upper atmosphere which influence the C^{14} production rate. The cosmic-ray changes may be due to variable screening of the charged flux either by the solar plasma or by the earth's magnetic field, or to variations in the galactic component or the solar-energetic-particle component of the cosmic-ray flux.

In all cases, however, the amplitudes of the variation in the causal factor must be much larger than the amplitude of the resulting variation in the atmospheric C^{14} concentration (de Vries, 1958; Wood and Libby, 1964). This is so because the amount of new radiocarbon introduced per year is smaller by a factor of about 8267 (mean life of C^{14}) than the total C^{14} inventory, and most of this inventory is found in the oceans, to which the atmospheric radiocarbon is transfered after an atmospheric residence time of only about 30 years. The attenuation factor depends on the frequency of the variations, and is such that the resulting C^{14} amplitude is of the order of 3 to 10 times smaller than the causal amplitude, for periods between roughly 10^4 and 10^2 years (Houtermans, 1966).

Evidence for the causal factors have been derived from correlations with climate (de Vries, 1958; Suess, 1965 and 1968; Damon, 1966, 1968 and 1970; Lal and Venkatavaradan, 1970); with solar activity as measured by the existing 250 years of sunspot records (Stuiver, 1961 and 1965; Suess, 1965; Grey et al., 1966; Houtermans et al., 1967); and with variations in the earth's magnetic dipole moment (Elsasser et al., 1956; Kigoshi and Hasegawa, 1966; Bucha, 1967; Bucha and Neustupnỳ, 1967; Ramaty, 1967; Grey, 1969). The question of the correct causes has not yet been settled, partly because correlations are usually at least to some extent subjective, and also because they indicate a relationship which may be only coincidental. However the following two relationships are perhaps generally accepted:
1) the large-scale behaviour over the last 7000 years is probably due to a varying modulation by the earth's magnetic field of the total cosmic-ray flux incident on the earth's atmosphere;
2) a negative correlation (or at least a significant coherence in the two frequencies of 0.5 and 2.0 cycles per century (Houtermans et al., 1967)) does exist between the solar activity, as measured by yearly average sunspot numbers, and the atmospheric C^{14} concentration. The first of these effects and perhaps also the second is due to a varying production rate. The second may instead be due to climatic effects, since correlations between solar activity and the weather have also been observed. The higher frequency ΔC^{14} variations probably are caused by both production rate and climatic variations.

The present work is an analysis of the radiocarbon measurements made by H.E. Suess on bristlecone pine wood from the past 7000 years, which were the subject of his two papers presented in the radiocarbon conference held in Uppsala in 1969 (Suess, 1970a and 1970b), in which most of the data here analysed was presented in graphical form. These measurements were carried out in La Jolla, California, during the past five years, for part of which time I was an assistant to Professor Suess in both his tritium and radiocarbon laboratories.

The following four chapters contain:

Chapter I

A short description of the measurement techniques, and the representation of the large-scale trends of the ΔC^{14} data by various analytical functions.

Chapter II

The development of an efficient technique for the Fourier analysis of unequally spaced data, and the proposal and discussion of criteria for choosing an optimal cut-off frequency for such data.

Chapter III

The application of the above technique of Fourier series analysis to the residual ΔC^{14} data, after the removal of a 10400 year period sine wave, and the application of the Fourier transform to the residual and the original data. Power spectra and smooth interpolation functions approximating the data are presented and discussed.

Chapter IV

The determination of the C^{14} production rate which would be necessary to account for the analytical ΔC^{14} functions found above, were they the sole cause of these variations. For this purpose a two-reservoir model of the atmosphere-ocean system is used. Its relationship to three-reservoir models, which for other purposes may be more realistic, is discussed.

CHAPTER I

THE RADIOCARBON MEASUREMENTS AND THEIR LARGE-SCALE TRENDS

Introduction

The subject of the analysis presented in this paper is a set of measurements of the radiocarbon concentration in dated samples of bristlecone pine extending over the last 7000 years, which were carried out by Professor H.E. Suess, who has kindly made the data available to me for this work. The purpose of the analysis is to extract from this set of data the maximum information about major trends, about physical periodicities, and about the function most nearly representing the true variations over the last 7000 years of the atmospheric radiocarbon concentration. This knowledge will assist in the investigation of the geophysical factors responsible for the variations, and in the calibration of the radiocarbon dating method.

Because of the data's oscillatory character, the use of Fourier series is clearly indicated as a means of analysis. The power spectrum may be found, and an interpolation function which fits the data in the sense of least squares may be synthesized from the terms having frequencies less than some cut-off frequency, chosen in such a way as to achieve a reasonable compromise between degree of fidelty and degree of smoothness. The Fourier analysis of unequally spaced data such as this, however, presents certain difficulties in computation and in assessment of the power spectra for the determination of a reasonable cut-off frequency. Chapter II contains the development of a general method of Fourier analysis to meet these difficulties, and Chapter III contains its particular application to the C^{14} data.

In addition to a description of the measurements, the present chapter treats the large-scale trends of the data, approximating them analytically in a variety of ways. This is important for the subsequent Fourier analysis, as well as interesting from a physical point of view. The Fourier series expansion of a data series of finite length T_1, which is the result of measurements of a phenomenon that does not happen to have the period

T_1, must nevertheless produce a periodic function with this period. The real discontinuities at the series' end-points result in the spurious behaviour of the Fourier approximation function near these end-points (Gibbs phenomenon). This may be minimized by the initial removal of any generally monotonic trend in the data to produce an approximately flat residual data series.

C^{14} variations and measurement techniques

The fluctuations in the atmospheric C^{14}/C^{12} ratio as a function of time are found by comparing the age-corrected C^{14} activity of a sample of known age with that of a standard sample. Both age-corrected activities must also be corrected for possible differences between the extents to which the fractionation of C^{14} with respect to C^{12} took place during their respective assimilation of CO_2 from the atmosphere. The C^{14} fractionation-correction is based on the measured C^{13} content of a sample, and is twice the corresponding C^{13} correction. The fractionation-corrected C^{14} activity A (of sample or standard) is

$$A = A'\left(1 - \frac{2(\delta C^{13} + 25)}{1000}\right) \quad ,$$

where A' is the measured C^{14} activity (of sample or standard), and δC^{13} is the per mil difference between the measured C^{13} content (of sample or standard) and the standard belemnite sample of Craig (1957a). (The value, $\delta C^{13} = -25$ ‰, is characteristic of wood and other biological material.)

The deviations in per mil of the atmospheric C^{14} activity from the activity at the time of the standard sample may then be expressed as

$$\Delta C^{14} = \frac{A \cdot e^{t/\tau} - A_0 \cdot e^{t_0/\tau}}{A_0 \cdot e^{t_0/\tau}} \cdot 1000 \quad ‰$$

$$= \left(\frac{A}{A_0}\, e^{(t-t_0)/\tau} - 1\right) \cdot 1000 \quad ‰ \quad ,$$

where A and A_0 are the fractionation-corrected activities at the time of measurement of the sample and standard, respectively;

t is the time between sample formation and its activity measurement; and t_0 is the time between the formation of the standard wood (see below) and its activity measurement. Thus $A \cdot e^{t/\tau}$ and $A_0 \cdot e^{t_0/\tau}$ are the age- and fractionation-corrected activities of sample and standard, respectively, where $\tau = T_{1/2}/\ln 2$ is the radioactive mean-life of C^{14}. The half-life, $T_{1/2}$ = 5730 y (τ = 8267 y), is used throughout, although conventional radiocarbon dates are reported using the half-life 5568 y (Olsson, 1968). The standard samples for these bristlecone pine measurements were from a fir tree grown in Oregon between 1870 and 1890. The U.S. National Bureau of Standards oxalic-acid standard was not used "because of the possibility that different procedures [from those which had been in use] could lead to different sources of error" (Suess, 1970a). The above equations are entirely equivalent, however, to those derived by Broecker and Olson (1959 and 1961) which use the NBS oxalic-acid standard.

The techniques of measurement have been described by Suess (1970a). Most of the 331 measurements under consideration were made on samples of bristlecone pine wood, supplied and dendrochronologically dated by C.W. Ferguson, of the Laboratory of Tree-Ring Research, University of Arizona. The samples consisted of bundles of 10 annual tree-rings and amounted to 20 g of wood. Each sample was cleaned by washing with acetone, acid, and hydroxide; burned and converted to acetylene (Suess, 1954), utilizing lithium carbide; and counted in two different counters (Houtermans and Oeschger, 1958) provided by Oeschger and constructed at the University of Bern. They had backgrounds of 1.0 and 1.8 counts per minute, and counting rates for nineteenth century wood of 18 and 21 counts per minute, respectively. Each sample was counted twice, for two days in each of the counters. One or two standards were counted after from five to eight sample measurements. The statistical counting errors are between 4 and 7 %. Malfunctioning of either system could be detected easily from differences, or systematically changing differences between the two counting rates. The C^{13} measurements were carried out in the laboratory of Professor H. Craig, also at the University of California in La Jolla.

The ΔC^{14} data

The ΔC^{14} measurements considered here are listed in table 11 which gives the La Jolla sample number; the tree-ring date, and radiocarbon date, based on the half-life of 5730 y (A.D. dates are positive and B.C. dates are negative); the ΔC^{14} value as a per mil deviation from the A.D. 1870-1890 standard wood; and the residual per mil ΔC^{14} value, $C(t_i)$, which results from the removal of the sine wave with 10400 y period discussed below.

The measurements are irregularly distributed over the range between 5290 B.C., and A.D. 1855. The mid-point of this range is at 1718 B.C., while the average of all dates is 376 B.C. The standard deviation from this mean (root-mean-square, or rms deviation from the mean) is 2094 y. The distribution of intervals, in order of decreasing frequency, are 20 y, 10 y, and 15 y. The largest intervals are 425 y, 190 y, and 100 y (twice) (*). These are located at about 4600 B.C., 5200 B.C., 3550 B.C., and A.D. 160, respectively. The mean interval is 21.6 y, and the standard deviation from this mean is 35.4 y, the distribution being skewed strongly toward large intervals (see figure 1).

The ΔC^{14} values are distributed between maxima of about 110 ‰ at about 3300 B.C., 4200 B.C. and 4400 B.C., and minima of about -25 ‰ at A.D. 24, and A.D. 1200. The mean of the ΔC^{14} values is 26.4 ‰, and the standard deviation from this mean is 33.0 ‰. The statistical counting errors of the measurements are between about 4 and 7 ‰. The ΔC^{14} data are shown in figure 2 with error-bars of ±5 ‰.

The radiocarbon dates, t_i^{14}, corresponding to the atmospheric radiocarbon data, $\Delta C^{14}(t_i)$, for the true dates t_i, are

$$t_i^{14} = t^{14}(t_i) = t_i + 8267 \cdot \ln\left(1 + \frac{\Delta C^{14}(t_i)}{1000}\right) \quad \text{A.D. y.} \qquad (0)$$

(*) As is mentioned in Chapters II and III, the 425 y interval limited the Fourier analysis to such low frequencies that in the second "run" (complete analysis of some part of the data) two equally spaced points were interpolated in this interval by means of an approximation function found in the first run. Runs III and IV omitted the earliest data in order to avoid the 425 y gap and the need for interpolation.

Figure 1

INTERVAL DISTRIBUTION

(NUMBER OF INTERVALS OF LENGTH Δt)

5290 B.C. TO 1855 A.D.

331 DATA

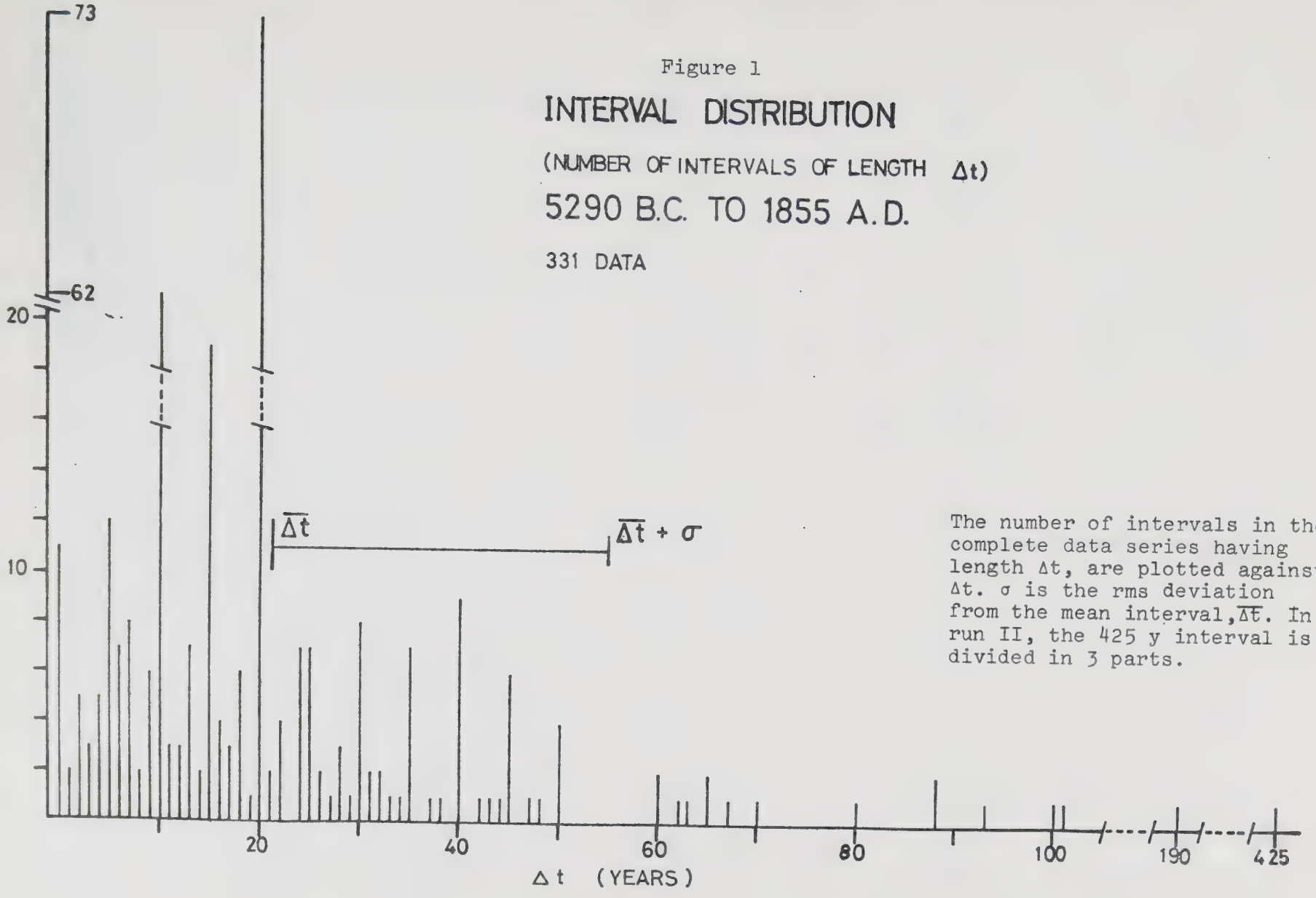

The number of intervals in the complete data series having length Δt, are plotted against Δt. σ is the rms deviation from the mean interval, $\overline{\Delta t}$. In run II, the 425 y interval is divided in 3 parts.

They are listed in table 11, and shown in figure 5 (and in plate 1). This figure is a graph of $t^{14}(t)$ versus t, i.e. radiocarbon dates versus bristlecone pine (true) dates. It may be used to find the (approximate) true age of a radiocarbon sample from its measured radiocarbon age. However, even if the real atmospheric C^{14} concentration were known exactly as a function of time, a given radiocarbon date must not necessarily correspond to a unique true date.

In order to save space figure 5 shows only the region lying near the center line which represents the agreement between the two kinds of dates. The scales have both A.D. - B.C. dates and B.P. dates (before present, i.e. A.D. 1950). The one-sigma error-bars shown correspond to about ±71 y, or 8.6 ‰ in ΔC^{14} (5 ‰ was intended, but the error-bars have been drawn as stated).

Large-scale trends

Suess has proposed that the large-scale trend of the atmospheric ΔC^{14} data is well-represented by a sine function. Figure 2 shows clearly that it is indeed an extremely natural analytical form for a first approximation to the data. The particular sine wave which best fits the ΔC^{14} data under consideration here is given by

$$\hat{C}_S(t) = 42.71 + 49.69\sin[\frac{2\pi}{10402}(t + 7388)] \text{ ‰ }, \qquad (1)$$

where t is in A.D. years ($t < 0$ for years B.C.). The residual ΔC^{14} data C_i are

$$C_i = C(t_i) = \Delta C^{14}(t_i) - \hat{C}_S(t_i) \; . \qquad (2)$$

The mean value of the C_i, and the standard error of estimate of $\hat{C}_S(t)$ are

$$\bar{C}_i = 0.002 \text{ ‰ } ; \; \sigma_S = \sqrt{\frac{1}{m}\sum_{i=0}^{m} C_i^2} = 9.86 \text{ ‰ } .$$

Thus the sine wave $\hat{C}_S(t)$ fits the data to within about twice the statistical error of measurement, over about seven tenths of its

period of 10400 years. This length is insufficient to prove the existence of a physical periodicity, and the good fit may be only fortuitious.

On the other hand, a real periodicity is of course not excluded. Suess (1970b) has reported the excellent agreement between this sine wave (*) which expresses the large-scale behaviour of the measured ΔC^{14} variations, and another sine wave which expresses the atmospheric ΔC^{14} variation deduced theoretically from the magnetic data of Bucha (1967). This deduction was made by first fitting the measurements of the earth's magnetic dipole moment $f(t)/f_0$ (in units of the present one, f_0), raised to the -0.52 power (Elsasser et al., 1956), by an 8000 y period sine wave which is then a first approximation to the large-scale behaviour of the atmospheric C^{14} production rate. This sine wave, attenuated by a factor of about 7, and phase-shifted by about 700 y (Suess, 1970b), should then represent the large-scale behaviour of the atmospheric ΔC^{14} variations. The agreement in period, phase and amplitude between this 8000 y period sine wave and $\hat{C}_S(t)$ is very good over most of the range of the ΔC^{14} tree-ring measurements. In addition, the decrease in ΔC^{14} with increasing age prior to about 5000 B.C., which is predicted through $\hat{C}_S(t)$ is not in disagreement with the earliest magnetic data of Bucha which shows low values of $(f/f_0)^{-0.52}$ at about 7000 B.C. In Chapter IV a theoretical C^{14} production rate sine wave, $\hat{Q}_S(t)$, is deduced from $\hat{C}_S(t)$ and is compared with this magnetic data.

The residual values $C(t_i)$ are listed in table 11, and are plotted in figure 3. It may be seen that the function $\hat{C}_S(t)$ serves remarkably well in removing the "monotonic" trend of the data. This figure shows also that in spite of the relatively large errors of the measurements (~5 ‰) in comparison with the scatter of the points about the zero-line (~10 ‰), there remain in the residual data general trends which are clearly distinguishable from purely random behaviour. Thus further information is definitely available from the measurements, and the Fourier analysis in Chapter III of the residual data $C(t_i)$ is made in order to extract this information.

(*) The small difference of 50 years between the 10350 y period reported by Suess, and that given here is due to a few subsequent measurements in what is essentially the same set of data.

In addition to the best sine fit $\hat{C}_S(t)$, figure 2 also shows linear and exponential least-square fits to the original ΔC^{14} data. These two functions are almost identical to each other over the range of the data. They are given by

$$\hat{C}_L(t) = 9.28 - 0.0155 \cdot t \quad ‰ ,$$

and

$$\hat{C}_E(t) = (1.0091 \cdot e^{-t/66900} - 1) \cdot 1000 \quad ‰ , \qquad (3)$$

where t is in A.D. years. The standard error of estimates of these functions with respect to the data are 16.7 ‰ for the linear function, and 16.5 ‰ for the exponential function. Thus they do not fit as closely as does the sine wave $\hat{C}_S(t)$.

The slope of $\hat{C}_L$ is -15.5 ‰/10^3y. The behaviour of $\hat{C}_E$ is that which would result from an atmospheric radiocarbon activity which decreases with a half-life of 46'400 y, and which had a ΔC^{14} value of 9.1 ‰ at the time of Christ. This would mean that 50'000 years ago the atmosphere had about twice its present-day C^{14} activity. Such a behaviour might be connected with a drastic change in world-wide climatic conditions such as the end of the ice age, and the subsequent exponential decrease to a new equilibrium.

The residual data $C_E(t_i)$ which result from the subtraction of the exponential curve from the original ΔC^{14} data are

$$C_E(t_i) = \Delta C^{14}(t_i) - \hat{C}_E(t_i) . \qquad (4)$$

The $C_E(t_i)$ values are plotted with 5 ‰ error-bars in figure 4, which shows that this residual data retains a large-scale oscillation. It does not correspond quite as naturally to a sine function as does the original ΔC^{14} data, but a best-fit sine wave, $\hat{C}_{ES}(t)$, was nevertheless determined:

$$\hat{C}_{ES}(t) = 1.301 + 17.89 \cdot \sin\left[\frac{2\pi}{6077}(t + 5280)\right] ‰ . \qquad (5)$$

Compared with the previous sine wave, $\hat{C}_S(t)$, this new sine wave has a period smaller by six tenths, an amplitude smaller by one third, and a minimum that occurs earlier by about 1000 years.

FIGURE CAPTIONS

Figure 2 ΔC^{14} DATA pages 16 and 17

The bristlecone pine data, $\Delta C^{14}(t_i)$, measured by Suess (1970a), are plotted vs. the calendar date. Error-bars are ±5 ‰. The 2 artificial points (triangles), used in run II for Fourier smoothing, are discussed in pages 43 and 44. The best fitting sine wave $\hat{C}_S(t)$ (period, 10,400 y, equation 1), line $\hat{C}_L(t)$ (slope, -15.5 ‰/10^3y, above equation 3), and exponential $\hat{C}_E(t)$ ($T_{1/2}$ = 46,400 y, equation 3) are shown.

Figure 3 RESIDUAL ΔC^{14} DATA page 16

The residual data, $C_S(t_i) = C_i = \Delta C^{14}(t_i) - \hat{C}_S(t_i)$, after the subtraction of the 10,400 y period sine wave, are plotted vs. the calendar date.

Figure 4 RESIDUALS FROM THE EXPONENTIAL FIT page 17

The residual data, $C_E(t_i)$ (equation 4), after the subtraction of the exponential ($T_{1/2}$ = 46,400 y, equation 3), which best fits the original ΔC^{14} data, are plotted vs. the calendar date. The curve shown is the sine wave $\hat{C}_{ES}(t)$ (equation 5), which best fits the residual data shown, and has the smaller period, 6077 y. It is <u>not</u> the difference between the sine curve and line (or exponential) of figure 2.

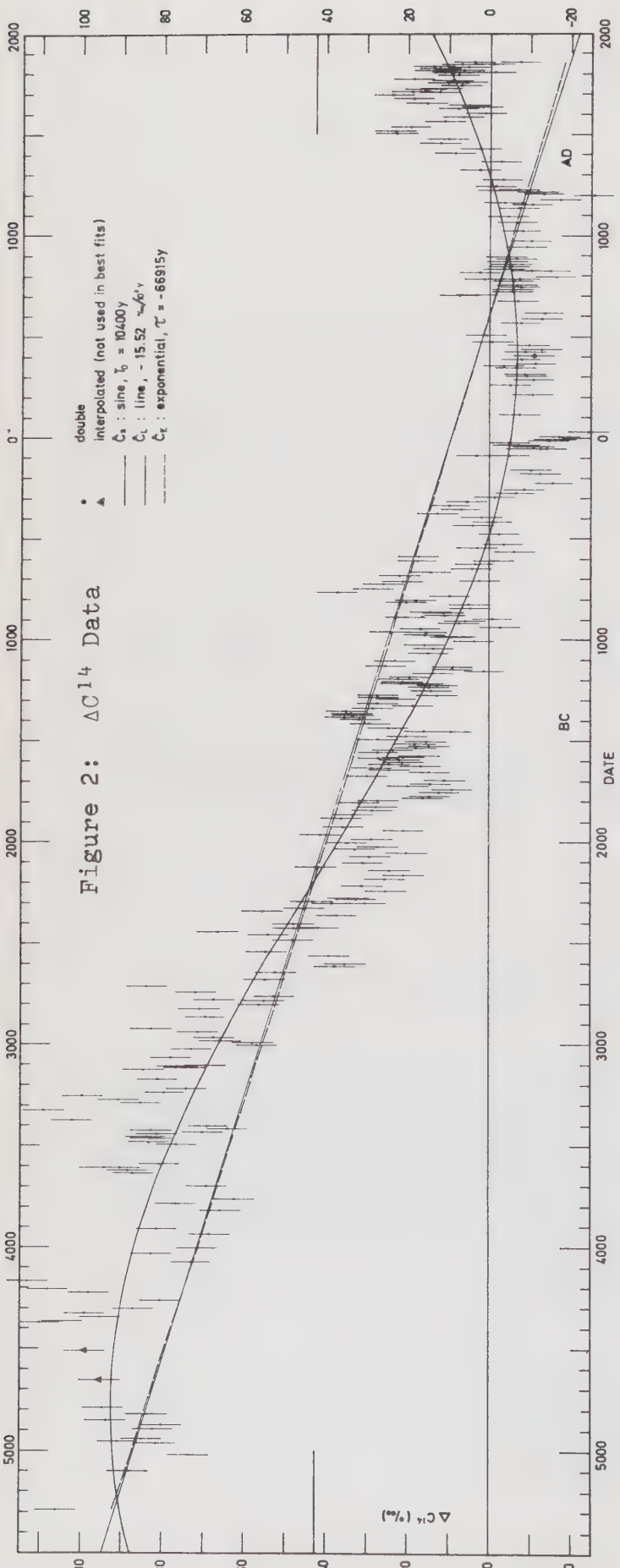

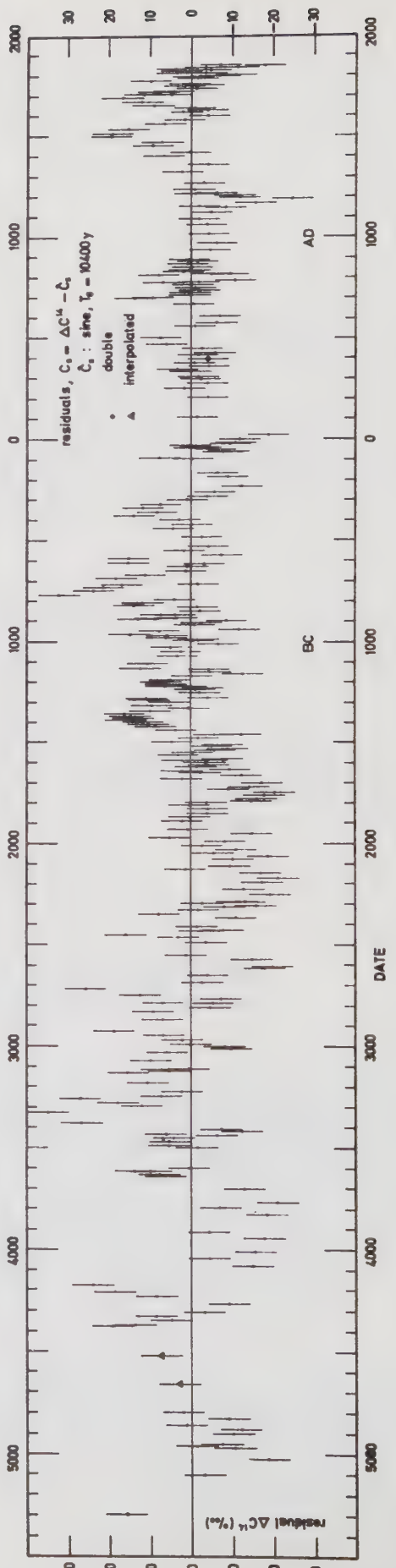

Figure 3: Residual ΔC^{14} Data

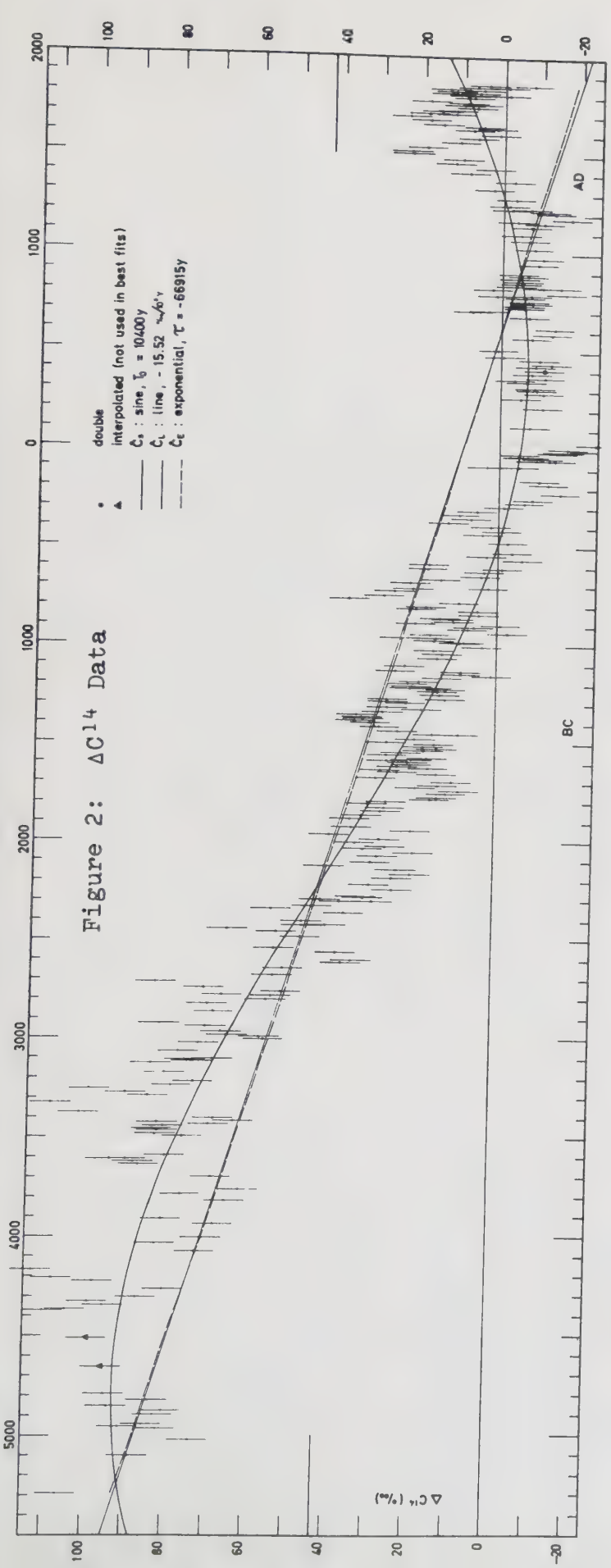

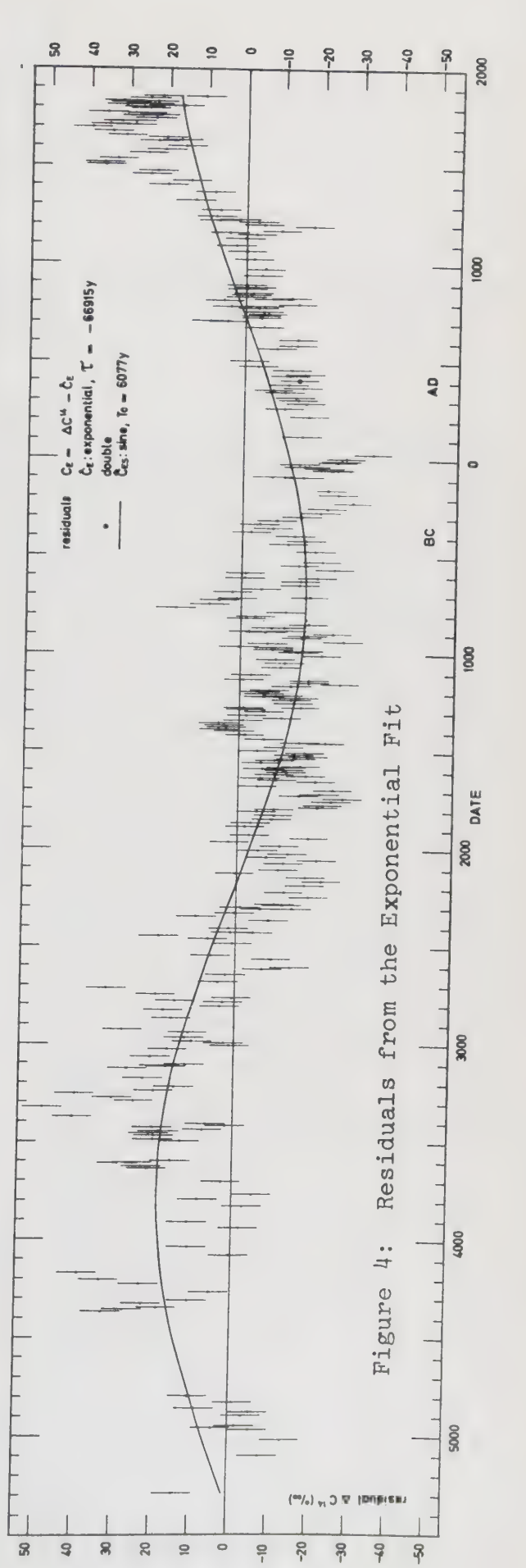

Figure 4: Residuals from the Exponential Fit

FIGURE CAPTION

Figure 5 and Plate 1 — CALIBRATION OF RADIOCARBON DATES — page 19 end insertion

Radiocarbon dates [t_i^{14}, equation (0)] of bristlecone pine samples, measured by Suess (1970a), and based on the 5730 y half-life, are plotted against the bristlecone pine (or true) date (on a diagonal to save space). The center line represents agreement between the two kinds of dates. B.P. (before 1950), and A.D.-B.C. dates are given; the 2 sections have an 1000 y overlap. Error-bars are ±71 y (±8.6 ‰, although ±5 ‰ was intended).

The smooth curve $\hat{t}^{14}(t)$ is based on the 10,400 y period sine wave $\hat{C}_S(t)$, best fitting the ΔC^{14} data (see page 43).

The other two curves are the Fourier fits from run II, with cut-off degree N, and smallest period T_n. The 2 artificial points near 6500 B.P., used in these fits, are not shown. See pages 12, 62 and 67 for explanations and examples of use.

Plate 1 is a factor 1.5 larger than figure 5, but is otherwise the same.

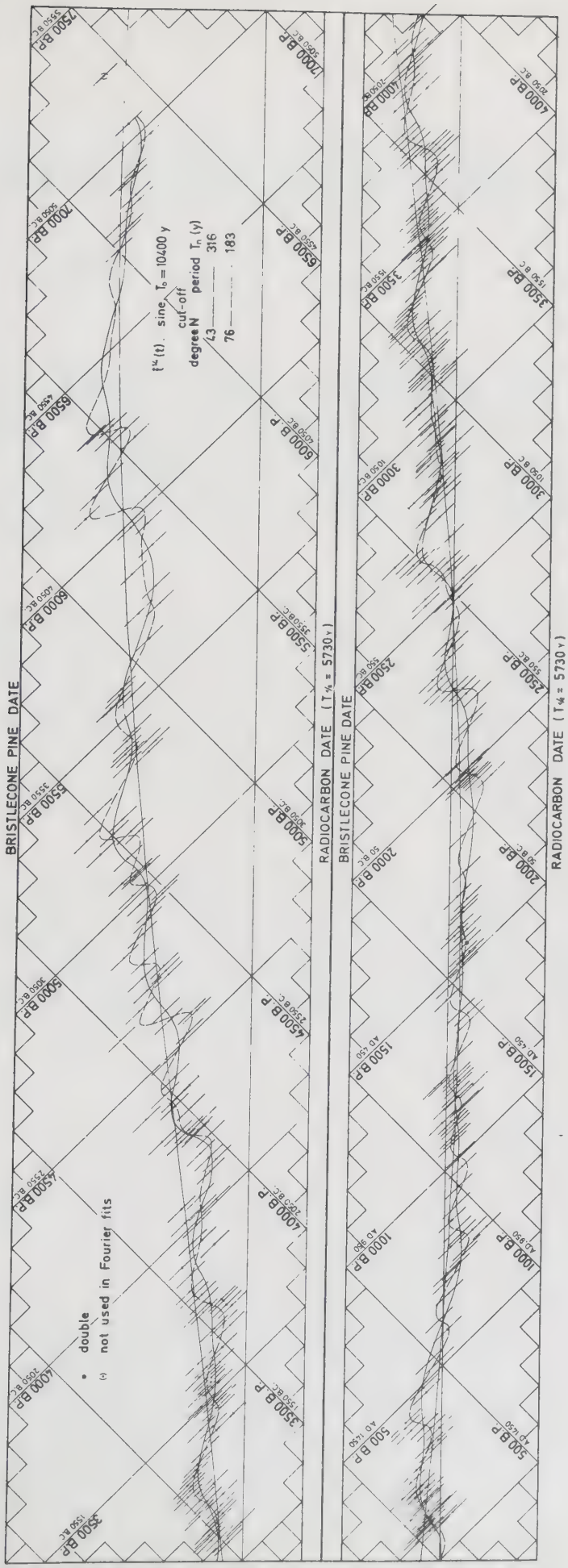

Figure 5: Calibration of Radiocarbon Dates

The standard error of estimate, with respect to the original ΔC^{14} data, of the exponential function plus the new sine wave is

$$\sigma_{E+ES} = \sqrt{\frac{1}{m}\sum_{i=1}^{m}[\Delta C^{14}(t_i) - (\hat{C}_E(t_i) + \hat{C}_{ES}(t_i))]^2} = 10.6 \text{ ‰} .$$

(This is of course also the standard error of estimate of the new sine wave $\hat{C}_{ES}(t)$ with respect to the residual data $C_E(t_i)$.) Thus the ΔC^{14} data is fitted a little better by the 10400 y period sine wave (σ_S = 9.9 ‰), than by the exponential ($T_{1/2}$ = 46400 y) plus the 6077 y period sine wave, even though the latter function has two more parameters than the former.

No Fourier series analysis was made for the residual data $C_{ES}(t_i) = \Delta C^{14}(t_i) - [\hat{C}_E(t_i) + \hat{C}_{ES}(t_i)]$. However, in Chapter IV the production rate, $\hat{Q}_E(t) + \hat{Q}_{ES}(t)$, which would be needed to cause the ΔC^{14} variation given by $\hat{C}_E(t) + \hat{C}_{ES}(t)$ is determined and compared with the magnetic data. The agreement is not as good as that between the magnetic data and the production rate $\hat{Q}_S(t)$ deduced from $\hat{C}_S(t)$. Using a different exponential function than the one given here, Suess (1970b) has found better agreement than in this latter case.

While the linear and exponential least-square fits are straightforward, the latter being the best linear fit to the points $(t_i, \ln[(\Delta C^{14}(t_i) + 1)/1000])$, a mention is made of the method used for a best sine fit. As a 0^{th}-approximation the form $\hat{C}_0(t) = A_0 + B_0\sin(\omega_0 t + \phi_0)$ was assumed, and the four parameters were graphically estimated. The function $\hat{C}_1(t)$ was then defined as

$$\begin{aligned}\hat{C}_1(t) &= A_1 + B_1\sin(\omega_1 T + \phi_1) \\ &= (A_0 + \Delta A_0) + (B_0 + \Delta B_0)\sin[(\omega_0 + \Delta\omega_0)t + (\phi_0 + \Delta\phi_0)] \\ &\simeq \hat{C}_0(t) + \Delta A_0 + \Delta B_0\sin(\omega_0 t + \phi_0) + \\ &\qquad + B_0(\Delta\omega_0 t + \Delta\phi_0)\cos(\omega_0 t + \phi_0).\end{aligned}$$

The last form is linear in the four unknown delta quantities, so that minimization with respect to them of

$$\sum_i [\Delta C^{14}(t_i) - \hat{C}_1(t_i)]^2$$

now leads to four simultaneous linear equations which can be solved by computer. The process is easily repeated and converges rapidly to the best sine, if, as is the case here, the data has a reasonable resemblence to a sine function. (The earliest data point at 5290 B.C. was used in the sine fits, while the two artificial points in the 425 y gap referred to above were not.)

CHAPTER II FOURIER ANALYSIS OF UNEQUALLY SPACED DATA

Introduction

The method of Fourier analysis is appropriate for investigating data series which, like the radiocarbon data, have an oscillating character. It can give information about periodicities occuring in the data, and can supply analytical interpolation functions that are objective approximations to the real underlying behaviour of the measured quantity. In the case of the radiocarbon data the latter is important both for the calibration or correction of the radiocarbon dating method, as well as for making deductions about the time dependence of the possible factors which cause the variation of the atmospheric radiocarbon. Thus in Chapter IV variations in the C^{14} production rate are deduced from the analytical interpolation functions found through Fourier analysis of the ΔC^{14} data, by assuming that these variations are the sole causal factor, and adopting a particular model to describe their effect on the atmospheric radiocarbon concentration.

However, the Fourier analysis of data spaced at intervals of irregular lengths presents difficulties, both computational and more fundamental, which arise from the fact that the ordinary harmonic functions, sinkt and coskt, when evaluated at the irregularly spaced times t_i, are not "orthogonal" to each other, as they would be were the t_i regularly spaced. (The term "orthogonality" is used here for functions evaluated at discreet values of the argument, to denote the property that the sum over these arguments of the product of two different functions of the arguments is zero. This is analogous to the orthogonality of functions of a continuous variable, where the integral over a range has been replaced here by a summation.) The consequence of this failure of orthogonality is that the coefficients of the basis functions, sinkt and coskt, used in the expansion of any function, will be dependent on the degree of the expansion. Thus the determination of these coefficients can be made only after the degree of the expansion has been chosen. But the latter is essentially the only unknown parameter in the problem of finding an optimal interpolation function for the data, so that in order to find this parameter by examining the Fourier expansions, it would seem that a set of coefficients must be determined for <u>each</u> degree of expansion, this being the computational difficulty referred to above.

Even if all sets of coefficients were found, however, these would yield not one power spectrum, but a set of power spectra, one for each possible degree of expansion, and this gives rise to the more fundamental difficulty. In the ordinary Fourier analysis of equally spaced data the one complete and invariant power spectrum yields information about the importance of the various frequencies occuring in the expansion, and therefore in the data. A choice of an optimal cut-off frequency may be based on this power spectrum, and may be made in such a way as to include relatively important frequencies and exclude relatively unimportant ones, the latter being attributed to random errors of measurement or "noise". Furthermore, this choice, although made on the basis of the complete spectrum, is also made with the assurance that the truncated spectrum is identical to the spectrum of the truncated expansion. On the other hand, in the case of unequally spaced data where there is one power spectrum per degree of expansion, one must find alternative criteria for the determination of an optimal cut-off frequency. For the information contained in these power spectra does not include a clear distinction between the extent to which a frequency is important because the data (or the underlying phenomenon) "really" oscillates with that frequency, and the extent to which it is important because of the accidental occurrence of a particular distribution of interval lengths.

In this chapter, and in Appendix A, a method of Fourier analysing unequally spaced data is described. It enables a tentative choice to be made of a small number of candidates for an optimal cut-off frequency prior to the determination of any Fourier coefficients. This initial choice is based on a number of related criteria, including measures of the deviation of the data from the approximation curve as a function of the degree of the expansion, and a new kind of "power spectrum" which <u>is</u> invariant to the degree of expansion. All these criteria functions, as well as other numbers from which the Fourier coefficients for any desired degree may be found subsequently, are determined by a recursive procedure up to any highest degree specified. Thus only after finding a small set of promising degrees of expansion is it necessary to calculate the Fourier coefficients, Fourier power spectra and Fourier series, and indeed only for these few cases. Finally, a choice of one or perhaps a few of the best cut-off frequencies may be based on an examination of the original criteria functions, the few Fourier power spectra and the few approximation functions themselves.

Because the difficulties with unequally spaced data arise from the non-orthogonality of the ordinary harmonic functions, the basis of the method described here is the introduction of new basis functions which are orthogonal over the particular given set of unequally spaced arguments, and are themselves linear combinations of sinkt and coskt. Such an introduction of orthogonal basis functions has been used, for example, by W.E. Milne (1949) in the power series expansion of functions of a continuous variable and, by analogy, of functions of equally spaced discreet arguments. Hüsser (1957 and 1968) has given a treatment, also for power series expansions, of functions of unequally spaced discreet arguments, and has supplied a computer program for this case. I have been unable to discover a treatment of harmonic expansion for unequally spaced data, although harmonic interpolation formulae for such data have been known for a long time. (For references and formulae due to Cauchy (1841), Gauss (1866), and Hermite, see Whittaker and Robinson (1940).)

The expansion in terms of the orthogonal functions introduced here provides a short-cut for the determination of the Fourier coefficients, and also a new "power spectrum" which is invariant to the degree of the expansion, but which does not have a clear interpretation because of the rather peculiar and artificial nature of these new basis functions. I have found indications "experimentally" that the new kind of invariant "power spectrum" (or rather "spectra", since alternative normalizations of these functions may be chosen) may be a very revealing source of information, at least in the case of the ΔC^{14} data, about the data itself apart from its accidental spacing. That is, it might give a better approximation to the "real" power spectrum associated with the data, than do any of the Fourier power spectra, it having in some sense corrected for the unequal spacing. However, no demonstration for the validity, if any, of such an interpretation has been found.

It should be remarked that an alternative approach of initially interpolating equally spaced values between the given data points was rejected, even though this has led to the still relatively cumbersome technique reported here. The desire to treat the data as a whole, including even regions where large gaps existed, has led to this decision. The amount of interpolation that would have been necessary to achieve a reasonable overall density of points would have been highly unreasonable in these gaps, giving far too much weight to regions where relatively little data is available. However in practice it was found that in the largest gap

some interpolation was necessary after all. Furthermore, the dependence of the approximation function at time t on data far removed from t was found to be very small indeed, thus weakening the argument for treating all the data at once. It would still be a valuable contribution to apply interpolation and ordinary Fourier analysis to separate regions of the ΔC^{14} data which singly have relatively constant densities of measurement. Problems of continuity at the end-points of such regions, and the limited resolution of peaks in the power spectrum for regions of small length would still present some difficulties.

The remainder of this chapter is devoted to a fuller description of the technique of Fourier analysis which has been employed, and then to a discussion of the functions of degree and frequency used to choose a cut-off frequency. Chapter III concerns the application of this technique to the ΔC^{14} data.

Fourier analysis

We consider the m+1 arbitrarily distributed data points (t_i, w_i), i=0,1,2,...m, where $w_i = w(t_i)$, and the t_i have been normalized to the interval $(t_0=0, t_m=2\pi)$. The number of independent data points is $M \leq m$, since multiple points at the same time are permitted, and since any function analysed must have the fundamental period $T_1=2\pi$. If $w_0 \neq w_m$, both should be set equal to their average, perhaps only a minor adjustment if a trend has already been removed.

In order to fit this data we define the harmonic series $Z_N(t)$ of degree N (N = 2n for even N, and N = 2n-1 for odd N, where n is the highest frequency number) as

$$Z_N(t) = \frac{1}{2} d_{N0} + \sum_{k=1}^{n} (c_{Nk}\sin kt + d_{Nk}\cos kt), \quad 0 \leq N \leq M, \qquad (1)$$

where $d_{Nn} = 0$, for odd N (N = 2n-1).

Thus $Z_N(t)$ has N+1 coefficients (*), a highest frequency n, and a term in cosnt only for even N. Note that in general

---

(*) For equally spaced data, $t_i = 2\pi i/m$, there are only N coefficients if N = M = m = 2n, since $\sin nt_i = 0$.

the coefficients require the additional index N. They are determined by minimizing the total square deviation $\mathcal{E}_N^2$ of the data from $Z_N(t_i)$:

$$\mathcal{E}_N^2 = \sum_{i=0}^{m-1} [w_i - Z_N(t_i)]^2, \qquad (2)$$

which provides N+1 simultaneous linear equations in the N+1 unknown coefficients.

For equally spaced data these equations may be reduced immediately by using the "orthogonality" property of sinkt and coskt:

For $t_i = 2\pi i/m$, and for k and j integers, $0 \leq k,j \leq m/2$,

$$\sum_{i=0}^{m-1} \text{sinkt}_i \text{cosjt}_i = 0$$

$$\sum_{i=0}^{m-1} \text{sinkt}_i \text{sinjt}_i = \begin{cases} \frac{m}{2}\delta_{kj}, & k \neq 0 \text{ and } k \neq m/2 \\ 0, & k = 0 \text{ or } k = m/2 \end{cases} \qquad (3)$$

$$\sum_{i=0}^{m-1} \text{coskt}_i \text{cosjt}_i = \begin{cases} \frac{m}{2}\delta_{kj}, & k \neq 0 \text{ and } k \neq m/2 \\ m\,\delta_{kj}, & k = 0 \text{ or } k = m/2 \end{cases}$$

This leads to the well known expressions for the Fourier coefficients:

$$\left.\begin{aligned} c_{Nk} = c_k &= \frac{2}{m}\sum_{i=0}^{m-1} w_i \text{sinkt}_i \\ d_{Nk} = d_k &= \frac{2}{m}\sum_{i=0}^{m-1} w_i \text{coskt}_i \end{aligned}\right\} \begin{cases} k = 0, 1, 2, \ldots, n < m/2 \\ N = 0,1,2,3,4,\ldots,2n-1,2n < m \end{cases} \qquad (4)$$

$$[c_{N0} = c_{m-1,m/2} = c_{m,m/2} = c_{m/2} = 0;$$

$$d_{m,m/2} = d_{m/2} = \frac{1}{m}\sum_{i=0}^{m-1} w_i \text{coskt}_i \text{ ; for even m.}]$$

Thus the coefficients may be calculated easily up to any desired

maximum degree N_{max}. The power, $p^2_{Nk} = p^2_k = c^2_k + d^2_k$ is invariant to the degree of expansion, so it may serve as the basis for choosing a cut-off frequency or degree for which $Z_N(t)$ will in some sense be an optimal interpolation function for the data.

On the other hand, for unequally spaced data the orthogonality conditions (equations 3) do not hold, so that in a direct approach N+1 simultaneous equations in the N+1 coefficients must be solved for each $N \leq N_{max}$, in order to find the N_{max} different power spectra. (For $N < L$, the power spectra p^2_{Nk}, k=0,1,...n, are in general not the same as the spectrum p^2_{Lk}, k=0,1,...n.) For reasonably large N_{max} the task of finding these spectra in this manner would be formidable even for a computer.

However, if the power spectra are found, they will exhibit variations from one spectrum to the next in the heights of peaks belonging to certain frequencies. As may be seen from figure 12, these variations may be substantial for some frequencies. Clearly, a large but unstable peak does not indicate the importance of a frequency in the same sense as does a large peak in an ordinary invariant power spectrum. Such an unstable peak contains information about, and is a consequence of both the data values and the data times. Large unstable peaks can occur at a frequency which may or may not be really important in the measured phenomenon, the instability arising from an interaction between the frequency, the time intervals and the data values. One purpose of the subsequent analysis is therefore to find criteria which will help in assessing the significance of large peaks.

Orthogonal basis

The alternative technique of introducing new basis functions is primarily a short-cut in the task of calculating sets of Fourier coefficients and finding Fourier power spectra, but in addition it provides a new kind of power spectrum which is invariant to the degree of expansion, but whose physical meaning is not as clear as that of a Fourier power spectrum. The introduction of new basis functions cannot provide more information than is already contained implicitly in the Fourier power spectra, but perhaps it can order the same information in a more illuminating way.

We define the new basis functions $P_K(t)$ as linear combinations of sinjt and cosjt, having degree K (K = 2k for even K, and K = 2k-1 for odd K), in formal analogy to the functions $Z_N(t)$ of equation 1:

$$P_K(t) = \frac{1}{2} b_{K0} + \sum_{j=1}^{k} (a_{Kj} \sin jt + b_{Kj} \cos jt), \quad 0 \leq K \leq M, \qquad (5)$$

where $b_{Kk} = 0$, for odd K (K = 2k-1).

The K+1 coefficients of $P_K(t)$ can be determined by the K+1 equations of the orthogonality condition

$$\sum_{i=0}^{m-1} P_K(t_i) P_L(t_i) = \frac{m}{2} \delta_{KL} , \qquad (6)$$

(if the coefficients of the $P_L(t)$, $0 < L < K$, have been found already). This orthogonality condition and normalization are analogous to those satisfied by the functions sinkt and coskt for equally spaced data times t_i (equations 3), being in that case entirely identical to them.

These orthogonal basis functions are determined by the particular distribution of the times t_i, and not by the data values w_i. Their values at the times t_i are of interest only in so far as they are needed in the calculation of the various functions to be introduced below. Other functions, $P'_K(t) = \Gamma_K P_K(t)$, will also be introduced. These involve an alternative normalization to that given by equation 6 when K=L. Appendix A shows how the $P'_K(t_i)$ may be found recursively from the previous four functions $P'_{K-v}(t_i)$, v=1,2,3,4, using four quantities α_{Kv} which are also necessary for the subsequent determination of the Fourier coefficients, c_{Nk} and d_{Nk}, in equation 1. Thus the coefficients, a_{Kj} and b_{Kj}, in the expression for $P_K(t)$ (equation 5) need not be found explicitly.

In the case of equally spaced data, both the functions $P_K(t)$ and $P'_K(t)$ reduce to the ordinary harmonic functions, sinkt and coskt. For unequally spaced data they contain additional terms of lower frequencies which prevents their simple interpretation in terms of simple oscillations. This disadvantage is of course the price for the simplicity of the coefficients of $P_K(t)$ in the expansion of $Z_N(t)$.

The "gower spectrum"

The functions $Z_N(t)$ now may be expanded in terms of the new basis functions $P_K(t)$:

$$Z_N(t) = \sum_{K=0}^{N} G_K P_K(t) = \sum_{K=0}^{N} G'_K P'_K(t) \qquad (7)$$

The coefficients G_K may be determined by the minimization of $\mathcal{E}_N^2 = \sum_{i=0}^{m-1} [w_i - Z_N(t_i)]^2$. The orthogonality of the P_K then leads to the simple result:

$$G_K = \frac{\sum_i w_i P_K(t_i)}{\sum_i P_K^2(t_i)} = \frac{2}{m} \sum_{i=0}^{m-1} w_i P_K(t_i) \text{ , (Appendix A).} \qquad (8)$$

These coefficients are not dependent on N, so that a new kind of power spectrum, defined in analogy to the ordinary power as a function of frequency k,

$$g_k^2 = G_{2k-1}^2 + G_{2k}^2 \text{ , } k=0,1,2,3,\ldots \text{ , } (*) \qquad (9)$$

will be invariant to the degree N of expansion of $Z_N(t)$. This new power spectrum will be called the "gower spectrum".

The equality of the two ways of expanding $Z_N(t)$, (equations 1 and 7) leads to a solution for the Fourier coefficients:

$$c_{Nk} = \sum_{K=2k-1}^{N} G_K a_{Kk} \text{ , } k= 1,2,3,\ldots n,$$

$$d_{Nk} = \sum_{K=2k}^{N} G_K b_{Kk} \text{ , } k=0,1,2,3,\ldots n. \qquad \text{(Appendix A)} \qquad (10)$$

As mentioned above, it is not necessary to find the coefficients

---

(*) See footnote on next page.

a_{Kj} and b_{Kj}, since the Fourier coefficients may be determined more easily from the G'_K and a set of quantities α_{Kv}, v=1,2,3,4. These quantities may also be used to find the values $P'_K(t_i)$ recursively from the previous four sets of values $P'_{K-v}(t_i)$, v=1,2,3,4 with degrees less than K.

The total square deviation may also be found recursively:

$$\mathcal{E}^2_K = \sum_{i=0}^{m-1} [w_i - Z_K(t_i)]^2$$

$$= \mathcal{E}^2_{K-1} - G_K \sum_{i=0}^{m-1} w_i P_K(t_i) \qquad \text{(Appendix A)}$$

$$= \mathcal{E}^2_{K-1} - G^2_K \sum_{i=0}^{m-1} P^2_K(t_i) \qquad \text{(equation 8a)}$$

$$\mathcal{E}^2_K = \mathcal{E}^2_{K-1} - \frac{m}{2} G^2_K \ , \ -1 \leq K < M \ (*) \qquad \text{(equation 8b).} \quad (11)$$

Thus the improvement in fit resulting from using one additional basis function is

$$\mathcal{E}^2_{K-1} - \mathcal{E}^2_K = \frac{m}{2} G^2_K \ , \ -1 \leq K < M \ (*) \qquad (12)$$

and from using two additional basis functions (one additional frequency) is

$$\mathcal{E}^2_{2k-2} - \mathcal{E}^2_{2k} = \frac{m}{2} g^2_k \ , \ 0 \leq k < \frac{M}{2} \ (*). \qquad (13)$$

This property of the gower g^2_k is entirely analogous to the equivalent property of the power p^2_k for equally spaced data.

(*) The cases K=0 and K=-1 in equations 11 and 12, and the case k=0 in equations 9 and 13, may be included by defining $G_{-1} \equiv 0$, and $\mathcal{E}^2_{-2} \equiv \mathcal{E}^2_{-1} \equiv \sum_{i=0}^{m-1} w_i^2$. This corresponds to the correct expressions:

$$Z_0 = \frac{1}{m} \mathcal{E}^2_{-1}; \ P_0 = \sqrt{2}/2; \ G_0 = \sqrt{2}\, Z_0; \text{ and } \mathcal{E}^2_0 = \mathcal{E}^2_{-1} - mZ^2_0.$$

Alternative normalizations

The fundamental property of the basis functions $P_K(t)$ is their orthogonality over the irregularly spaced arguments t_i. The particular normalization, $\sum_{i=0}^{m-1} P_K^2(t_i) = m/2$, was chosen in analogy to the behaviour of $\sin kt_i$ and $\cos kt_i$ for equally spaced arguments. The choice of the value 1 instead of m/2 for the normalization constant would result of course in only trivial changes, for example the difference

$\mathcal{E}_{K-1}^2 - \mathcal{E}_K^2$, would be G_K^2 instead of $\frac{m}{2} G_K^2$.

Less trivial consequences result from another alternative normalization in which the last coefficient occuring in $P_K(t)$ is set equal to 1. Using primes for these new functions, we define $P'_K(t)$ as in equation 5, but with the additional condition: $a'_{2k-1,k} = b'_{2k,k} = 1$. The orthogonality condition, equation 6, remains the same for $K \neq L$. For $K = L$ the new normalization becomes

$$\sum_{i=0}^{m-1} P'^2_K(t_i) = \sum_{i=0}^{m-1} \Gamma_K^2 P_K^2(t_i) = \frac{m}{2} \Gamma_K^2 \quad ,$$

where $P'_K(t) = \Gamma_K P_K(t)$.

The ratio

$$\Gamma_K^2 = \frac{P'^2_K(t)}{P_K^2(t)} = \frac{G_K^2}{G'^2_K} = \frac{2}{m} \sum_{i=0}^{m-1} P'^2_K(t_i) \qquad (14)$$

is a function which generally decreases with increasing K, but is not monotonic (see figures 9 , 10, and 11). However, as also shown in these figures, the function of frequency

$$\gamma_k^2 = \frac{1}{2} (\Gamma_{2k-1}^2 + \Gamma_{2k}^2) \quad , \quad K>0 \qquad (15)$$

is a monotonic non-increasing function, although I have not proved this.

In the limit of equally spaced data where $P_{2k-1}(t) = P'_{2k-1}(t) = \sin kt$ $(k > 0)$, and $P_{2k}(t) = P'_{2k}(t) = \cos kt$ $(k \geq 0)$, we have $\Gamma_K^2 = \gamma_k^2 = 1$, for all k between 0 and M/2 = m/2. For unequally spaced data the figures show that γ_k^2 goes to 1 as k approaches 0, and goes to 0 as 2k approaches m, the number of data points (less 1). In the first limit the spacing of the data is irrelevant, since the best fit is a horizontal line through the mean of the data. In the second limit all frequencies are used, up to the frequency number m/2 with period $2T_1/m$, which is twice the average interval length and is much smaller than other intervals occuring in the data. The fact that this frequency is much too high to give reasonable results in these other intervals, may be thought of as expressed by the low value of γ_k^2 for high frequency number k. Thus γ_k^2 can be interpreted as an index of the importance of the irregularity of the spacing relative to the frequency k, and as such is used below to indicate the approximate upper limit for a reasonable cut-off frequency.

Program of calculation and criteria for cut-off

Of the two ways of expanding $Z_N(t)$, the first has simple basis functions but complicated coefficients, and the second has complicated basis functions, but simple coefficients. Thus the first fails to give unique information about how important certain frequencies are for the measured phenomenon, while the second fails to tell of what it speaks when it says exactly how much of it there is. Indeed these are mathematically identical ways of saying the same thing, and therefore neither can contain more information than the other. The advantages of the second method are primarily its greater convenience for calculation but perhaps also the greater clarity with which it presents the available information. This is a somewhat subjective quality refering to the relative ease with which the behaviour of a unique spectrum or related unique functions of the frequency, independent of cut-off frequency, may be assessed, as opposed to the relative difficulty of understanding the information contained in a whole series of power spectra.

The next section summarizes the steps in the Fourier analysis and the calculation of the various functions which will be used as criteria for the choice of a good cut-off frequency. These functions are then described and discussed in the succeeding section.

Calculation

The details of the calculation will be treated first. The first approach requires the solution of many sets of simultaneous equations for the Fourier coefficients, and the subsequent evaluation of the functions $Z_N(t_i)$, in order to permit an examination up to some large N_{max} of both the power spectra and the degrees of fit as measured for example by $\mathcal{E}_N^2$. On the other hand, the new approach permits the immediate calculation of $\mathcal{E}_N^2$, so that a few candidates for an optimum cut-off frequency may be chosen prior to any evaluation of the Fourier coefficients and the functions $Z_N(t)$. This choice will be based on a few functions of degree K and frequency k, which may be determined recursively. Subsequently and for only the few chosen values (K=N) the Fourier coefficients, the power spectra, and the $Z_N(t)$ themselves may be examined in detail, along with the original criteria functions, in order to make a final choice of optimal cut-off frequency.

The calculation may be summarized as follows:

A. The recursive determination for K = 0,1,2,...N_{max}(*) of:

1. four recursive parameters α_{Kv}, v=1,2,3,4, to be used for finding $P'_K(t_i)$, and subsequently the Fourier coefficients (Appendix A);

2. $P'_K(t_i)$ by means of the α_{Kv} and the four sets of values $P'_{K-v}(t_i)$, v=1,2,3,4, [$P'_{K-4}(t_i)$ are no longer needed];

3. Γ_K^2 (equation 14);

4. $G'_K = \frac{2}{m} \sum_{i=0}^{m-1} w_i P'_K(t_i) / \Gamma_K^2$;

5. $Z_K(t_i)$, an optional step (equation 7);

(*) For a possible choice for N_{max} see the discussion of equations 17 and 18, below.

6. the following additional functions of K or k which are independent of cut-off degree N (*), and are to be used as criteria for N:

   a. $G_K = \Gamma_K G'_K$;

   b. the total square deviation $\mathcal{E}^2_K$ (equation 11);

   c. the "inefficiency of fit" $\eta^2_K = \mathcal{E}^2_K/(M-K-1)$;

   d. the standard error of estimate $\sigma_K = \sqrt{\mathcal{E}^2_K/m}$;

   e. the "gower" g^2_k, K=2k (equation 13);

   f. the renormalized gower $g'^2_{k-1} = G'^2_{K-1} + G'^2_K$, K=2k ;

   g. the "irregularity index" γ^2_k, K=2k (equation 15);

   h. the total power A^2_K/π (equation 16).

B. The examination of these functions of K and k, and the choice, based on their behaviour, of a small set of values of N which, hopefully, will include the desired cut-off degree that is in some sense optimal.

C. The calculation for the chosen N's of the Fourier coefficients c_{Nk} and d_{Nk}, k=0,1,2,...n, and the Fourier power spectra, using the α_{Kv} and G_K (Appendix A).

D. The evaluation for the chosen N's of $Z_N(t)$, using the Fourier coefficients, either at the original arguments t_i, or at equally spaced arguments, or both.

(*) "independent of N" in the sense that they depend only on K, not on both N and K < N. In some of these functions, for example the total power up to degree K, both K and N refer to cut-off degrees, and these are of course functions of K.

Parts A, C and D may be done as separate computer runs. Part D may include a computer plotting routine for $Z_N(t)$ at equally spaced t. Due to rounding errors some differences exist between the values $Z_N(t_i)$ at the original t_i as found using the $P'_K(t_i)$ (step A.5.) and as found from the Fourier coefficients (step D.). The former are probably slightly more accurate (Hüsser, 1968).

Criteria for the choice of N

These many functions of the degree N or the frequency n (*) will now be examined for the information they contain relevant to the choice of an optimal cut-off frequency.

A. The total square deviation and related functions

1. $\mathcal{E}_N^2$, G_N^2 and g_n^2

The total square deviation $\mathcal{E}_N^2$ measures the degree to which $Z_N(t)$ fits the data, that is at the data times t_i. It is a monotonic non-increasing function of N. The relative importance of a degree N in improving the fit is shown by the size of the decrease,

$$\mathcal{E}_{N-1}^2 - \mathcal{E}_N^2 = \frac{m}{2} G_N^2,$$

and the relative importance of a frequency n is shown by the size of the decrease,

$$\mathcal{E}_{2n-2}^2 - \mathcal{E}_{2n}^2 = \frac{m}{2} g_n^2.$$

Once certain ranges of N have been ruled out by other means, the function $\mathcal{E}_N^2$, or equivalently the functions G_N^2 and g_n^2, are the most important guides to the detailed choice of an optimal N. In other words, large peaks in the gower spectrum g_n^2, just as in an ordinary power spectrum, may indicate important frequencies. In both cases spurious peaks, probably at high frequencies, must be identified by other means such as the behaviour of the total power and the relationship between interval length and frequency (see section B. below).

(*) In the following, degree and frequency will be called N and n, rather than K and k, unless both are necessary.

2. η_N^2

The "inefficiency of fit", $\eta_N^2 = \mathcal{E}_N^2/(M-N-1)$, is relatively large either for large $\mathcal{E}_N^2$ or for large N. If it has a minimum value for some N, this might be called the least inefficient or most efficient N, having the smallest $\mathcal{E}_N^2$ per N. The number of remaining degrees of freedom after imposing N+1 equations on the M independent data points is M-N-1 (*). $\mathcal{E}_{M-1}^2$ need not be zero when this is zero, so η_N^2 may have a minimum. However, this occurs at such a high value of the degree N, that it clearly cannot be interpreted as "optimal" in a sense useful in this context. (It is possible that some variation of this idea, taking for example $(M-N-1)^2$ in the denominator, might have a useful interpretation which <u>is</u> supported by a statistical argument.) On the other hand, η_N^2 does have local minima (see figures 6, 7, and 8), and these of course coincide with relative peaks of the function G_N^2. Thus η_N^2 throws no additional light on the situation.

3. σ_N

The standard error of estimate, $\sigma_N = \sqrt{\mathcal{E}_N^2/m}$, is the root-mean-square of the deviation of the data from $Z_N(t_i)$, being just so large that 68.3 % of the data w_i lie within $\pm\sigma_N$ of the curve $Z_N(t)$. Equating σ_N to the data's standard error of measurement σ, provides a possible <u>a posteriori</u> criterion for N, based on additional information about the data. However since σ is a rather slowly changing function of N (see figures 6, 7, and 8), this criterion is not very helpful. Nevertheless it can be regarded either as a rough criterion for N, or conversely as a useful check on the standard error of measurement.

(*) For an exception, see footnote page 25.

B. The Nyquist frequency and the total power

The distribution of interval lengths in a data time series is related to the highest frequency and the smallest period which can reasonably be used in its Fourier analysis. In the case of equally spaced data the limiting frequency is called the Nyquist frequency, n_q. It corresponds equivalently to an exact fit, where the number of independent data points equals the number of coefficients ($M = m = N = 2n_q$, M even), and to a smallest allowable period T_q, equal to twice the interval length Δt:

$$n_q = \frac{M}{2} = \frac{T_1}{2\Delta t} = \frac{T_1}{T_q} \quad \text{(equally spaced data).}$$

The larger is the data's random character relative to the real character of the phenomenon (noise to signal ratio), the lower the optimal cut-off frequency will be relative to the limiting Nyquist frequency. That is, at some point already before reaching the Nyquist frequency, the function $Z_N(t)$ may begin to exhibit wild behaviour, since while trying to fit even the random part of the data it is free to take any value in the intervals. One recommendation (Hartree, 1952) for the smallest period T_{min} which may reasonably be used in the analysis of equally spaced data is that it should include at least 6 data points:

$$T_{min} = 6\Delta t = 3T_q$$
$$N_{max} = 2n_{max} = \frac{M}{3} \quad \text{(equally spaced data).}$$

One measure of the amplitude of oscillation of $Z_N(t)$ in the gaps is its total square deviation from zero over the continuous interval from 0 to 2π, i.e. the square area

$$A_N^2 = \int_0^{2\pi} Z_N^2(t)dt = \pi \sum_{k=0}^{n} p_{Nk}^2 \quad (*) \; . \qquad (16)$$

Because of the orthogonality of sinkt and coskt over this continuous interval, this is equal to π times the total power up to the frequency n (Parseval's formula). Whereas

---

(*) Contrary to the previous notation, p_{N0}^2 here is $d_{N0}^2/2$.

for equally spaced data, A_N^2 is of course monotonic non-decreasing, possibly becoming very large for $N >> N_{max}$, for unequally spaced data this is not the case. It also begins at some point to reach large values, but may return again to lower ones (see figures 6 , 7 , and 8). This pronounced piqued character is one of the few good indications (along with marked instabilities in the Fourier power spectra) that a frequency is too large for intervals existing in the data series.

For unequally spaced data the condition, $2n \leq M$, is of course still valid, but its interpretation in terms of an analogous Nyquist frequency n_q is not so clear since there is no constant interval $\Delta t = T_1/m$. However it would be convenient to have such an analogous limit based on the given distribution of interval lengths Δt_i. Letting δt be some kind of "average" interval for unequally spaced data, we would have

$$n_q = \frac{T_1}{2\delta t}$$

$$T_{min} = 6\delta t \qquad \text{(unequally spaced data)}$$

$$N_{max} = 2n_{max} = \frac{1}{3}\frac{T_1}{\delta t} \qquad (17)$$

The following suggestion for such an average interval δt is based on my experience with the C^{14} data. In particular, the total power A_N^2, the Fourier power spectra and the $Z_N(t)$ themselves begin to behave strangely at a degree $N = N_{max}$ which corresponds roughly to δt equal to the root-mean-square interval length:

$$\delta t = \sqrt{\frac{1}{m}\sum_{i=0}^{m-1} \Delta t_i^2} \qquad \text{(unequally spaced data).} \qquad (18)$$

The initial recursive calculation therefore may be carried to a highest degree perhaps slightly larger than $N_{max} = T_1/3\delta t$. The rms interval length δt corresponds to an effective number of data points, $M_{rms} = T_1/\delta t$, which will be used below in conjunction with the "irregularity index" γ_n^2 to determine a maximum cut-off frequency based on information available only after the initial calculation has been finished.

N_{max} would be too small if δt were taken as the largest of the gaps Δt_i. It would be too large if δt were to

equal either the average gap length or even a weighted average, using the Δt_i themselves as weights. The corresponding "Nyquist" frequency is

$$n_q = \frac{1}{2}\left(\sum_{i=0}^{m-1} \Delta t_i\right)\left(\frac{1}{m}\sum_{i=0}^{m-1} \Delta t_i^2\right)^{-1/2} \qquad \text{(unequally spaced data)}$$

Perhaps a statistical argument could be found to deduce its usefulness in this context.

C. The power of the gower

1. The power p_{Nk}^2

For equally spaced data the choice of an optimal cut-off frequency is essentially a judgement based on the unique power spectrum of the point at which the deviation of the data from the smooth function may be attributed solely to random errors of measurement. Usually this point is clear from the spectrum, being the end of a region of large "significant" peaks and the start of a region of small random values in the histogram.

As seen in figure 12, the set of many power spectra for unequally spaced data exhibit, in addition to some large peaks of relatively constant magnitude, peaks at particular frequencies which grow and disappear again over a range of different cut-off frequencies. For example in figure 12, note the behaviour of the power for frequency numbers k = 17, 24 and 27, in the spectra with cut-off degrees N = 50, 54, 64, 71 and 76.

Such instabilities in the power spectra are related to the data's interval distribution, reflecting the use of frequencies too high for some relatively large time intervals occuring in the data. They may be interpreted as contributions from these large gaps to the square area A_N^2 under $Z_N(t)$, caused by these frequencies. That the instabilities are not due to noise in the conventional sense of random power, and that they are not limited to frequencies of only small importance, has been shown by the Fourier analysis of unequally spaced data taken from a test function with known harmonic coefficients.

Since an instability in the power spectrum may or may not occur at a frequency which is also important in a real sense for the description of perhaps most of the data, the problem of judging the significance of peaks in the power spectra of unequally spaced data involves distinguishing both between signal and noise, and between the signal and these instabilities. For this purpose the power spectra p^2_{Nk} alone are not very helpful. It is true that the instability of large peaks at low frequencies is small, so that a cut-off frequency chosen from the power spectra to include only these low frequencies while excluding all subsequent large instabilities, would yield a smooth interpolation function having a high degree of certainty, but this choice might also discard unreasonably much information contained in the data.

2. The gower g^2_k ; g'^2_k and γ^2_k

The first normalization of $P_K(t)$ results in the proportionality of the gower, $g^2_k = G^2_{2k-1} + G^2_{2k}$, to the improvement in fit, $\mathcal{E}^2_{2(k-1)} - \mathcal{E}^2_{2k}$, so that this meaning of the gower is quite clear. However, its interpretation in terms of the importance of the functions $P_{2k-1}(t)$ and $P_{2k}(t)$ in the expansion of $Z_N(t)$ does not extend to the importance of the frequency k alone, since all frequencies less than k are also included in P_{2k-1} and P_{2k}.

This applies also to the basis functions $P'_K(t)$ which were normalized so as to have at least one of the coefficients sinkt and coskt equal to one. For low frequencies, and especially for large peaks in the spectra, g^2_k and g'^2_k are nearly the same, and are both about equal to the ordinary power $p^2_{2k,k}$, in the spectrum K=2k in which sinkt and coskt first appear. Thus for "low" frequencies the gower may be interpreted as an ordinary power after all, and signifies the relative importance of each frequency.

For "high" frequencies the various spectra are no longer even approximately the same. The point at which they begin to convey only very doubtful information about frequencies in the data may be judged from

1) sudden increases or peaks in the total power A_N^2,

2) the appearance of marked instabilities in the power spectra p_{Nk}^2, and

3) downward kinks in the graph of γ_k^2.

Figures 6 and 9 show that for the case there depicted, these three criteria give an upper limit for the cut-off degree which lies between about N=50 and N=80, and that the only reasonable candidates for a good cut-off above N=50 are N=54, 66 and 76.

By using γ_k^2, the index of the importance of the irregularity of the spacing for any frequency k, these judgements may be summarized into one objective criteria. It is based on the assumption that the effective interval length is the rms interval length δt (equation 18), so that the effective number of data points is $M_{rms} = T_1/\delta t$; and on the assumption that the effective number of data is also given by $M_{eff}(k) = m\gamma_k^2 \leq m$. Equating these two expressions, we have

$$M_{eff}(k) = m\gamma_k^2 = M_{rms} = \frac{T_1}{\delta t} . \qquad (19)$$

This equation may be solved graphically for k, and gives a value for the upper frequency limit which agrees with the rougher limits found by inspecting the various graphs. For example in the case shown in figure 9, with T_1 = 6955 y, one finds δt = 29 y and M_{rms} = 240, which corresponds to a cut-off degree of N = 60.

It should be stated finally that the reasons for accepting the above two assumptions and this criteria have been, at least up to now, purely empirical ones, since the above explanations are not more than plausibility arguments.

CHAPTER III FOURIER ANALYSIS OF RADIOCARBON CONCENTRATIONS IN BRISTLECONE PINE

Introduction

In this chapter the method of Fourier analysis described in Chapter II is applied to the bristlecone pine radiocarbon measurements which were carried out by H.E. Suess, and which have been described in Chapter I.

A number of curves approximating this data to various degrees were chosen by means of criteria discussed here and in chapter II, and these results are presented in the accompanying figures. Various power spectra and other functions of frequency such as the standard error of estimate are also given. Calibration curves for radiocarbon dating have been calculated from the smooth ΔC^{14} functions using the 5730 y half-life. Finally, for the investigation of physical periodicities, the power spectra as found by means of the Fourier transform are given for various sections of the ΔC^{14} data time series, for comparison with the power spectra from the Fourier series analysis.

Data preparation

The original ΔC^{14} data consists of 331 radiocarbon values measured by H.E. Suess (1967 and 1970) for bristlecone pine wood.

$$\Delta C^{14}(t_i) \pm \sigma_i = [(\frac{A(t_i)}{A_0} - 1)\cdot 1000 \pm \sigma_i]\ ‰\ ,$$
$$i = 0,1,2,\ldots,m=330.$$

for the dates t_i which are irregularly spaced from 5290 B.C. (negative) to A.D. 1855 (positive), and which were determined dendrochronologically by C.W. Ferguson (1968). The fractionation- and age-corrected activities of the standard wood, A_0, and of the sample wood, $A(t_i)$ have been discussed in Chapter I. The statistical counting errors σ_i are between 4 ‰ and 7 ‰, and will be referred to collectively as σ. Using the half-life $T_{1/2}$ = 5730 y, the radiocarbon dates of these data are

$$t_i^{14} = t^{14}(t_i) = t_i + 8267\cdot\ln(1 + \frac{\Delta C^{14}(t_i)}{1000})\ \text{A.D. y},$$

where t_i is the bristlecone pine (true) A.D. date.

The original ΔC^{14} data was reduced to the residual values

$$C_i = C(t_i) = \Delta C^{14}(t_i) - \hat{C}_S(t_i)$$

by the subtraction of the best-fitting sine function

$$\hat{C}_S(t) = 42.71 + 49.69\sin[\frac{2\pi}{10402}(t + 7388)] \text{ ‰ ,}$$

with period 10400 years (see Chapter I). The standard deviation from the mean of the original ΔC^{14} data, 33.0 ‰, was thereby reduced to 9.9 ‰, for the standard deviation from the mean (zero) of the residual C_i data. The "sine" function for the radiocarbon date, in A.D. years, which corresponds to the ΔC^{14} sine function $\hat{C}_S(t)$ is

$$t^{14}(t) = t + 8267\cdot\ln(1 + \frac{\hat{C}_S(t)}{1000}) \text{ A.D. y ,}$$

where t is the true A.D. date.

The residual ΔC^{14} data, C_i, was analysed in four independent "runs" treating different sections of the data. The first of these, run I, included all the 331 data points in the 7145 y range from 5290 B.C. to A.D. 1855, which contains a largest gap of 425 y between 4795 B.C. and 4370 B.C., limiting the analysis to rather low frequencies. The root-mean-square (rms) interval length was δt = 35 y, so that the effective or rms number of data points was $M_{rms} = T_1/\delta t$ = 201. By graphically solving the equation, $\delta^2 n_{eff} = M_{rms}/m$, for $N_{eff} = 2n_{eff}$ (see equation 19, Chapter II), an effective maximum cut-off degree of N_{eff} = 32 was found. This corresponds to a maximum frequency of only about 2.2 cycles per millenium (cpM) and a minimum period of about 450 years.

For this reason, in run II, two artificial points were added to the residual data series, C_i, in the large gap, and the initial 190 y interval was eliminated by omitting the first point. By reducing the largest interval to 142 y, this allowed a much more detailed analysis, up to a frequency of about 5.5 cpM. Also, the end point values, C_0 and C_m, became closer together in this arrangement. The interpolated data points used in run II were: C(-4563 y) = 2.9 ‰, and C(-4511 y) = 7.4 ‰. (ΔC^{14}(-4563 y) = 94.9 ‰, and ΔC^{14}(-4511 y) = 99.1 ‰). These values of C_i were taken from the approximation functions $Z_{26}(t)$ from run I, which had a cut-off frequency of 1.8 cpM, well below the boundary of about 2.2 cpM between reasonable and unreasonable approximation functions.

Although the introduction of these artificial points violates to a slight extent the spirit of an objective and comprehensive treatment of the data, it has only an extremely small effect on the resulting approximation curves for dates more than a few hundred years away from the region of interpolation. The sections of the resulting smooth curves which are near this region should simply be regarded with an appropriate degree of scepticism, particularly in the 425 y interval itself, where in any case no better information is available.

Runs II and IV are analyses of the data before and after about 200 B.C., respectively. Run IV begins at 4370 B.C., so that both runs exclude the 425 y gap and the interpolated points. This particular division of the data series was made at the suggestion of Professor Suess who had observed a change in phase, occuring roughly at this point, of an oscillation with a period of about 400 y, which is apparent in at least parts of the data series.

The results from only the runs II, III and IV will be presented in this paper. Whereas information about frequency dependence is given graphically for all three of these, the time dependence, in the form of a few smooth approximation functions, is shown only for run II. Approximation functions from different runs, which corresponded to each other in that they had cut-off frequencies as nearly equal as possible, were the same within 1 or 2 % over most of their common ranges. The exceptions to this were only in the few hundred years near the end-points of either data series, where agreement would be expected only if the radiocarbon concentration happened to vary with the fundamental periods equal to the artificial lengths of both of these data series.

The agreement between the three runs, containing different sections of the data, shows that the influence on the approximation functions at time t, exerted by the data points at time t', must fall off rapidly with increasing distance $|t - t'|$. This conclusion reduces the importance which I had previously attached to treating all the data at once, and suggests that it would be worth-while to separately analyse smaller, more homogeneous sections of the data up to higher frequencies than would otherwise be possible. On the other hand, the agreement confirms to some extent the independence of the results from the accidental nature of the fundamental period T_1, and supports the view that the real general character of the ΔC^{14} variations is given correctly.

Table 1 gives some descriptive parameters for the four runs: the range, and the length T_1 of the data series; the number of data, m+1, and of independent data, M (M is m minus the number of double points); the maximum interval length Δt_{max}, the average interval $\overline{\Delta t}$, and the rms interval δt. The effective number of data points, $M_{rms} = T_1/\delta t$, is also given, as is the much smaller number $T_1/\Delta t_{max}$. The former number is used below to find an upper frequency limit.

Table 1

Data Series Parameters

RUN	RANGE (A.D. date)	PERIOD T_1 (y)	m+1 M	MAX. INT. Δt_{max} (y)	$\frac{T_1}{\Delta t_{max}}$	AV. INT. $\overline{\Delta t}$ (y)	rms INT. δt (y)	$M_{rms} = T_1/\delta t$
I	-5290 1855	7145	331 319	425	17	22	35	201
II	-5100 1855	6955	332 320	142	49	21	29	240
III	- 180 1855	2035	110 102	101	20	19	26	79
IV	-4370 -225	4145	210 205	100	41	20	25	166

Choice of cut-off frequency

Three sets of figures for the three runs show the various functions of degree N, frequency number n (n = N/2 or (N+1)/2 as N is even or odd), and frequency $f_n = n/T_1$. These functions illustrate various features of the three data series and have been presented and described in Chapter II. Figures 6, 7 and 8 (for runs II, III and IV, respectively) show: the total square deviation $\mathcal{E}_N^2$ of the data from the curves $Z_N(t)$; the related functions $\eta_N^2 = \mathcal{E}_N^2/(M-N-1)$, and $\sigma_N = \sqrt{\mathcal{E}_N^2/m}$; and the total power $\sum_k p_{Nk}^2 = A_N^2/\pi$, where A_N^2 is the total squared area "under" $Z_N(t)$, i.e. over the continuous time interval, rather than at just the discreet data times t_i. Figures 9, 10 and 11 show the "gower" spectra, $g_n^2 = \mathcal{E}_{2n-2}^2 - \mathcal{E}_{2n}^2 = G_{2n-1}^2 + G_{2n}^2$, $g_n'^2$, and G_N^2; and the "effective number of data points", $M_{eff}(n) = m\gamma_n^2$, which is a function of frequency number n, and is proportional to $\gamma_n^2 = (\Gamma_{2n-1}^2 + \Gamma_{2n}^2)/2$, where $\Gamma_N = G_N/G_N' = P_N'(t)/P_N(t)$ is the

ratio between the two orthogonal but alternatively normalized basis functions P'_N and P_N. Finally, figures 12, 13 and 14 show a number of Fourier power spectra $p^2_{Nk} = c^2_{Nk} + d^2_{Nk}$, as functions of frequency number $k \leq n$, for various degrees N, and illustrate their variability especially for some peaks, and their behaviour (in run II) for extremely large N.

Initially, only the functions $\mathcal{E}^2_N$ and A^2_N were used to choose a few cut-off frequencies: by first eliminating those ranges of N with high values of, and peaks in A^2_N, which indicated "wild" behaviour of $Z_N(t)$ in the largest intervals, and then making a detailed choice within the remaining range, of those degrees where relatively large decreases in $\mathcal{E}^2_N$ occured. Figures 6, 7 and 8 show that extremely large values of A^2_N begin to be encountered at N = 81, 32 and 71 in runs II, III and IV, respectively, so that these degrees are therefore too high. On the other hand, the function $\mathcal{E}^2_N$ indicates that reasonable lower limits for the degree in the three runs are N = 13, 6 and 4, respectively (see table 3), for which values the approximation functions $Z_N(t)$ will certainly represent the main features of the data, although perhaps some available information may thereby be ignored. Some of the initially chosen N-values are listed in table 2, and a few of these are indicated by arrows in figures 6, 7 and 8. More values were taken than needed, for the purpose of investigating the method itself.

Table 2

Initially chosen Degrees N

run

II: N = 5, 7, 13, 24, 31, 43, 48, 50, 54, 64, 71, 76, 82, 94, 96, 100

III: N = 3, 6, 16, 19, 22, 24, 27, 32, 36

IV: N = 4, 8, 11, 13, 19, 26, 30, 31, 37, 41, 45, 60

The Fourier power spectra were found for the selected degrees, and some of them are shown in figures 12, 13 and 14. Note the marked instabilities in the spectral peaks at the frequency numbers n = 24 and 27, which are shown for the spectra which have cut-off degrees N = 64 and 71, in run II (figure 12); and compare with the peaks in A^2_N/π at N = 65 and 72. An examination of the curves $Z_N(t)$ confirmed their expected wild behaviour. The presence of these unstable peaks may be at least partly due to the real importance of these frequencies

FIGURE CAPTION

Figures 6	CRITERIA FUNCTIONS	Run II	pages 49
7		III	52
8		IV	55

These functions of the degree N of expansion, and the corresponding frequency $f_n = n/T_1$ [n=N/2 or (N+1)/2] are defined and discussed in Chapter II, as criteria for the choice of an optimal cut-off frequency. They are: the total square deviation $\mathcal{E}_N^2$, of the data from the approximation curve; the standard error of estimate σ_N, of the fit; the "inefficiency" of fit $\eta_N^2 = \mathcal{E}_N^2/(N-M-1)$; and the total power, $2A_N^2/T_1$, up to the cut-off N, where A_N^2 is the total square area "under" the approximation curve. Lower $\mathcal{E}_N^2$ means a better fit, but higher A_N^2 means this is at the expense of a "wilder" oscillation between the data points, which may become extreme, as shown here.

The arrows indicate N-values for which $Z_N(t)$ were investigated further as promising or interesting. Note the local minima in η_N^2, large decreases in $\mathcal{E}_N^2$, and peaks in A_N^2.

FIGURE CAPTIONS

Figures 9	GOWER SPECTRUM	Run II	pages	50
10		III		53
11		IV		56

The "gower" g_n^2 (b) is the sum of G_{2n-1}^2 and G_{2n}^2 (a), G_N^2 being 2/m times the decrease, $\mathcal{E}_{N-1}^2 - \mathcal{E}_N^2$, in the total square deviation (figures 6, 7 and 8). Unlike the power spectrum, the gower spectrum is invariant to cut-off degree. The steeples (c) are the renormalized gower $g_n'^2$ (Chapter II). Γ_N^2 is the ratio $G_N^2/G_N'^2$, and $\gamma_n^2 = (\Gamma_{2n-1}^2 + \Gamma_{2n}^2)/2$ is roughly the same ratio, but is monotonic. $M_{eff}(f_n)$ has been interpreted here as the effective number of data points "seen" by the analysis, as though they were equally spaced over T_1. The horizontal dashed line is the rms number of data points $[T_1/(\text{rms interval})]$, and meets M_{eff} at a reasonable upper limit for the cut-off degree.

Figures 12	POWER SPECTRA	Run II	pages	51
13		III		54
14		IV		54

The Fourier power spectra, $p_{Nk}^2 = c_{Nk}^2 + d_{Nk}^2$, are shown vs. frequency number k, for various cut-off degrees N. Note the stability of large peaks and the similarity to the gower spectrum at low frequencies; the instability of some peaks at higher frequencies; and (in run II) the slow transformation of the spectra into a quasi-Gaussian distribution, related to the Fourier integral transform of the data time-series, or the distribution of time intervals between data points.

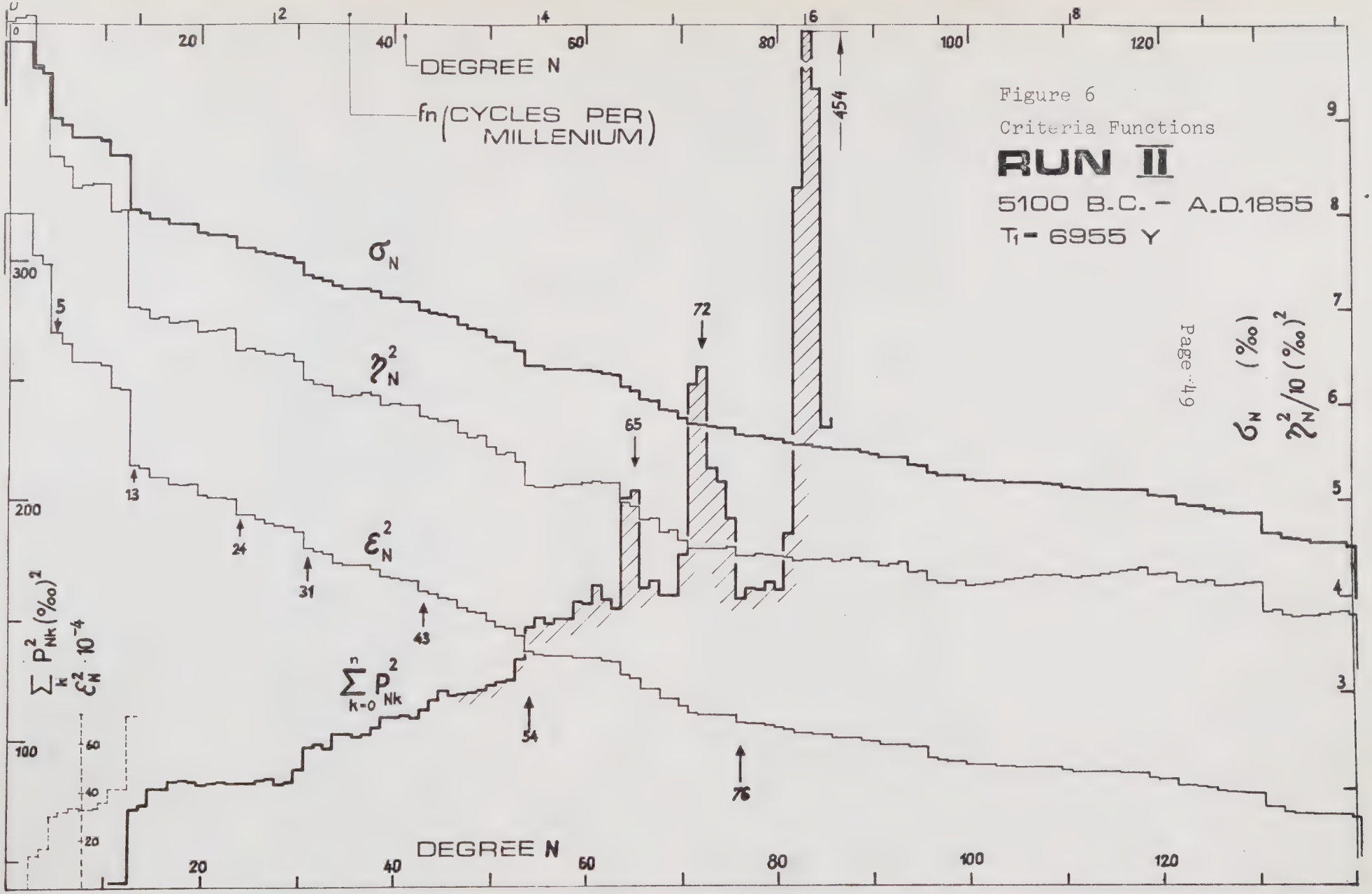

Figure 6

Criteria Functions

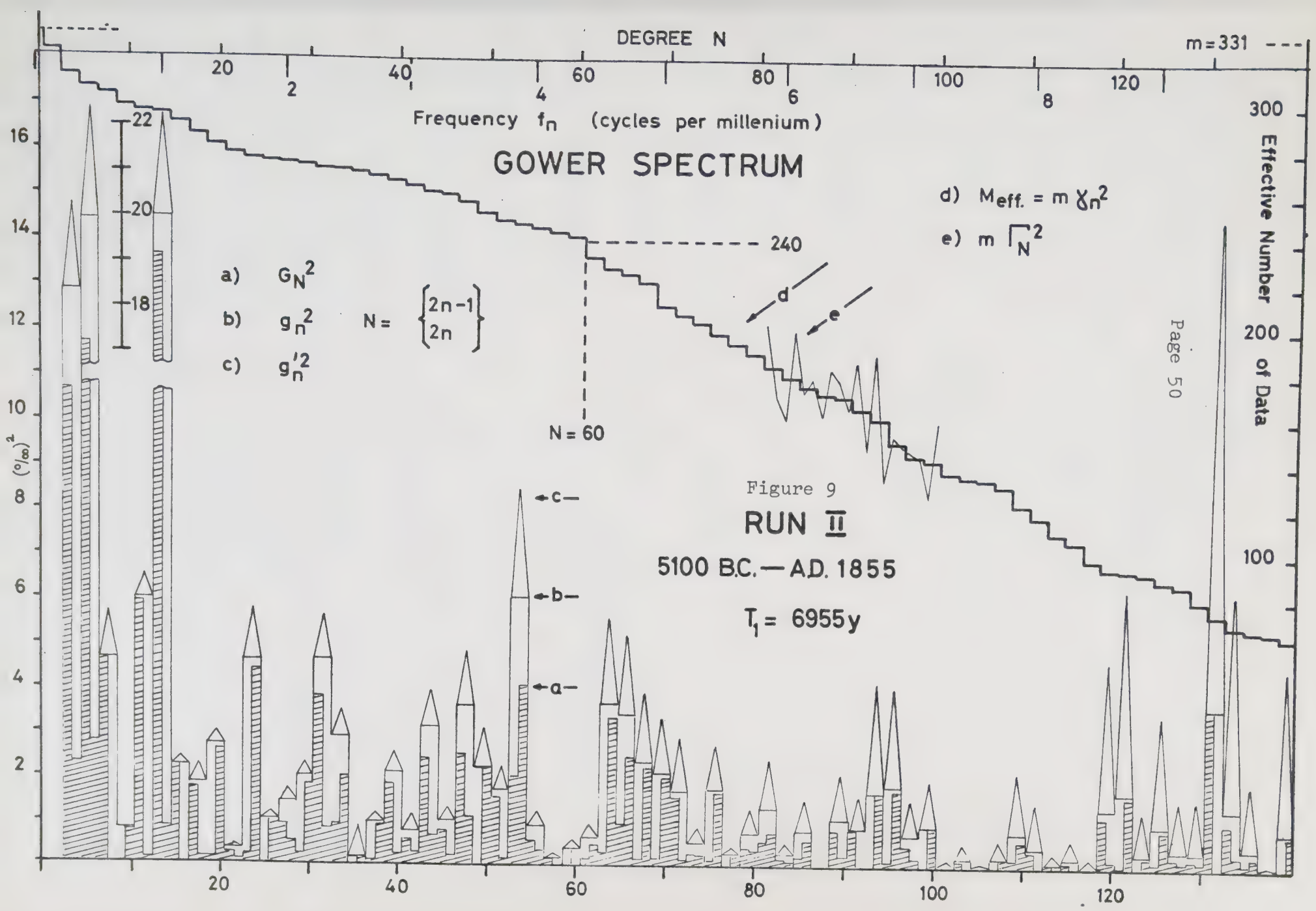
DEGREE N
m=331
Frequency f_n (cycles per millenium)
GOWER SPECTRUM
d) $M_{eff.} = m\,\gamma_n^2$
e) $m\,\Gamma_N^2$
a) G_N^2
b) g_n^2
c) $g_n'^2$
$N = \begin{Bmatrix} 2n-1 \\ 2n \end{Bmatrix}$
240
N = 60
Effective Number of Data
$(‰)^2$
RUN II
5100 B.C. — A.D. 1855
T_1 = 6955y

Figure 9

Figure 12

POWER SPECTRA

P^2_{Nk}

RUN II

5100 B.C. to A.D. 1855

T_1 = 6955y

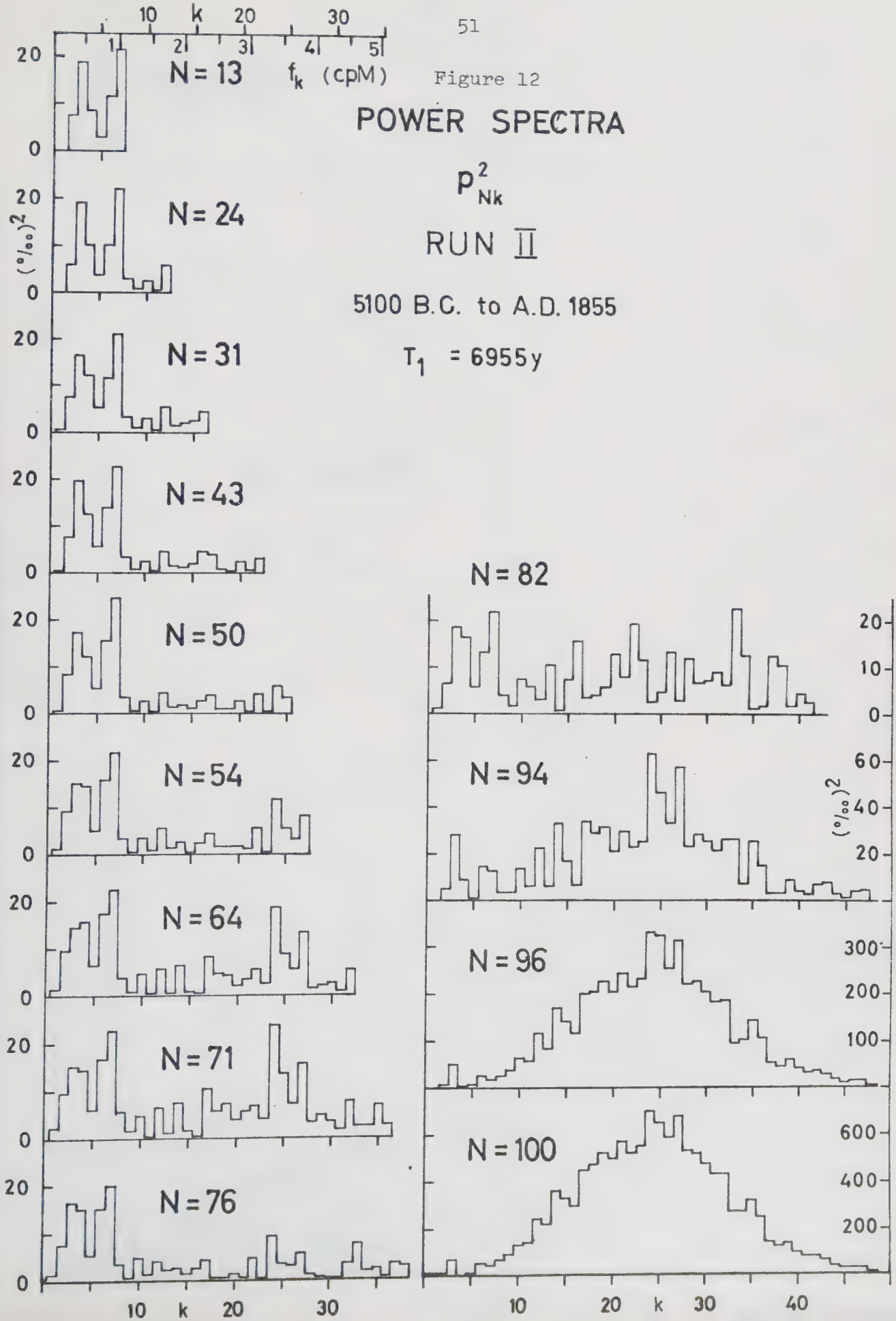

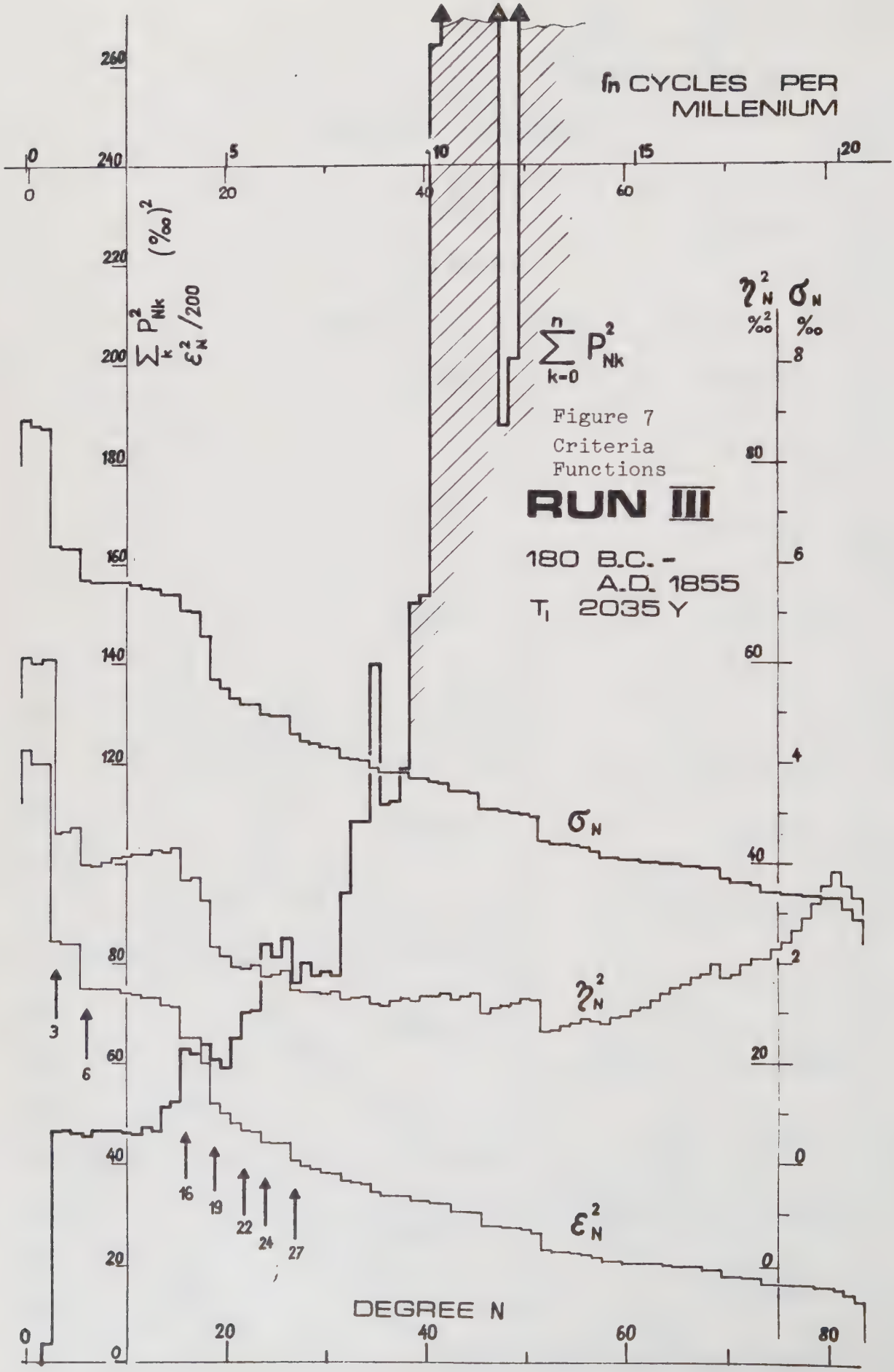

Figure 7
Criteria Functions

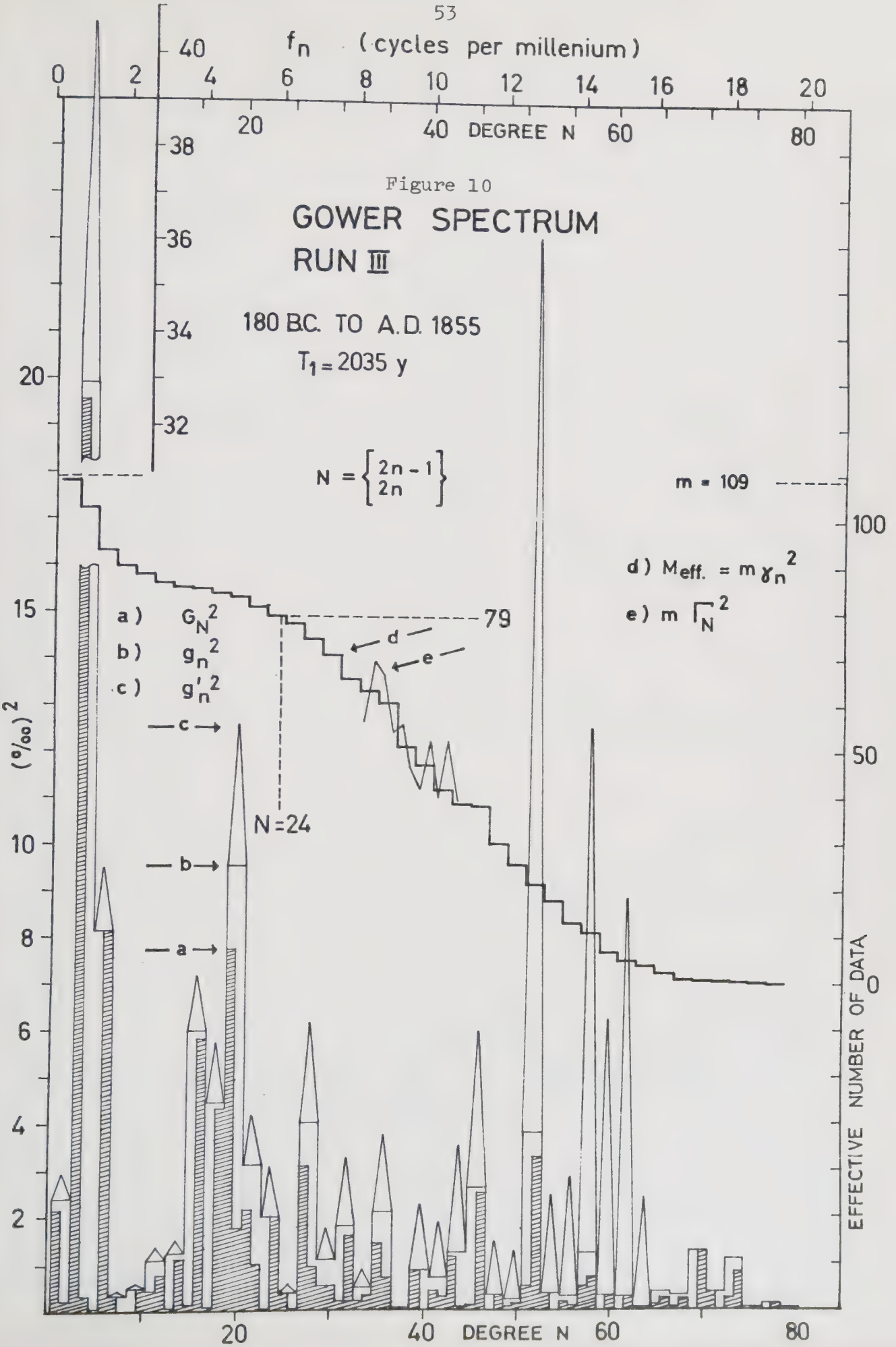
f_n (cycles per millenium)
0
2
4
6
8
10
12
14
16
18
20
40
38
36
34
32
20
40 DEGREE N 60
80
GOWER SPECTRUM
RUN III
180 B.C. TO A.D. 1855
$T_1 = 2035$ y
$N = \left\{ \frac{2n-1}{2n} \right\}$
m = 109
100
50
0
79
N=24
a) G_N^2
b) g_n^2
c) g'^2_n
d) $M_{eff.} = m\gamma_n^2$
e) $m\Gamma_N^2$
$(‰)^2$
15
10
8
6
4
2
EFFECTIVE NUMBER OF DATA
20
40 DEGREE N 60
80

Figure 10

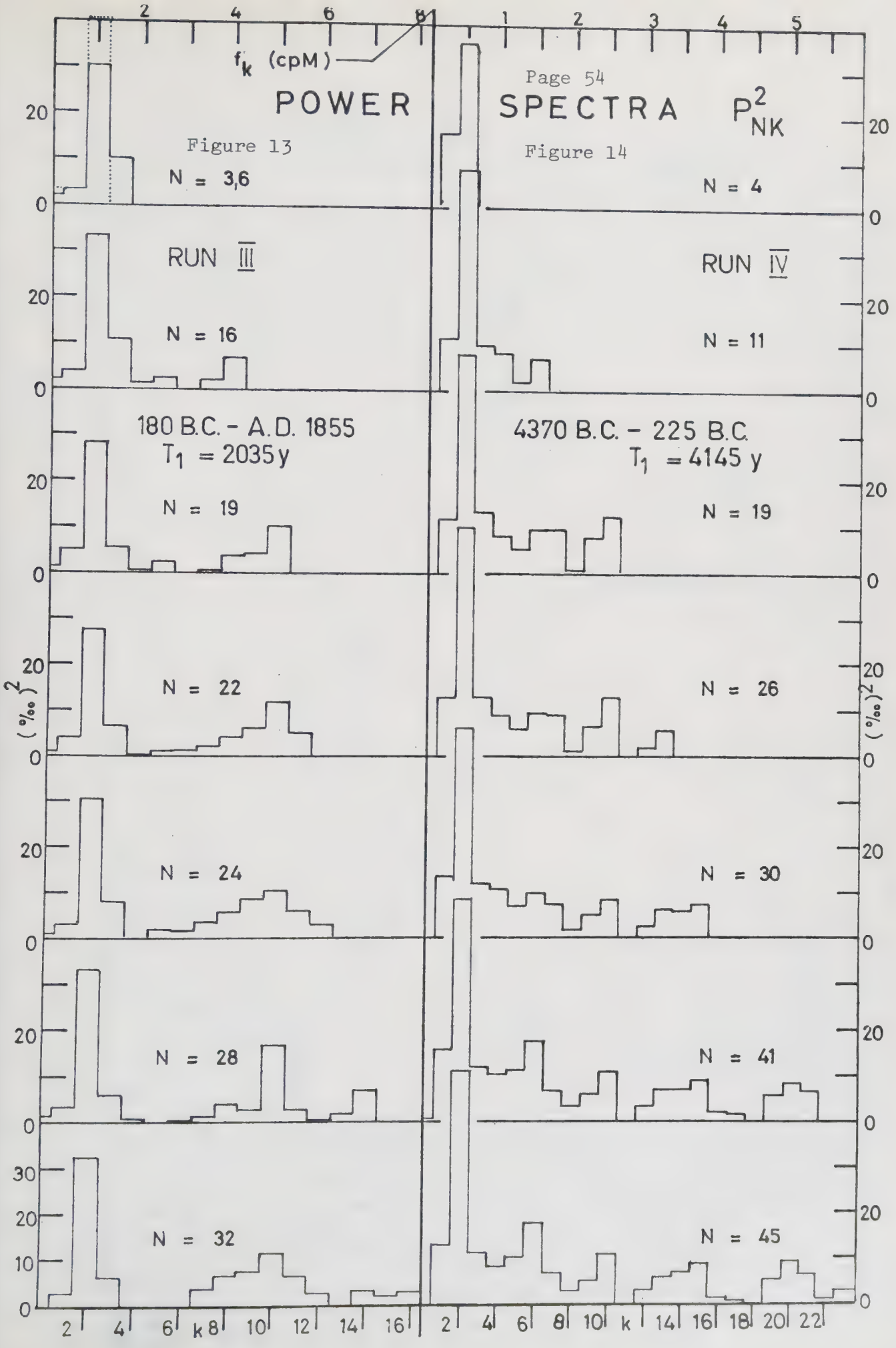
POWER SPECTRA P^2_{NK}
Figure 13
Figure 14
f_k (cpM)
RUN III
RUN IV
N = 3,6
N = 4
N = 16
N = 11
180 B.C. - A.D. 1855
T_1 = 2035 y
4370 B.C. - 225 B.C.
T_1 = 4145 y
N = 19
N = 19
N = 22
N = 26
N = 24
N = 30
N = 28
N = 41
N = 32
N = 45
(‰)²
k

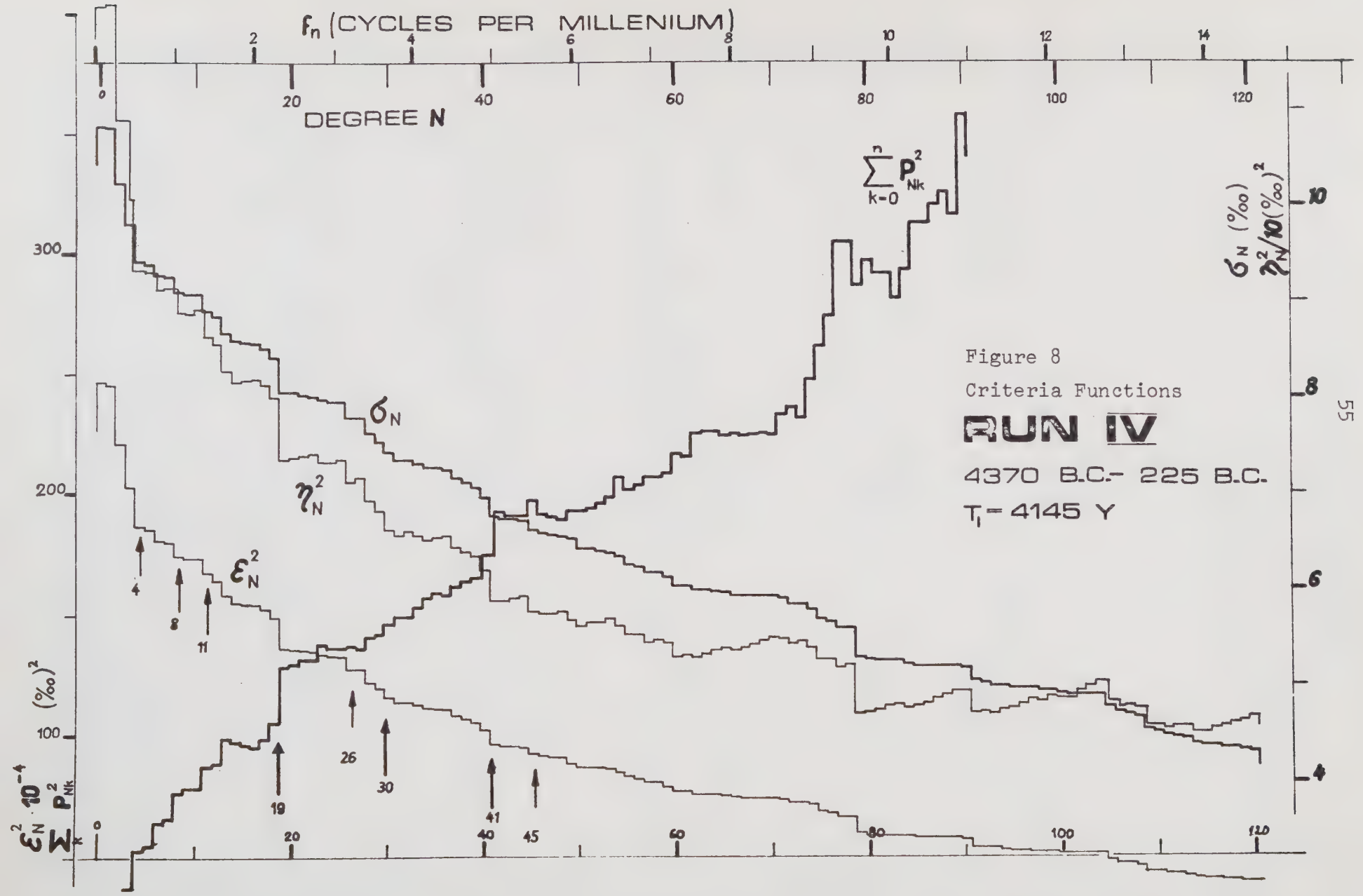

Figure 8
Criteria Functions

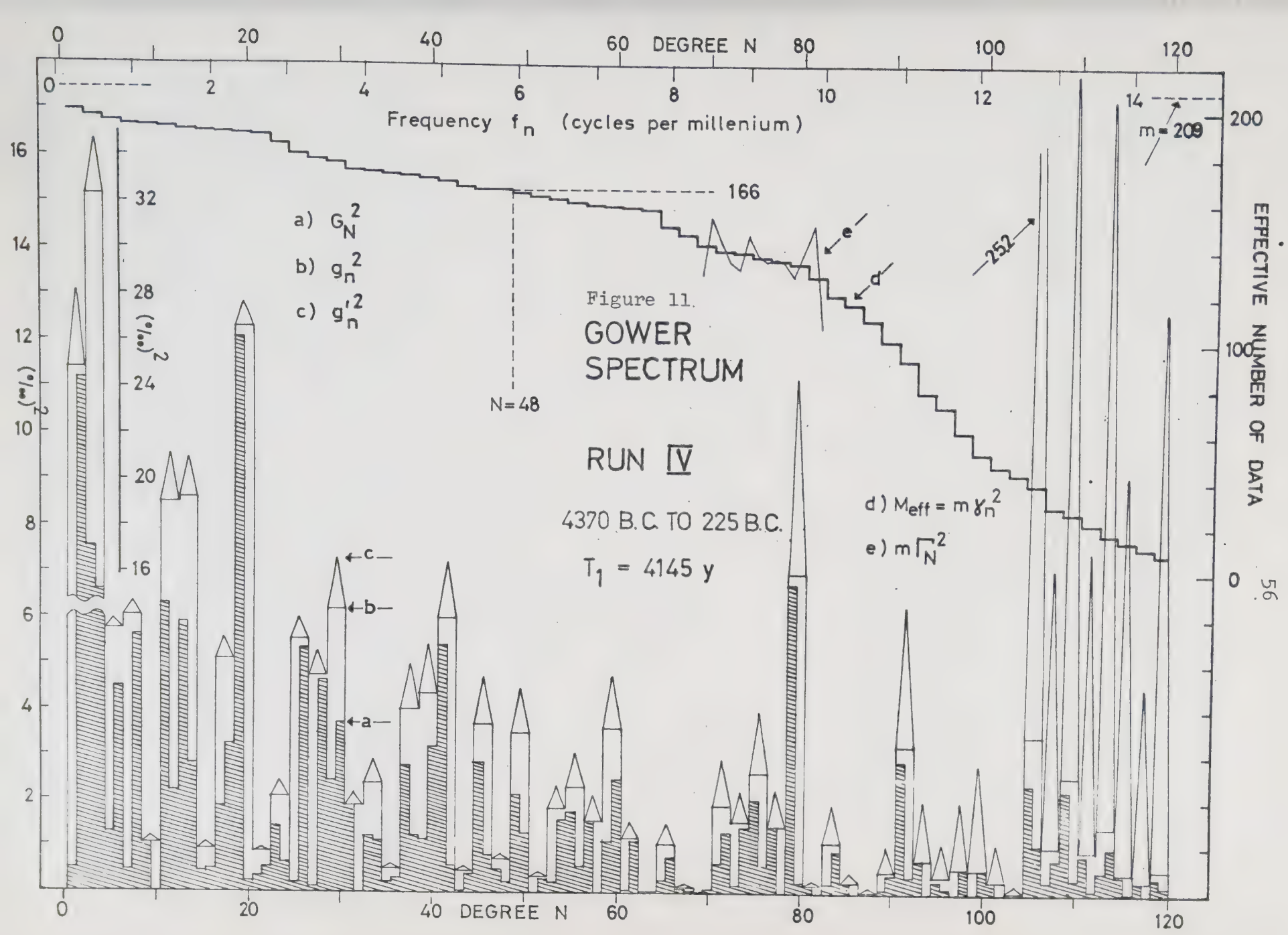

Figure 11.
GOWER SPECTRUM

for $\Delta C^{14}(t)$, but this can probably not be determined from the given data series, because of its particular interval distribution which gives rise to the instabilities at these frequencies. Evidence for physical periodicities will be discussed in another section.

Figure 12 also shows that for very high degrees the power spectra first become very roughly flat (see N = 82), and then begin to approach a Gaussian distribution (see N = 100).

In figures 6, 7 and 8 it may be seen that the "inefficiency of fit" η_N^2 occasionally attains local minima, but this function is of very little use. The standard error of estimate σ_N of the various $Z_N(t)$ with respect to the data may be compared with the statistical counting error σ ($4\ \text{‰} \leq \sigma \leq 7\ \text{‰}$). Table 3 gives the bounds of σ_N, for N in the "reasonable" range described above.

Table 3

Standard Error of Estimate

run	range of N		range of σ_N	
	min.	max.	max. ‰	min. ‰
II	13	80	8.0	5.6
III	6	30	5.8	4.2
IV	4	70	8.9	5.9

This comparison with σ is not used as a criterion for the determination of N. That the values $\sigma_N \approx 7$ ‰ for the two longer series, and $\sigma_N \approx 5$ ‰ for the shorter one, are in the range of σ may be regarded as a kind of reciprocal confirmation, which is nice to have, but which should not be over-emphasized.

The significance of the relationship between the two gower spectra, g_n^2 and $g_n'^2$, shown in figures 9, 10 and 11, was not realized at first. The "objective criterion" which was described in Chapter II, for an upper limit, N_{eff}, of a reasonable cut-off, is the graphical solution for $N_{eff} = 2n_{eff}$ of the equation

$$M_{eff}(n) \equiv m\gamma_n^2 = M_{rms} \equiv \frac{T_1}{\delta t} ,$$

by means of the above figures. The choice here of the rms interval δt, i.e. of M_{rms}, was based on the earlier work

described above, which indicated by means of other criteria [e.g. A_N^2, p_{Nk}^2 and $Z_N(t)$] the range of reasonable values of N. In fact other possibilities for an "average" interval (e.g. Δt_{max}, $\overline{\Delta t}$, and $\Sigma \Delta t_i^2 / T_1$) were all rejected in favor of δt, which best corresponded to the "known" range of reasonable frequencies. If this empirically determined gower criterion also has general validity, its use would save considerable time in the determination of an upper frequency limit for the Fourier analysis of unequally spaced data.

Table 4 gives for the three runs, the cut-off degree, frequency number, frequency, and period, determined from the M_{rms} values (table 1) and $m_{\gamma_n^2}$ (figures 9, 10 and 11).

Table 4

Maximum (rms) Cut-offs

run	N_{eff}	n_{eff}	$f_{n_{eff}}$ (cpM)	$T_{n_{eff}}$ (y)
[I	32	16	2.2	450]
II	60	30	4.3	232
III	24	12	5.9	170
IV	48	24	5.8	173

An examination of the figures shows that these maximum cut-off degrees are reasonable from the point of view of the other criteria functions. High values and peaks in A_N^2, and instabilities in p_{Nk}^2 are indeed excluded, while on the other hand, the limits are by no means too low. The detailed choice of cut-off frequency can be made from among the frequencies below this maximum, on the basis of large peaks in the gower spectrum.

Table 5 is a list of the cut-off degrees, frequencies and periods which were chosen so as to include in the expansion significant peaks of successively higher frequencies, and therefore to produce approximation curves $Z_N(t)$ that represent the ΔC^{14} data with successively increasing fidelity but decreasing "smoothness". Values of the standard error of estimate σ_N are also shown. The curves indicated by stars (*) are illustrated in the accompanying figures.

Table 5

Representative Cut-off Frequencies

	N	n	f_n (cpM)	T_n (y)	σ_N (%)
run II *	13	7	1.01	994	8.0
*	24	12	1.73	580	7.6
	31	16	2.30	435	7.4
*	43	22	3.16	316	7.0
	48	24	3.45	290	6.8
	54	27	3.88	258	6.4
*	76	38	5.46	183	5.7
run III	16	8	3.93	254	5.4
	19	10	4.92	204	4.9
	22	11	5.41	185	4.6
	27	14	6.88	145	4.3
run IV	19	10	2.42	414	8.0
	30	15	3.62	276	7.4
	41	21	5.06	197	6.8
	45	23	5.55	180	6.60
	48	24	5.80	173	6.55

As may be seen from the plateaus which occasionally occur in the total squared area A_N^2, the functions $Z_N(t)$ are often insensitive to the exact choice of cut-off degree. (It may be that there is a slight advantage to taking even cut-off degrees, but this was not always done here.) Values of N for which peaks occured in A_N^2 were avoided, but in each run one cut-off degree was chosen from a subsequent valley in A_N^2 where the $Z_N(t)$ curves had calmed down again. For example, the value $N_{II} = 76$ was taken, even though it is higher than the upper limit of 60 found above. It may be seen from figure 15 that $Z_{76}(t)$ is indeed reasonable over much of the densely populated sections of the data series, although it also has frequencies which are clearly too high for some less dense sections. (The curve for N = 66, also in a valley of A_N^2, may have been a better choice than N = 76.) The approximation curve $Z_{76}(t)$ from run II agreed, in the overlapping regions except near any end-points, within 1 or 2 % with the curves from run III, Z_{22}, and from run IV, Z_{45}, all of which have about the same cut-off frequency (see table 5).

A final choice of the "best" cut-off frequency can of course be made only after a more definite statement of the real problem has been given. This question has been left until now, because for any choice, certain methods and information had to be found regardless of the exact purpose of the analysis. Now that these are available, the purpose should be examined more closely, so that a final choice of cut-off degree may be made.

In the next section the approximation curves are presented and discussed from the point of view of interpolation functions having varying degrees of fidelity to the data and inversely varying degrees of smoothness and certainty of fit. The main use of a radiocarbon interpolation function will probably be its application to the radiocarbon dating method. During those regions of time where the various approximation curves are in good agreement with each other, so that it is unimportant which one is taken, they give a better indication than does the data alone of a sample's true age as a function of its radiocarbon age. And in those regions where agreement between the curves is not so good, for example because of the importance of higher frequencies (either in these regions or elsewhere), it should be clear from the data itself whether or not the more rapid oscillations are warranted. In case these higher frequencies are not warranted by the data, then at least the difference between the approximation curves in this region gives a better indication of the magnitude of the possible error in the corrected age of a sample, than is given by the standard errors and scatter of the data itself.

For the deduction of the possible time dependence of the atmospheric radiocarbon production rate Q, from the time dependence of the atmospheric radiocarbon concentration, an approximation function with relatively low cut-off frequency should be taken. This is so partly because of the uncertainties in the model connecting the two functions, and the uncertainties in the ΔC^{14} curves themselves which are amplified in the production rate curves. In addition, it is not known to what extent the ΔC^{14} variations are caused by production rate variations alone. For example, the highest frequency variations may be caused primarily by climatic variations. In Chapter IV production rates are found from the ΔC^{14} curves from run II, using cut-off degrees N = 13, 24 and 43. The most important for this purpose is the curve for N = 13, which, as may be seen from figures 6 or 9, includes only the two most significant and clearly existing frequencies in the data, namely those with periods of 2320 y (n=3) and 994 y (n=7). (The production rate curves for N = 24 and 43 illustrate the greater attenuation at higher frequencies.)

In the last section of this chapter the frequency dependence is discussed from the point of view of evidence from the ΔC^{14} data for the existence of physical periodicities.

Analytical ΔC^{14} approximation functions

Using the Fourier coefficients c_{Nk} and d_{Nk} in equation 1 of Chapter II, the analytical functions

$$Z_N(t) \equiv C_N(t) = \Delta C_N^{14}(t) - \hat{C}_S(t)$$

which are approximations to the residual ΔC^{14} data, C_i, were computed at equally spaced values of the time, for various cut-off degrees N. Approximation functions for the original ΔC^{14} data, $\Delta C^{14}(t_i) = C_i + \hat{C}_S(t_i)$, where $\hat{C}_S(t)$ is the constant plus sine function with 10400 y period, are then simply

$$\Delta C_N^{14}(t) = C_N(t) + \hat{C}_S(t) \ .$$

The Fourier coefficients for run II (5100 B.C. to A.D. 1855) and for the cut-off degrees N = 13, 24, 43, 54 and 76 are given in table 12. The corresponding values of the power, $p_{Nk}^2 = c_{Nk}^2 + d_{Nk}^2$, are given in table 13. (No analysis has been made of the accuracy of these Fourier coefficients, and therefore of the approximation curves, in relation to the statistical errors of the measurements.)

The approximation functions, both $\Delta C_N^{14}(t)$ for the ΔC^{14} data, and $C_N(t)$ for the residual data C_i, are given in various figures as follows:

1. for N = 24, 43 and 76

	in figure	
$\Delta C_N^{14}(t)$	15	without data error-bars
$C_N(t)$	16	
$\Delta C_N^{14}(t)$	17	with 5 ‰ error-bars
$C_N(t)$	18	

2. for N = 13, 24 and 43, with the corresponding production rates (see Chapter IV)

   a) for N = 24 and 43

	in figure
$\Delta C_N^{14}(t)$	27
$C_N(t)$	26

   b) for N = 13

	in figure
$\Delta C_N^{14}(t)$	24
$C_N(t)$	25

3. for N = 43 and 76, as radiocarbon dates vs. true dates

   $t_N^{14}(t)$ in figure 5.

Figure 17 is a photographic superposition of figures 2 and 15, and figure 18 is a superposition of figures 3 and 16, in order that the curves may be inspected with or without the error-bars.

The approximation functions $\Delta C_N^{14}(t)$ of the original ΔC^{14} data were also translated into C^{14} ages (or dates) as functions of the bristlecone pine or true ages (or dates) using $T_{1/2}$ = 5730 y. These are shown in figure 5, for N = 43 and 76, together with the "sine" function $\hat{t}^{14}(t)$ with 10400 y period.

FIGURE CAPTIONS

Figure 15 and Figure 24 — FOURIER-SMOOTHED ΔC^{14} — page 64, page 99

Three curves, of different degrees of smoothness, are fitted to the original ΔC^{14} data of Suess (1970a). They are found by adding the Fourier fits of the residual data in run II (figure 16), to the 10,400 y period sine wave $\hat{C}_S(t)$ shown here (see equation 1, Chapter I).

Figure 24 shows the curve for N = 13.

Figure 16 and Figure 25 — RESIDUAL FOURIER FITS — page 64, page 100

The three curves shown here are harmonic series which fit the residual ΔC^{14} data, C_i, in the sense of least squares, and have cut-off degrees N and smallest periods T_n, chosen to include the most important frequencies. The Fourier coefficients are given in table 12.

Figure 25 shows the curve for N = 13.

Figure 17 — FOURIER-SMOOTHED ΔC^{14} (2) — page 65

Figure 17 is a photographic superposition of figure 15 and figure 2, and therefore shows the Fourier approximation curves together with the ΔC^{14} data and their ±5 ‰ error-bars. (The three large-scale trend curves are therefore all shown.)

Figure 18 — RESIDUAL FOURIER FITS (2) — page 65

Figure 18 is a superposition of figure 16 and figure 3.

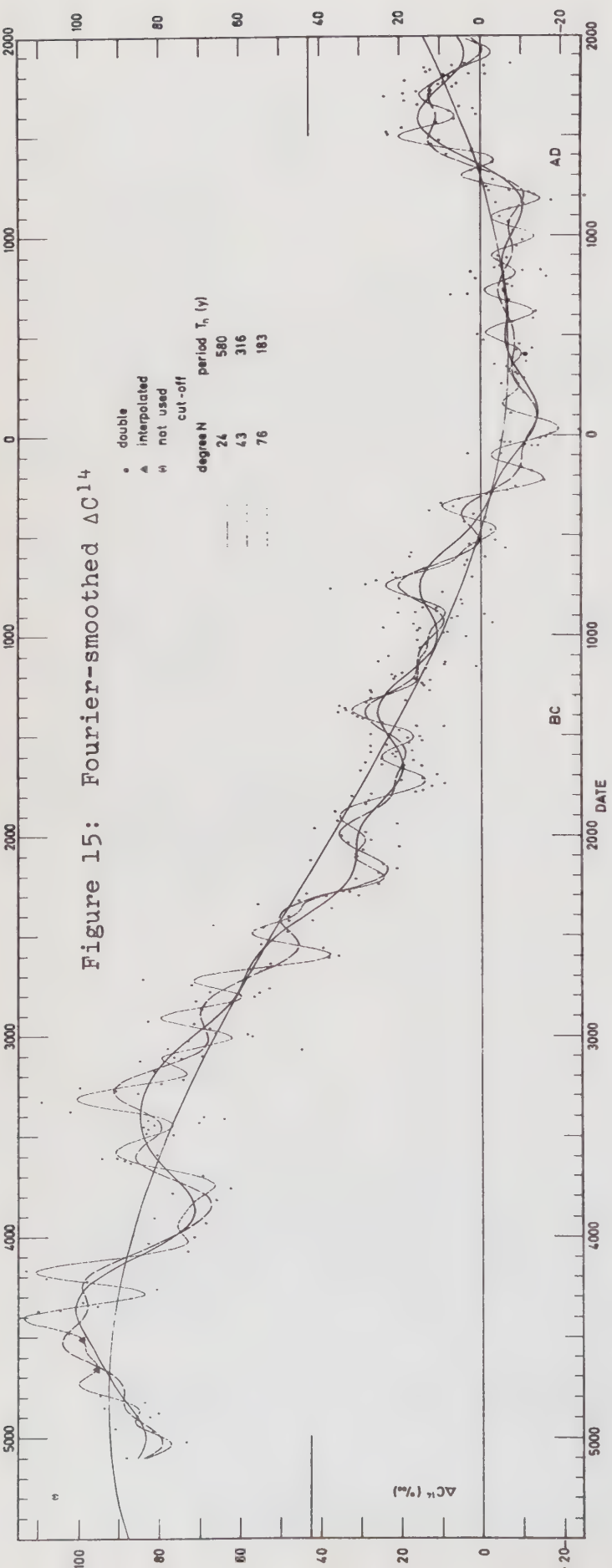

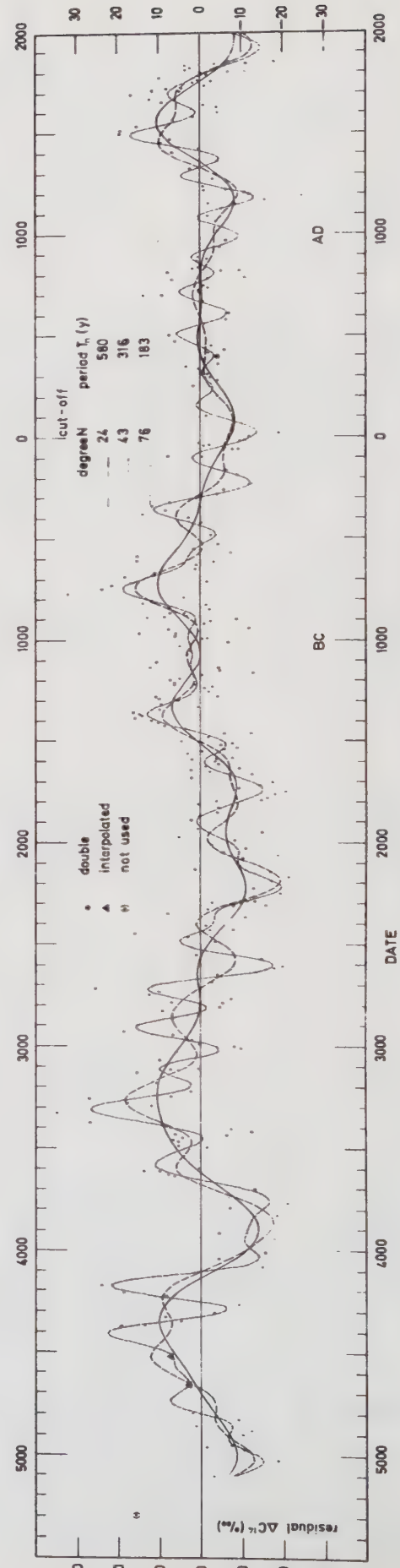

Figure 16: Residual Fourier Fits

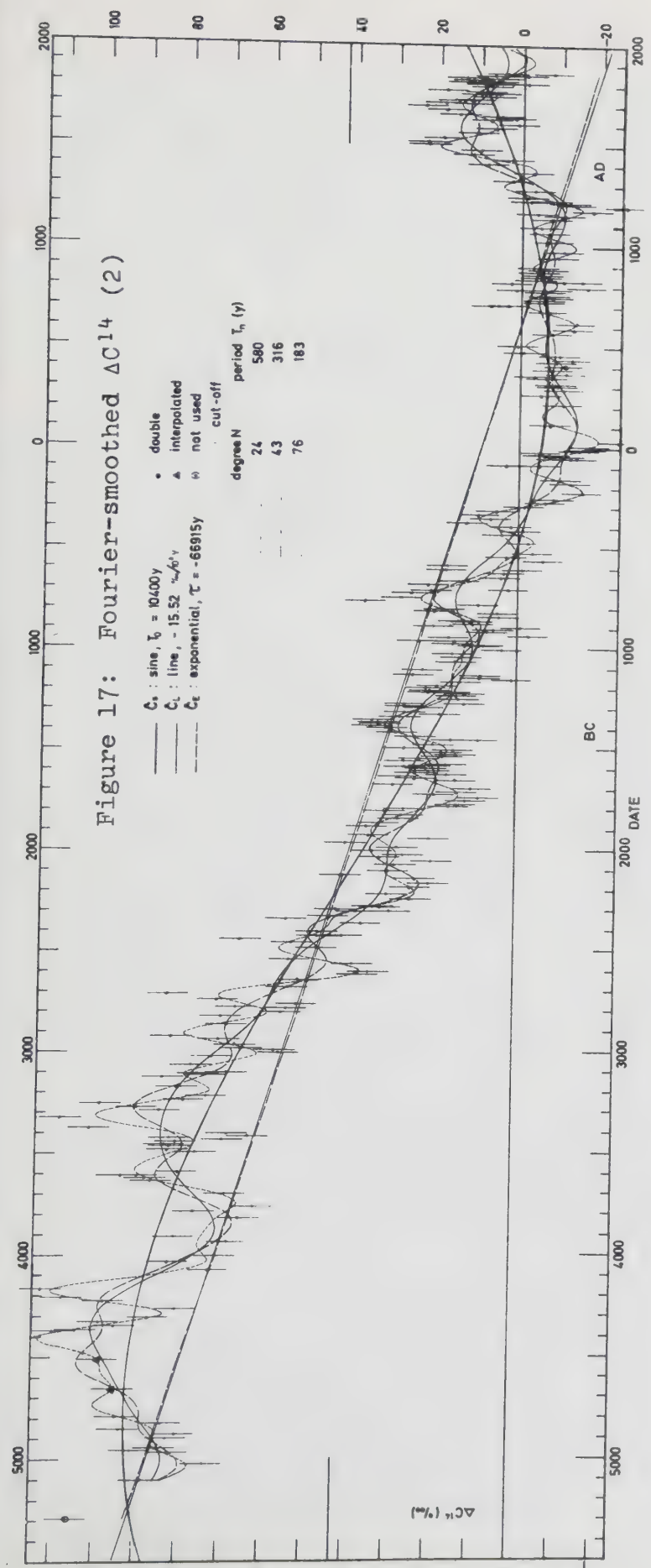

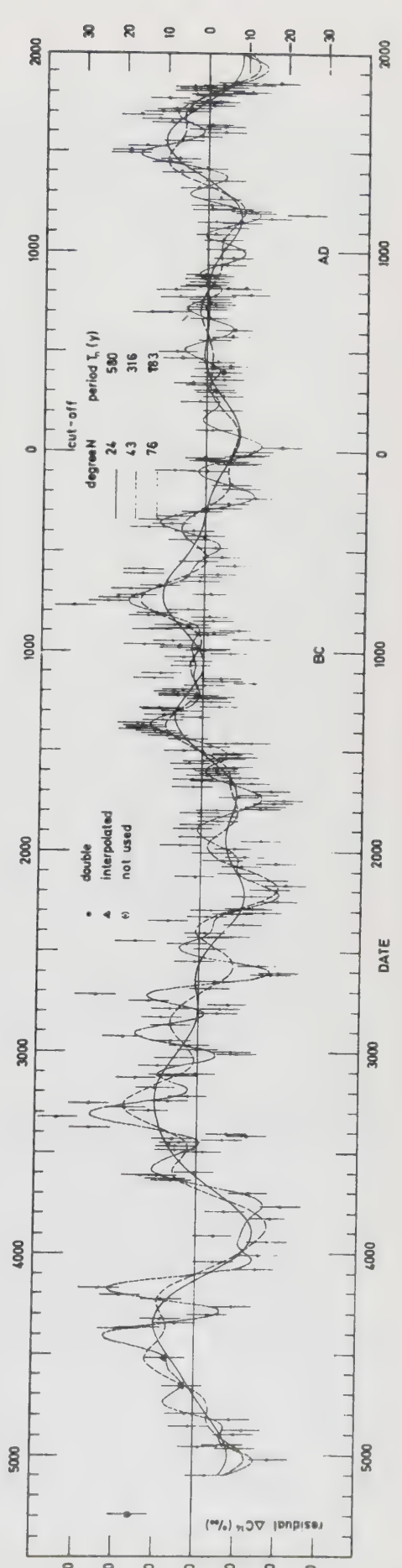

Figure 18: Residual Fourier Fits (2)

All of these curves have the fundamental period of 6955 years, and therefore have continuous values and slopes at the end-points, 5100 B.C. and A.D. 1855. Thus near these points the curves are not good approximations to the data, and their slopes of course cannot be used for predicting the ΔC^{14} behaviour outside the region of measurement.

The curve with cut-off degree N = 43 is probably the one best over-all approximation function of the ones shown. (In some respects the curves with N = 48 and 54 are slightly better, except for a few short regions, but it has not been possible to present them here.) The curves with N = 13 and 24 give the general low-frequency behaviour best, and therefore in some regions fail to follow trends of higher frequency which are very clearly present in the data. The curve with N = 76 gives the correct high-frequency behaviour in a large fraction of the time span, although in some regions it clearly oscillates too rapidly.

For purposes of interpolation it is possible to use the higher frequency curves (e.g. N = 76) in regions of dense measurement, whenever a clear trend is evident in these measurements, and to use the lower frequency curves (e.g. N = 13 or 24) either in regions of sparse measurement or whenever no trend is evident. In particular, in the 425 y interval between 4370 B.C. and 4795 B.C., only the curves for N = 13 and 24 have any validity, since the two interpolated data points in this gap influence these curves hardly at all, in clear contrast to the curves with N = 43 and especially N = 76.

At the other extreme of measurement density, the data in the last 500 years, which exhibit the two well-known ΔC^{14} peaks at about A.D. 1500 and A.D. 1700, are not represented well except in the case of N = 76, where the two peaks are at least clearly resolved. Owing to the frequency limitations imposed by large intervals elsewhere in the data series, more detail cannot be achieved while treating all the data at once. Run III gave somewhat better results in this region, and in general smaller data sections should be analysed to achieve better resolution in time.

However, the general behaviour of the measured atmospheric radiocarbon variations are represented well by these curves, and therefore they give some idea of the possible true radiocarbon variation. For example the steep rises in ΔC^{14} between about 1700 and 1600 B.C., and between about 1550 and 1400 B.C. are shown by the N = 76 curve; and the peaks at about 800 B.C. and the valley at about 2200 B.C. are also clearly shown.

Figure 5 and plate 1 are the same calibration graph for correcting radiocarbon dates. The smooth approximation curves are given in the form of radiocarbon dates as functions of bristlecone pine or true dates. The top scale gives the bristlecone pine date, the bottom scale gives the radiocarbon date (5730 y half-life), and the horizontal center line represents agreement between the two kinds of dates ($\Delta C^{14} = 0$), and is at an angle of 45° to the coordinate axes. The scales give both calendar dates and B.P. dates (ages in A.D. 1950). The scale interval is 50 years. The picture has been split into two parts, the region from 3000 to 4000 B.P. appearing in both.

The graph contains the data points, with error-bars of ± 71 y (± 8.6 ‰ in ΔC^{14}, although ± 5 ‰ was intended), the "sine" function with 10400 y period, and the approximation functions for N = 43 and 76.

If a radiocarbon B.P. date is known as a conventional date based on the 5570 y half-life, it must first be converted to the 5730 y half-life basis by multiplying it by 5730/5570 = 1.029, before the calibration curve can be used. To illustrate this, the use of the table, and the non-uniqueness of the functional dependence, an example is given here. A sample with a conventional radiocarbon date of 5350 B.P., has a "real" radiocarbon date of 5500 B.P., and a corrected date found from plate 1 (2 cm / 20 y) of 6273 B.P., based on the N = 43 approximation; and the three possible dates of 6203, 6296, or 6378 B.P., based on the N = 76 approximation. This many-valued property is of course inherent in the radiocarbon dating method, depending on the slope of the $t^{14}(t)$ function. If the slope is greater than 90°, an isolated sample cannot be uniquely dated, but such a region can be useful in the accurate dating of a series of samples whose relative ages are otherwise known (e.g. a "floating" tree-ring chronology).

The cautionary remarks made above apply also to the radiocarbon calibration curves shown here. Their behaviour near the end-points and in the 425 y gap and other large intervals with little data are necessarily rather approximate. The density of measurement is an aid to deciding which of the three curves is best in a particular region and for a particular purpose. The difference between the curves may be an indication of the magnitude of the over-all error in a corrected radiocarbon date.

Periodicities in the ΔC^{14} data

Evidence for periodicities in the residual data C_i (ΔC^{14} minus the 10400 y period sine wave) is available, for the three sections of the data, from the "gower" spectra (figures 9, 10 and 11), and from the Fourier power spectra having various cut-off degrees (figures 12, 13 and 14). These figures do not have a common frequency scale so that comparison between the three runs, which are data sections of different lengths, is more difficult than in figure 19. This figure shows as functions of the frequency in cpM (cycles per 10^3 y), the gower spectrum (*) from each run, and the power spectra corresponding to those Fourier expansions having cut-off degrees: N_{II} = 24, 43 and 76 (for run II), N_{III} = 16 and 22, and N_{IV} = 20 and 42. These spectra were usually chosen as being typical of a neighborhood of N, the spectra being often rather insensitive to the exact value of N. The continuous power spectra found from the Fourier integral transform (discussed below) of the original ΔC^{14} data, and over the three data sections, is shown in the overlay of figure 19.

The prior removal of the oscillation with period 10400 y should be born in mind for its influence on the low frequency portion of these spectra. Also, the high frequency end is probably distorted by the properties of the interval distribution, i.e. by the finite intervals between data points.

The degree N (N+1 is the number of terms in the harmonic expansion) and the highest frequency number n are related by the relations: n = N/2 for even N, and n = (N+1)/2 for odd N. However, the general frequency number will also be called n here, and the corresponding frequency is $f_n = nf_1 = n/T_1$. The frequency resolution is limited to perhaps one half of $f_1 = 1/T_1$ (frequency limits below are $\pm f_1/2$) and is determined by the length T_1 of the data series. When f_n is comparable with f_1 the resolution of periods is of course poor. Since the power spectra vary with cut-off degree N (the gower spectrum is of dubious value for a frequency determination) the side peaks have not been included in determining the peak frequency value. A weighted average of three peaks would in any case yield a frequency within $\pm f_1/2$ of the central peak.

(*) The gower is the improvement in fit which results from increasing the frequency number by one, and which is measured by the total square deviation of the data from the Fourier series expansion.

The range, period T_1, and fundamental frequency f_1 of the three runs are listed in table 6, as they are ordered in figure 19.

Table 6

Run Parameters

	range	T_1 (y)	f_1 (cpM)
run IV	4370 B.C. to 225 B.C.	4145	0.241
run II	5100 B.C. to 1855 A.D.	6955	0.144
run III	180 B.C. to 1855 A.D.	2035	0.492

The most striking features of figure 19 are the two large peaks in run II (the whole data series), and the disappearance of a different one of them in each of the other runs. The first peak is at $f_3(II) = 0.43 \pm 0.07$ cpM, and must obviously be due to data common to run IV (the more ancient data), for which the only strong peak ist at $f_2(IV) = 0.48 \pm 0.12$ cpM. It is clearly not due to the data in run III (the more recent data) for which no peak at this frequency exists. This situation is reversed with respect to the second peak of run II at $f_7(II) = 1.01 \pm 0.07$ cpM, which corresponds to no peak in run IV, and corresponds instead to the only strong peak of run III at $f_2(III) = 0.98 \pm 0.24$ cpM. The various spectra within a run are all in agreement as to the importance of these two major frequencies.

Table 7 summarizes these important frequencies and gives their periods. Also included are the corresponding frequency and period values found from the Fourier integral transform of the original ΔC^{14} data, taken over the data sections corresponding to the three runs.

FIGURE CAPTION

Figure 19 and Overlay — POWER SPECTRA, RUNS II, III AND IV — page 71

The Fourier series power spectra (and the gower spectra) of the three runs, and for various cut-off degrees, are shown on a common frequency scale. Note the peaks common to runs II and III, and to runs II and IV. These spectra result from analyses of the residual data, while the continuous power spectra (of the corresponding data sections, shown in the overlay) are integral transforms of the original ΔC^{14} data, i.e. before removal of the 10,400 y period sine wave.

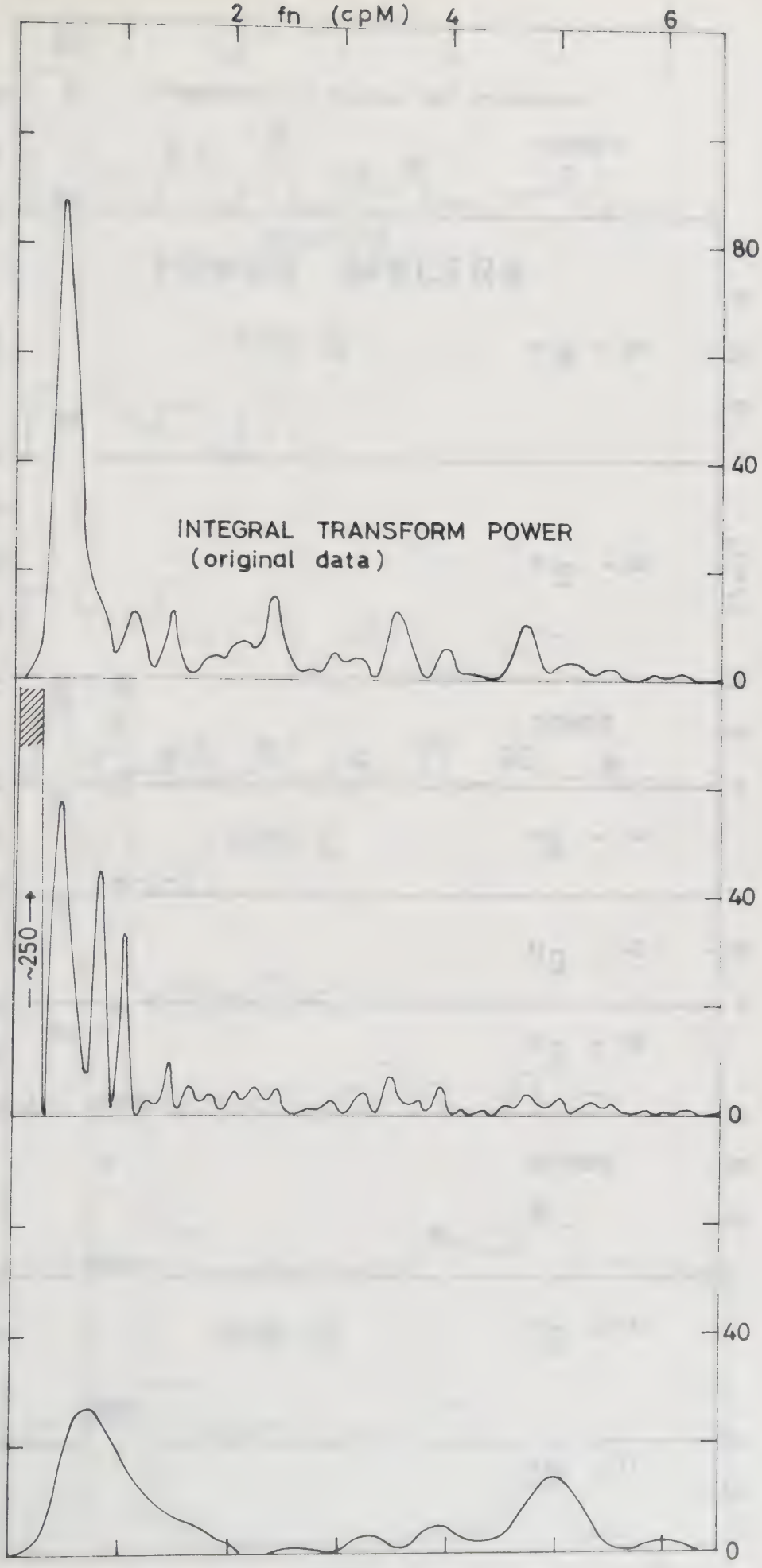
2 fn (cpM) 4
6
80
40
0
INTEGRAL TRANSFORM POWER
(original data)
~250
40
0
40
0

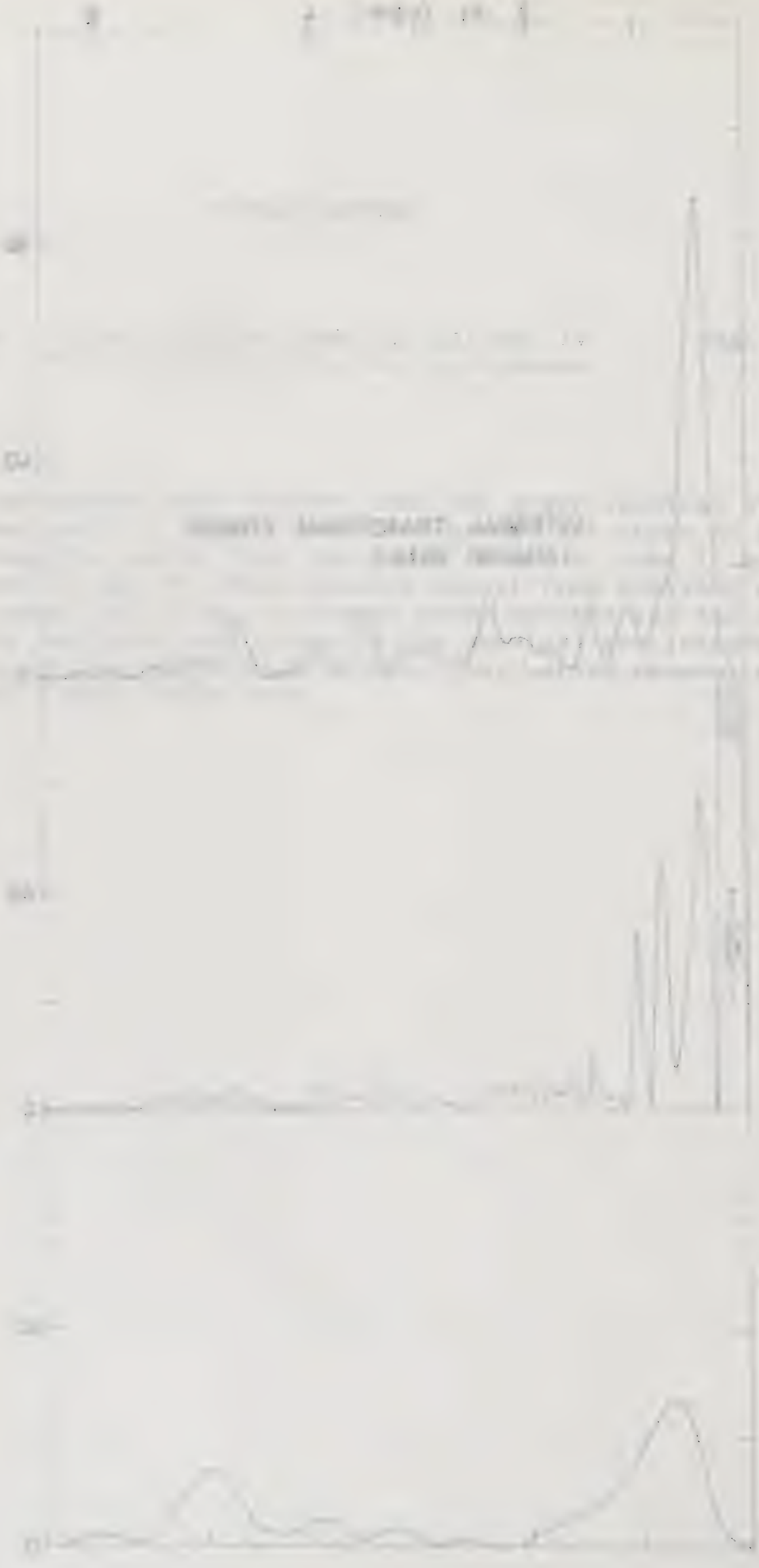

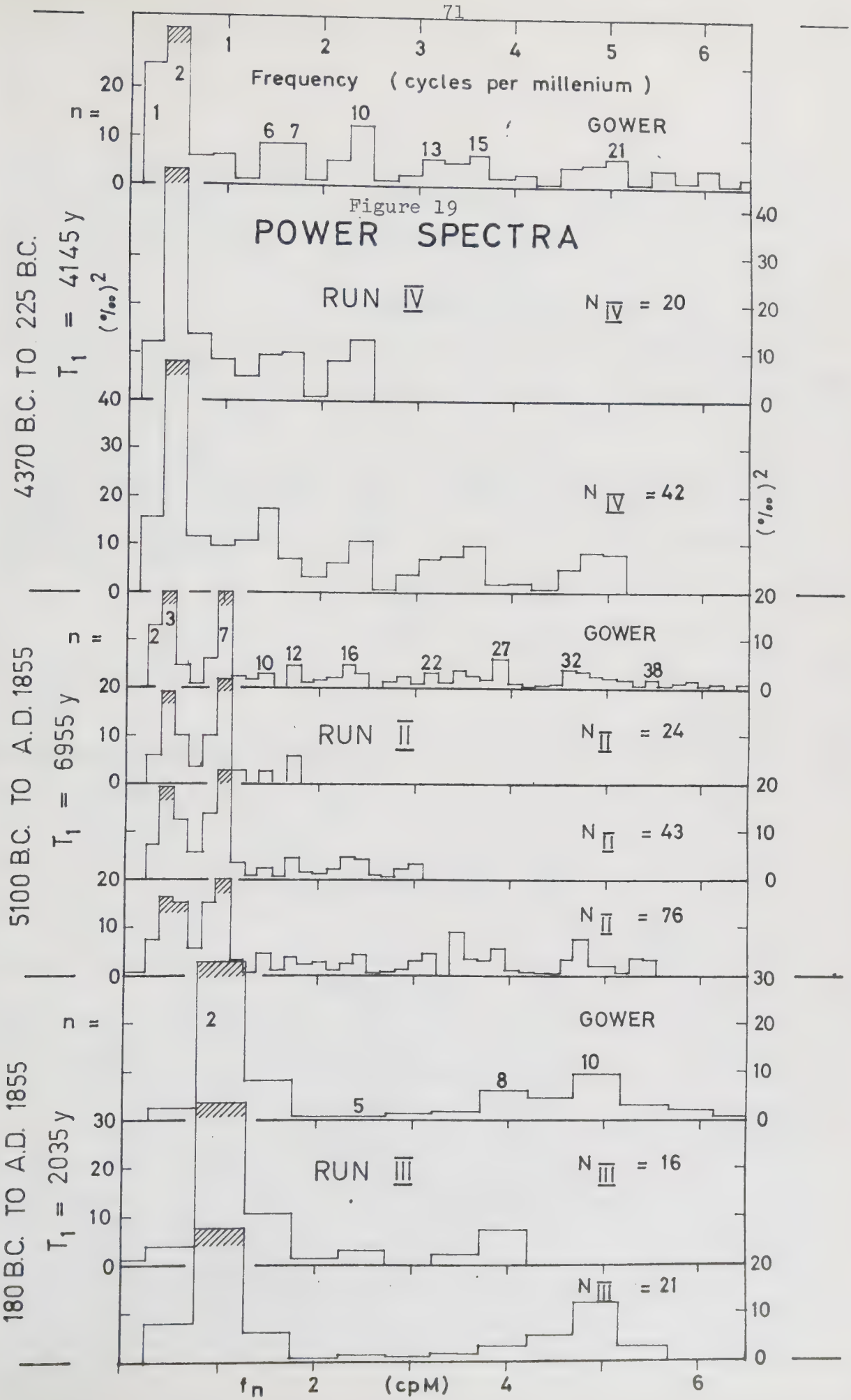
Frequency (cycles per millenium)
GOWER
Figure 19
POWER SPECTRA
RUN IV
N IV = 20
N IV = 42
4370 B.C. TO 225 B.C.
T1 = 4145 y
(‰)2
RUN II
N II = 24
N II = 43
N II = 76
5100 B.C. TO A.D. 1855
T1 = 6955 y
RUN III
N III = 16
N III = 21
180 B.C. TO A.D. 1855
T1 = 2035 y
fn
(cpM)

Table 7

Major Frequencies

Fourier Series

data section	n	f_n (cpM)	T_n (y)	n	f_n (cpM)	T_n (y)
run II	7	1.01 ±0.07	995 ±70	3	0.43 ±0.07	2320 ±380 ($^{-320}_{+460}$)
run III	2	0.98 ±0.24	1020 ±250 ($^{-200}_{+330}$)			
run IV				2	0.48 ±0.12	2070 ±510 ($^{-410}_{+1100}$)
II	1					[0.17 5900 y]
	2				0.42	2380
	3		[0.77	1300 y]		
	4	1.00	1000			
III	1		[0.72	1390 y]		
IV	1				0.43	2320
peak number		f	T		f	T

Fourier Integral

The frequency determination by the Fourier integral transform of such irregularly spaced data as this should not be accepted without some critical comment. In comparison with the Fourier series expansion of short data series, it has the advantage of finding values of the power at arbitrary frequencies. However, it gives far too much weight to individual measurements which are alone in large intervals of the data series, since some method of averaging in the intervals must be employed. Therefore, the Fourier series power spectra are at least of equal importance here in the frequency determination of physical periodicities.

The power spectrum was found by taking the Fourier transform of a function Z(t) which in some way represents the data w_i inside the measurement region of length T_1, and is equal to zero outside this region. The following form of the Fourier integral was used:

$$Z(t) = \int_0^{\infty} [c(\omega)\sin\omega t + d(\omega)\cos\omega t]d\omega$$

$$c(\omega) = \frac{1}{\pi} \int_{-T_1/2}^{+T_1/2} Z(t)\sin\omega t \, dt$$

$$d(\omega) = \frac{1}{\pi} \int_{-T_1/2}^{+T_1/2} Z(t)\cos\omega t \, dt$$

$$p^2(\omega) = c^2(\omega) + d^2(\omega)$$

The simplest and safest averaging method,

$$Z(t) = \frac{w_i + w_{i+1}}{2} \text{ , for } t_i < t < t_{i+1} \text{ , } i=0,1,2,\ldots,m-1,$$

was chosen since the results were found to be very similar to those from a few alternative methods. This simple average gives undue weight to lone data points since it is equivalent to weighting a measurement in proportion to the time interval between its two nearest neighbors. The resulting spectrum, at least for periods of the order of the largest interval length, is therefore certainly a distortion of the phenomenon's real spectrum.

The use of the finite interval T_1 in the integrals for $c(\omega)$ and $d(\omega)$, introduces side peaks in the power spectrum $p^2(\omega)$. For $z(t) = \sin 2\pi f_0 t$, the first side lobes are at the frequencies $f_\pm = f_0 \pm (3/2)/T_1$, and the ratio of peak heights is $p^2(f_\pm)/p^2(f_0) = 0.14$. For more general harmonic forms the result is not essentially different. The finite interval length, however, is not a prohibitive factor here.

The data series of length 7000 years, consisting of the original ΔC^{14} data was analysed for many sections of various lengths and starting points, only three of which are shown in figure 19. (The residual data C_i was also analysed, giving similar results above about 1 cpM.) In each case, the best linear fit to the original data, in the particular data section, was subtracted from this data before the analysis. The extremely large 5900 y peak (run II, figure 19) is certainly due to the 6077 y period sine wave, $\hat{C}_{ES}(t)$, found in Chapter II to be the best sine fitting the residual data, after the removal of the best exponential (almost linear) fit to the original data.

The second large Fourier transform peak, for run II at $\sim$0.42 cpM, is partly (at least 50 %) due to the side lobe (expected at about 0.38 cpM) of the large peak at 0.17 cpM (5900 y). On the other hand, this 0.42 peak is clearly repeated in run IV, whose largest peak at 0.43 cpM can of course not be a side lobe, and is clearly real. (No errors are quoted for the Fourier transform frequencies, but they are probably of the order of ±0.02 cpM, which will be used below.)

The major frequencies may be summarized as follows:

1. The complete ΔC^{14} data series is fitted well by a 10400 y period sine wave. The removal of the best linear trend from the data results in residual data which are best fit by a 6080 y period. The 7000 year span of these measurements is too short to give either of these periods very much significance outside of this interval.

2. There is a clear periodicity of about 2300 y or 2400 y: perhaps 2350 ±100 y (see table 7; these values are certainly better than the run IV value of 2070 ±570 y). This is seen in the complete and the ancient data, but not in the modern data, and is given by both Fourier series and integral spectra. Johnsen (1970) reports two periods, 400 y and 2400 y, in the long-term climatic record, as measured by the O^{18}/O^{16} ratio in a 100,000 y "long" ice core from Camp Century in Greenland.

3. The complete and the modern data show a strong Fourier series peak at about 1000 ±70 y. The Fourier transform seems to resolve this into two peaks at 1300 ±35 y, and 1000 ±20 y, in the complete data, and finds a 1390 ±40 y peak in the modern data. (The modern data seems to have a rather strange transform spectrum.)

The situation for higher frequencies is more problematical because the peaks are smaller, and because of the lack of agreement between the various spectra for many of the peaks.

There is little evidence for a period near 400 y in the modern data since Christ, but strong evidence in the older data before Christ. Since there has been some interest in this period, it will be discussed now in some detail.

The Fourier transform of the run IV data gives a strong peak for the period 425 y. The Fourier series spectra in run IV (n = 10) have relatively strong peaks at 415 ±20 y. In the complete data, the Fourier transform gives only a bump at about 415 y, while the Fourier series (N_{II} = 43) gives two small "peaks" at n = 16 and 17: 435 ±14 y, and 409 ±12 y. A series of data sections with roughly 2000 y lengths and successively shifted by 500 y was analysed by the Fourier transform, and confirmed the existence of an approximate 400 y period in some parts of the ancient data. A particularly large peak at a period of 446 y was found for the 2000 years starting at 3450 B.C.; strong peaks at 415 y were found both in the 3300 y long interval beginning at 4370 B.C., and in the 2000 years beginning at 2460 B.C. (these dates were rather arbitrarily chosen).

The remaining frequencies will not be discussed in detail. Figure 19 shows indications for the existence of some of the periods shown in Table 8. Values for stronger peaks have been underlined.

Table 8

Weak Peaks

	period (y)					
run IV	930	700	425	290	254	215
run II	980	710	435 409	290	260	211
run III			407	303	255	200

The other spectra confirm these values to varying degrees. In particular, a period of about 210 y seems to be present over the whole length of the measurements.

CHAPTER IV THE PRODUCTION RATE OF RADIOCARBON

Introduction

The general success of the radiocarbon dating method indicates that the radiocarbon production rate has been constant to a good first approximation over at least a few mean lives of C^{14}. It also means that the factors influencing the distribution of radiocarbon throughout the various carbon reservoirs have also remained essentially constant. The deviations from constancy of these two classes of causal factors have resulted in the observed variations in the radiocarbon concentration in the atmosphere over the last 7000 years. These deviations have a large-scale amplitude of about 5 % over this period. Superimposed on this large-scale trend are variations at higher frequencies (predominately, and approximately, 1000 y and 400 y periods) with amplitudes of the order of 2 or 3 %.

A variable production rate is very probably responsible for the observed long-term ΔC^{14} trend, and also for some portion of the higher frequency behaviour. This chapter will therefore concentrate on the production rate, both because of its importance, and because its influence on the atmospheric C^{14} concentration can be described by models which are simpler and whose parameters are better known, than those relating ΔC^{14} to the climatic factors. Of primary importance is the changing magnetic field strength of the earth, which modulates the cosmic-ray flux entering the atmosphere (Elsasser *et al.*, 1956).

The problem of identifying the correct causal factors for the various components of the radiocarbon variations has been approached by deducing theoretical C^{14} concentrations from the past history of the various possible causal factors. These include those factors which influence the production rate [modulation by the magnetic fields of the earth and the solar plasma, and variations in the galactic and solar components of the cosmic-ray flux before such modulation], and those factors which influence the distribution of carbon throughout the various exchangeable reservoirs [climatic influence on the reservoir sizes (temperature), and on the exchange rates ("storminess")].

In this chapter the reverse approach is used. Variations of the C^{14} production rates are deduced from the variations of the C^{14} concentration, under the assumption that the climatic factors are constant. The deductions are based on the variation of atmospheric radiocarbon, as reflected by the bristlecone pine ΔC^{14} measurements of Suess, and using the analytical functions of time which have been found to represent these measurements, and which must be used in this treatment instead of the data itself, because otherwise it would be necessary to solve an integral equation for Q(t).

The deduction of the production rate is made by means of a 2-reservoir model of the atmospheric and oceanic carbon systems, under the assumption of constant reservoir sizes and transfer rates. Various models have been used to describe the distribution of C^{14} on the earth after its production in the upper atmosphere. The main feature of this distribution is the delay, of the order of 30 years (Suess, 1954a), between the time of production and the time of exit to the oceans, which compromise the largest carbon reservoir in the context of radiocarbon, and in which most of the radioactive decay takes place. The two parameters describing this main feature are the ratio ν between the amount of C^{12} in the oceans and the amount in the atmosphere; and the residence time T_{as} of C^{12} in the atmosphere, defined as the mean time which a C^{12} atom spends in the atmosphere after its production and before its transfer to the sea.

Various values of the two parameters in the 2-reservoir model have been used, in order to investigate their influence on the production rate. The values $\nu \simeq 30$, and $T^* = 50$ y (and 30 y) were finally chosen. The more complex 3-reservoir model, which includes an upper and lower ocean, is also investigated, and is related to the 2-reservoir model. These two models are found equivalent in their predictions connecting a variable production rate with a variable atmospheric C^{14} concentration. Relationships, which are necessary for the equivalence of the models, are found between the parameters of the two models. These relationships aid in the interpretation of a parameter choice, and perhaps also in making this choice.

The theoretical C^{14} production rates found below can be compared with production rates deduced from the paleomagnetic data, or from other available evidence, in order to judge which parts of the C^{14} variations are due to a changing production rate, and which parts are not. Where agreement, within the various large uncertainties, is not found, additional or alternative causal factors or models may be sought.

The resulting production rate functions, although found by assuming all other causal factors constant, may themselves be interpreted as a test of this hypothesis, and perhaps also of the model. Oeschger has pointed out (Oeschger et al., 1970) that if one regards the atmosphere as a simple 1-reservoir system, there is a symmetry between source and sink, both being "production rates", but having opposite signs. To the extent that there is little feed-back of C^{14} from the oceans, this idea may be applied to the results found from a 2-reservoir model, in spite of the fact that the model automatically takes into account the transfer of C^{14} in both directions. In this view, the production rates found here may be net effective production rates, and therefore already include those parts of the climatic effects which influence C^{14} transfer rates, although not reservoir sizes. Damon (1970) explains the discrepancy between the observed relative phase, of the order of 10^2 y, between paleomagnetic production rates and $\Delta C^{14}(t)$, and the 2-reservoir prediction of the order of 10^3 y, by observing that this model allows more C^{14} feed-back to the atmosphere than occurs in reality.

The use of Argon-39 has been suggested for the purpose of determining the behaviour of the C^{14} production rate as a function of its various causal factors, since it does not participate, as does radiocarbon, in the complex distribution into reservoirs other than the atmosphere (Loosli and Oeschger, 1968; Oeschger et al., 1970).

Appendix B is devoted to the mathematical description of the 2- and 3-reservoir models. It gives the differential equations of the models and solutions of these equations; two relations between their respective parameter sets; and the solutions for $\Delta C^{14}(t)$ or for $Q(t)$, one in terms of the other, in the case that the known function is a series of harmonic terms. Equation numbers prefaced by "B" refer to this appendix.

2- and 3-reservoir models

For the particular purpose of relating fluctuations in the C^{14} production rate to fluctuations in the atmospheric C^{14} concentration, a 2-reservoir model is completely adequate, since it contains the two essential points of (1) a non-zero average delay between the production of a C^{14} atom and the time it leaves the atmospheric reservoir, which (2) is much smaller than the large oceanic reservoir into which it is transfered. The total C^{14} produced per year is about ⅟8000 times the total C^{14} inventory (more precisely, ⅟8270). Fluctuations in this production, on a time scale shorter than about 8000 y, will have only an extremely small effect on the world-average C^{14} concentration of the total exchangeable carbon. However, on a small portion of the total exchangeable carbon, the effect will be much greater, provided that a C^{14} atom, produced in this portion, does not immediately leave this reservoir, i.e. in a time short compared with the period of fluctuation.

It was recognized by Suess (1954a) that this situation could be sufficiently well described mathematically by assuming the existence of two homogeneous reservoirs of carbon. It was pointed out that such a description is valid even when dealing with reservoirs which are in reality not homogeneous (Bien et al., 1963), because the two homogeneous reservoirs may always be chosen to take this inhomogeneity into account. He estimated the residence time in the atmosphere (average delay time) as being about 30 y, and resisted attempts to lower this figure in spite of indications that made this appear necessary (Craig, 1957b; Bainbridge, 1963; Dockins, et al., 1967).

The present state of knowledge of the distribution and transfer of carbon in the exchangeable systems is still insufficient to improve appreciably the predictions of the 2-reservoir model. Nevertheless, it is tempting to incorporate new values of parameters into the more complex models, as these values become available through the analysis of various phenomona of transfer between reservoirs and through increasing oceanographic knowledge. For example in the 3-reservoir model, the transfer time from the atmosphere to the mixed ocean layer is probably closer to 10 y than the 30 y of the 2-reservoir model (Revelle and Suess, 1957; Craig, 1957b). There still remain, however, other parameters in the more complex models, which have uncertainties at least as large as those in the original simpler model, so that the prediction of the former models will not necessarily be more accurate.

An appropriately chosen 2-reservoir model can always lead to essentially the same result for C^{14} variations, as a particular three reservoir model, which may correspond more closely to the true situation. This was tested here by investigating the relationships between their effective parameters.

We consider both 2- and 3-reservoir models, the latter including a continuous variable β, which describes the extent of direct exchange between the atmosphere and the deep oceans, being zero for a "chain" model, and non-zero for a "cyclic" model (Craig, 1963). The 2-reservoir model consists of an "effective" atmosphere and an "effective" ocean (indices, j=a, for atmosphere, and j=s, for sea, will be used for the 2-reservoir model). The 3-reservoir model consists of the atmosphere; the mixed, upper layer of the ocean above the thermocline (top 75 m); and the deep ocean (indices i=1,2,3, respectively, will be used for these reservoirs). Other reservoirs such as the biosphere and the humus may be considered as part of an overall effective upper reservoir.

The C^{14} and C^{12} contents of these reservoirs, in atoms per cm^2 of the earth's surface, are $X_i(t)$ and Y_i, and the C^{14} concentrations are $R_i = X_i/Y_i$. The constant ratios of C^{12} in the various reservoirs to the C^{12} in the upper reservoir are $\nu = Y_s/Y_a$, and $\nu_i = Y_i/Y_1$. The atmospheric production rate of C^{14} averaged over the earth is Q(t), and the rate of sedimentation of C^{14} out of the sea is S; both are in C^{14} atoms/$(sec \cdot cm^2)$, and S is assumed constant. Lingenfelter and Ramaty (1970) find a lower limit for S of 0.16 $cm^{-2}sec^{-1}$. They give values for the production rate of Q (solar minimum, 1953-54) = (2.42 ±0.48) $cm^{-2}sec^{-1}$; and Q (solar maximum, 1957-58) = (1.93 ±0.39) $cm^{-2}sec^{-1}$. The influence of S is small, and enters into the solutions for $\Delta R_i/R_{i0}$, only in the form of a factor times the solution for S=0 (see equation B17). It therefore may enter the argument at any point, and can be assumed zero here. The possible effects on R_i of changing reservoir sizes and transfer rates are related to the climate, and are not treated here (see e.g., Houtermans, 1966; Lal and Venkatavaradan, 1970; and Damon, 1970).

All the reservoirs are assumed to be in exchange with each other (unless β=0), and to be well-mixed. Although the latter assumption is known to be wrong at least for the deep oceans, the resulting simplification may nevertheless provide an adequate description of the radiocarbon distribution for the purpose of predicting production rate variations. The validity of this and other assumptions of these models may themselves depend to some extent on the frequency of these variations.

The rates of exchange of carbon between the various reservoirs are assumed to be proportional to the rate constants $k_{uv} = 1/T_{uv}$, where T_{uv} is the residence time in reservoir u with respect to removal (of C^{12} or C^{14}) to reservoir v. It is defined as the mean time that an atom spends in reservoir u before it is transfered to reservoir v. Differences between k_{uv} for C^{12} and for C^{14}, due both to their mass difference and to radioactive decay, can be neglected in the present context. The low concentrations of carbon allow the use of first order removal rates from reservoir u to reservoir v, equal to $k_{uv}Y_u$ and $k_{uv}X_u$, for C^{12} and C^{14}, respectively. In both models an individual equilibrium is assumed between each pair of reservoirs which exchange carbon. This leads to the equations B1, relating the residence times, reservoir ratios, and β. The mean life of C^{14} is $\tau = 8267$ y, and the decay constant is $\lambda = 1/\tau$. The differential equations for the two models are given in Appendix B (B2 and B20).

The 2-reservoir model has 2 independent parameters: the ratio ν between the effective atmospheric and oceanic reservoirs; and the effective atmospheric residence time T_{as}, which may be replaced by the alternative parameter T^* (Wood and Libby, 1964). [$T^* = 1/\lambda^* = 1/(\lambda + k_{as} + k_{sa})$, is only a few per cent smaller than T_{as}.] The 2-reservoir predictions of $\Delta C^{14}(t)$ from Q(t), or <u>vice-versa</u>, will be approximately correct when these parameters take their best values. It is easy to see that the best value for ν must lie between 30 and 60, corresponding to the inclusion or exclusion of the mixed layer in the "atmosphere". The situation is not so clear with respect to the effective atmospheric residence time T_{as}. Values between about 3 y and 50 y have been used in various contexts. It should not be confused with the smaller residence time T_{12} of the 3-reservoir model.

Of the 5 parameters in the 3-reservoir model (S can be ignored in comparing the models), ν_2 and ν_3 can be taken as well-known [e.g., $\nu_2 = 1.2$, and $\nu_3 = 58.3$: Craig (1963)]. The remaining three independent parameters may be taken to be the residence time T_{12} (atmosphere to mixed layer); the residence time T_{32} (deep ocean to mixed layer); and the parameter β, which describes the extent to which the atmosphere and deep ocean are in direct exchange. [$\beta = T_{12}/T_{13}$.]

To investigate the relationships between the 2-reservoir and the 3-reservoir models, it is postulated that they must both make the same predictions for the case of a constant production rate. The two models must both give the same C^{14} concentration in the atmosphere, and the same concentration in the deep ocean. This provides two equations (B24) between the two sets of model parameters, which may be used, for example, either to express ν and T^* in terms of the five 3-reservoir model parameters, or to

express two of the latter in terms of other parameters. Equations B25 to B31 show some of the possible relations. Values for the 3-reservoir ratios of reservoir sizes: ν_2 = mixed layer/atmosphere = 1.2, and ν_3 = deep ocean/atmosphere = 58.3, have been taken from Craig (1963).

The 2-reservoir ratio ν, is almost independent of the 3-reservoir parameter β, and varies only with the ratio T_{12}/T_{32}, i.e. the ratio of atmospheric residence time to deep-sea residence time (both with respect to the mixed layer). The relationship is such that, for example, the fraction ε of the mixed layer, which is included in the effective atmosphere of the 2-reservoir model, is ½ when $T_{32} = (\nu_2+\nu_3)T_{12}$ (equations B25 and B26), and this corresponds to ν = 37. For T_{12}/T_{32} less than the reasonable limit of about 10/500, ν is less than about 40, and this would narrow somewhat the range (30 to 60) previously used for this effective parameter. Figure 20 shows ν as a function of the ratio T_{12}/T_{32}.

The second relation, as given in equation B29, is between, on the one hand, the ratio T_{32}/T_{12} (related to ν as above), and, on the other hand, β and the ratio T^*/T_{12}, of the upper reservoir residence times (with respect to the next lower ones) in the two models. For β=0 (Craig's chain model), this becomes an equation (B31) for T^*, linear in T_{12} and T_{32}, which says that T^* is the same as T_{12} plus 36 y for every 1000 y of deep-sea residence time T_{32}. Figure 20 shows this for T_{12} = 5, 10, and 15 y. In addition, curves for β = 0.15 and β = 0.3 are shown for these values of T_{12}.

Thus the above assumptions (for constant production rate) of equal concentrations in those reservoirs of the two models which must correspond to each other, enables a value of one parameter to be interpreted as particular values of other parameters, in the other model. For example, if T_{12} is fixed [the value T_{12}= 7 y is used below in all the production rate calculations (Craig, 1963)] then the choice of T_{32} determines both of the 2-reservoir model parameters, T^* and ν; or if T^* is fixed both ν and T_{32} are determined. (Here β is assumed known.)

The effect of increasing β from 0, is to decrease T^* from its maximum value, for a given T_{32}. The parameter β is equated by Craig (1963) to the ratio of ocean area where there is no thermocline separating a mixed layer from the deep sea, to the area where there is a thermocline. The value β = ⅓, corresponds to the latter area lying between ±45° lattitude. This value may be too large if, for example, a non-zero β be viewed as a consequence only of an Antarctic up-welling.

If the production rate is not constant, the equations (B16 and B22) of the reservoir models give the C^{14} concentration in terms of integrals of the production rate times exponential factors whose decay constants are the radioactive decay constant λ, and the rate constants $1/T^*$ (2-reservoir model), or $\lambda_0 \pm \alpha$ (3-reservoir model; see equation B9). If the production rate can be derived from measurements of factors other than C^{14} (for example solar activity, magnetic field of the earth, etc.) then these functions may be integrated, using some integral approximation, to find a theoretical C^{14} concentration, which may be compared to the measured concentration. On the other hand, if a theoretical production rate is to be deduced from the C^{14} measurements (which are much more precise than the measurements of the other factors), then it is necessary to first express these C^{14} data as a harmonic function, since the equations cannot be solved explicitly for Q(t). In Appendix B the attenuation factors are found which relate the coefficients of sines and cosines occuring in $\Delta C^{14}(t)$ to those occuring in Q(t).

Using the above relationships between the parameters of the two models (for the case of constant production rate), it was found that the two models are essentially equivalent for a varying production rate over the important frequency range between 0 and about one cycle per 100 y. In the relatively unimportant range above this frequency, the attenuation factor of the 2-reservoir model is about a factor of 2 greater than that of the 3-reservoir model.

The equivalence of the two models may be seen in figures 21 and 22. The former shows the power spectrum of the $\Delta C^{14}(t)$ approximation function for run II (the complete data series) with cut-off degree N = 43 (smallest period T_{22} = 316 y); and the power spectra of two production rates, Q(t), derived from it using the attenuation factors of the two different models. The 2-reservoir model case has parameters of T^* = 50 y and ν = 30; and the 3-reservoir case has parameters of β = 0, T_{12} = 10 y, and T_{32} = 1000 y. The latter parameters correspond to T^* = 46 y and ν = 33.5, but this 2-reservoir case is not shown, because it is practically identical to the 3-reservoir case. This figure shows the essential equivalence of the attenuation factors and production rates predicted by the two models. This equivalence is verified by figure 22, which shows a section of the resulting production rates as functions of time (between 2000 and 3000 B.C.), together with the $\Delta C^{14}(t)$ function. The agreement is much closer if the correct corresponding parameters are used. The large-scale, 10400 y period sine wave of ΔC^{14} and of ΔQ are also shown. The latter is the same for the two models.

For $\beta = 0$, and $T_{12} = 10$ y, $T^* = 50$ y corresponds to $T_{32} = 1100$ y; and $T^* \simeq 30$ y corresponds to $T_{32} = 550$ y; while for $\beta = 0.15$, and the same $T_{12} = 10$ y, these T^* values correspond to the higher T_{32} values of 2050 y and 850 y, respectively. Values for these parameters used recently by various authors are underlined in table 9, which gives examples of the approximate corresponding parameters in the model other than the one used by the author ($T_{12} = 5$ y is used for this illustration).

Table 9

Parameter values

	β	T_{32} (y)	T_{12} (y)	T^* (y)	ν
Lal and Venkatavaradan (1970)	0	1350	5	54	29
	0.15	1350	5	30	29
Damon (1970)	0	1200	5	48	30
	0.15	4250	5	48	27
Lingenfelter and Ramaty (1970)	0	550	5	25	33
	0.15	1025	5	25	30
	(perhaps 50?)		5		60

According to this picture, in order to have ν appreciably larger than 40, it is necessary to take absurdly small deep-sea residence times, and therefore the effective atmosphere must include not less than about one half of the mixed layer of the ocean. The independent implication for T^* is that it is probably not smaller than about 30 y, and could well be higher. This means that the attenuation factor (equation B33 gives the inverse attenuation factor), or ratio between the production rate's oscillation amplitude, and that of the C^{14} concentration, can be as much as a factor of 3 less than those attenuation factors corresponding to values of T^* of 10 or 20 y, which have occasionally been used (Houtermans, 1966). This would be of help, for example, in explaining the amplitude of the de Vries effect in terms of variations in sunspot number. Until now, the production rate amplitude, required to explain the approximate 1 % amplitude of the two ΔC^{14} peaks at 1500 and 1700 A.D., were a factor of 2 or 3 greater than the amplitude of the corresponding frequency variation in sunspot numbers, which are an indication of solar activity and the consequent magnetic shielding of cosmic-rays, and which agree in phase and period with the required production rate.

The equivalence between the two models can be summarized as follows. A 2-reservoir model can always be found which will give the same description as a particular 3-reservoir model, of how the atmospheric C^{14} concentration reacts to a variable production rate, at least for the important frequencies below about 1 cycle per 100 y. This can be done by equating C^{14} concentrations in reservoirs of one model with concentrations in corresponding reservoirs of the other model, for the case of a constant production rate. The two parameters ν and T^* of the 2-reservoir model are thereby related to the three parameters β, T_{12} and T_{32} of the 3-reservoir model (considering ν_2 and ν_3 to be fixed). The ratio T_{12}/T_{32} determines ν; and any set of 3 parameters [except the set (T_{12}, T_{32}, ν)] determines the other 2 parameters. For example, the three 3-reservoir parameters determine the two 2-reservoir parameters; or β, T_{12} and T^* determine T_{32} and ν.

This latter approach was used here: the value T_{12} = 7 y was taken from Craig (1963), and values of β and T^* were assumed which correspond, according to figure 20, to reasonable values of the 3-reservoir deep-sea residence time T_{32}. For β=0, the range of T^* between about 30 y and 50 y corresponds to T_{32} lying between about 500 y and 1000 y, which is a reasonable range for the deep-sea residence time (Craig, 1963). As seen in table 9, T^* = 50 y agrees with both Damon's (1970) 2-reservoir choice, and the 3-reservoir choice of T_{32} of Lal and Venkatavaradan (1970). For β=0.15, T^*= 50 y corresponds to the somewhat high value of about 2800 y for T_{32}, whereas T^*= 30 y corresponds to T_{32} = 1100 y.

The production rates presented below were calculated using a 2-reservoir model with T_{12} = 7 y, β=0, and T^*= 30 y and 50 y, thus determining ν for the calculation. T_{32} is also determined, and was used to find the 3-reservoir model production rates, which, as shown above, were essentially the same. Values of corresponding parameters are listed in table 10, which, as is described below, also gives numbers for the resulting production rate functions.

FIGURE CAPTIONS

Figure 20 MODEL RELATIONS page 89

Relationships are shown between the two parameters ν and T^* of the 2-reservoir model, and the three parameters β, T_{12} and T_{32} of the 3-reservoir model ($\nu_2 = 1.2$ and $\nu_3 = 58.3$ are assumed fixed). Upper picture: the 2-reservoir ratio ν (oceanic to atmospheric carbon ratio) vs. the 3-reservoir ratio T_{12}/T_{32} of residence times in the atmosphere, T_{12}, and in the deep-ocean, T_{32}, with respect to the mixed layer. Lower picture: the 3-reservoir deep-ocean residence time T_{32} vs. the 2-reservoir atmospheric residence time $T^* \simeq T_{as}$; each curve is labeled with two 3-reservoir parameters: $\beta = T_{12}/T_{13}$, and the atmosphere-to-mixed layer residence time T_{12}.

Figure 21 PRODUCTION RATE POWER SPECTRA page 90

Power spectra are shown of two C^{14} production rates, deduced from the same approximation function of the atmospheric C^{14} concentration, by using a 2-reservoir model (solid line) and a 3-reservoir model (dashed line). Scales are shown for both frequency (cycles per 10^3 y), and frequency number. The ΔC^{14} power spectrum (positive and negative steeples) is also shown. It is from Run II ($T_1 = 6955$ y), and has cut-off degree N=43 ($T_n = 316$ y; see Chapter III). The power scale is at the left. The production rates were found using: (1) a 2-reservoir model with T^* and ν as shown; and (2) a 3-reservoir model with β, T_{12} and T_{32} as shown. The latter corresponds (see figure 20) to the indicated values of T^* and ν, the use of which in a 2-reservoir model gives closer agreement than shown here between these two production rate spectra. Inverse attenuation factors are plotted for these two cases.

FIGURE CAPTIONS

Figure 22 COMPARISON OF MODELS page 91

A 1000 year portion is shown of the time dependences of the ΔC^{14} approximation function with $N_{II} = 43$; and the two production rates deduced from it by using 2-reservoir and 3-reservoir models which almost correspond to each other. The agreement is closer if the correct corresponding parameters are used (see explanation of figure 21). The ΔC^{14}, 10,400 y period sine wave $\hat{C}_S$, and the two (identical) production rate sine waves $\hat{Q}_S$, are also shown. The scale is in per cent.

Figure 23 LARGE-SCALE PRODUCTION RATE TRENDS page 92

Four production rate sine waves, $\hat{Q}_{S_i}(t)$ (equation 1) with a 10,400 y period are shown. They are deduced from the ΔC^{14} sine wave $\hat{C}_S(t)$ (equation 1, Chapter I) using a 2-reservoir model with the indicated parameter values. Except in the first case (solid line), the value of the ratio ν is determined from the correspondence with a 3-reservoir model, using $\beta=0$, $T_{12}= 7$ y, and the indicated values of T^*. Table 10 gives the corresponding values of T_{32}, the attenuation factors, and the phase relative to ΔC^{14}.

Also shown are the exponential production rate $\hat{Q}_E(t)$ (equation 4; $\tau = 67{,}000$ y) which is deduced from the ΔC^{14} function $\hat{C}_E(t)$ (equation 2; not shown); and the production rate of the exponential plus 6077 y period sine wave $\hat{Q}_{ES}$ (equation 3) which is deduced from the ΔC^{14} function $\hat{C}_{ES}$ (equation 2; also not shown).

The data points are production rate values (per cent deviations) derived from the indicated sources of paleomagnetic measurements of the earth's dipole moment (see text).

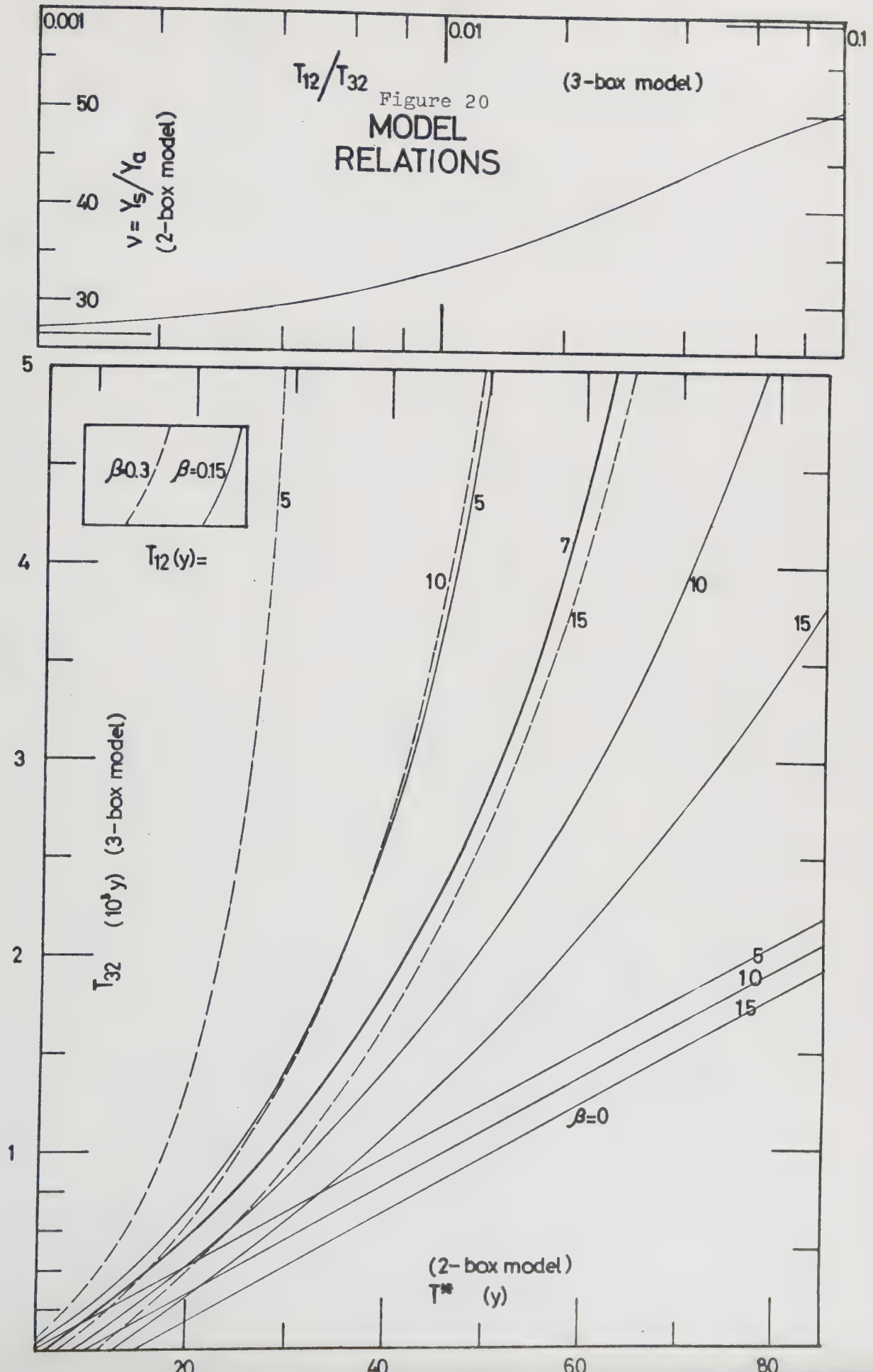

Figure 20
MODEL RELATIONS

Figure 21

Production Rate Power Spectra

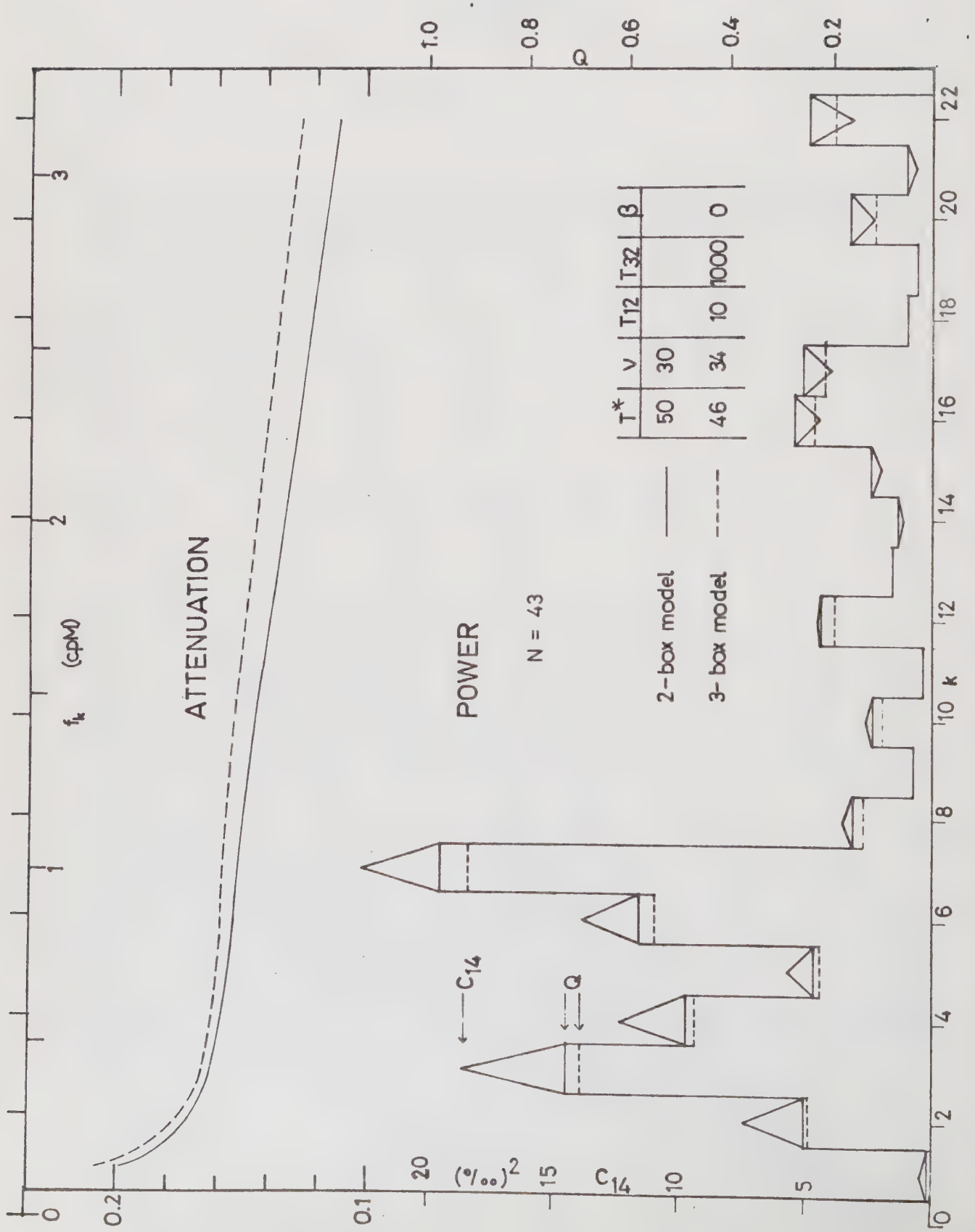

Figure 22

Comparison of Models

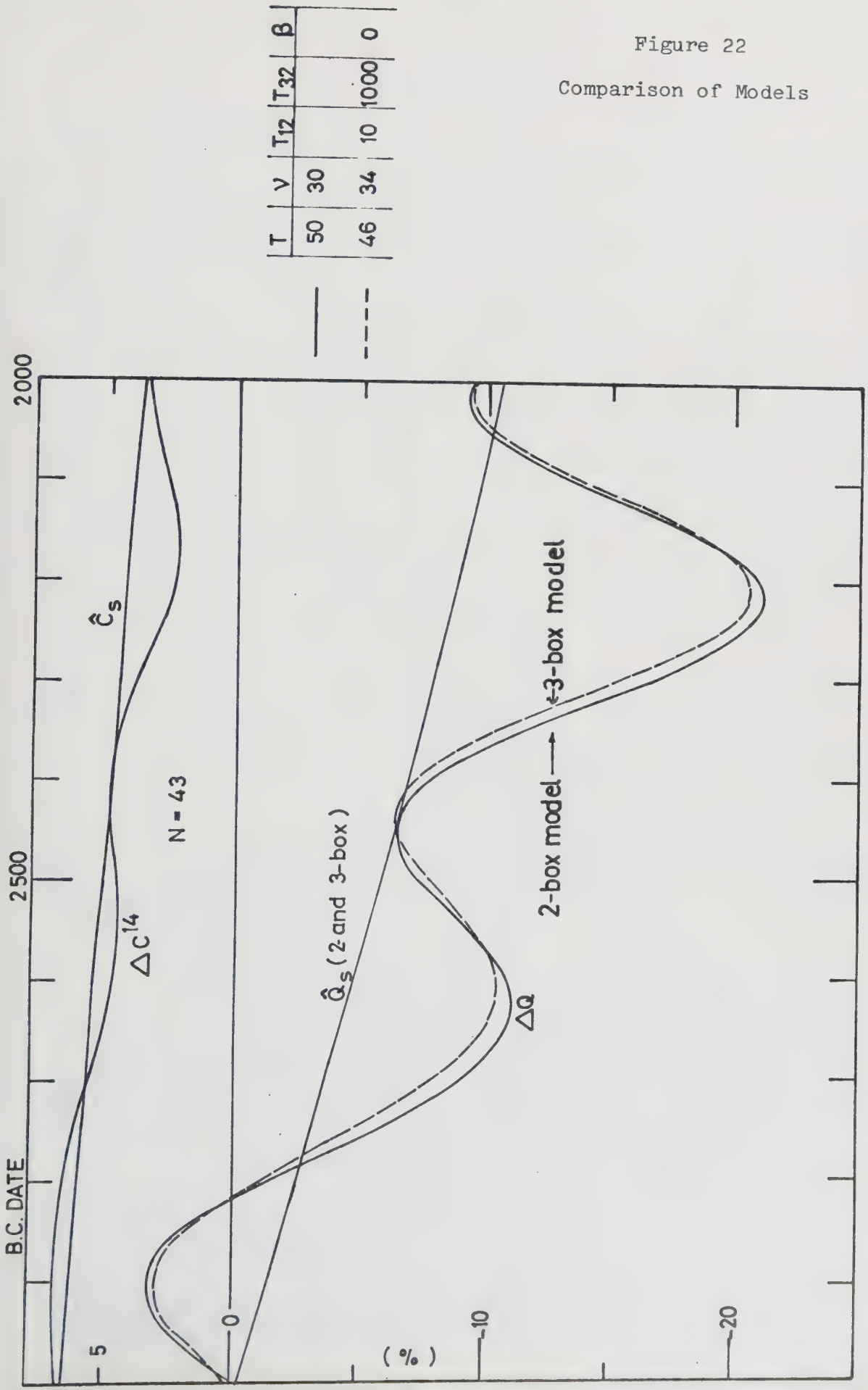

Figure 23

Large-Scale Production Rate Trends

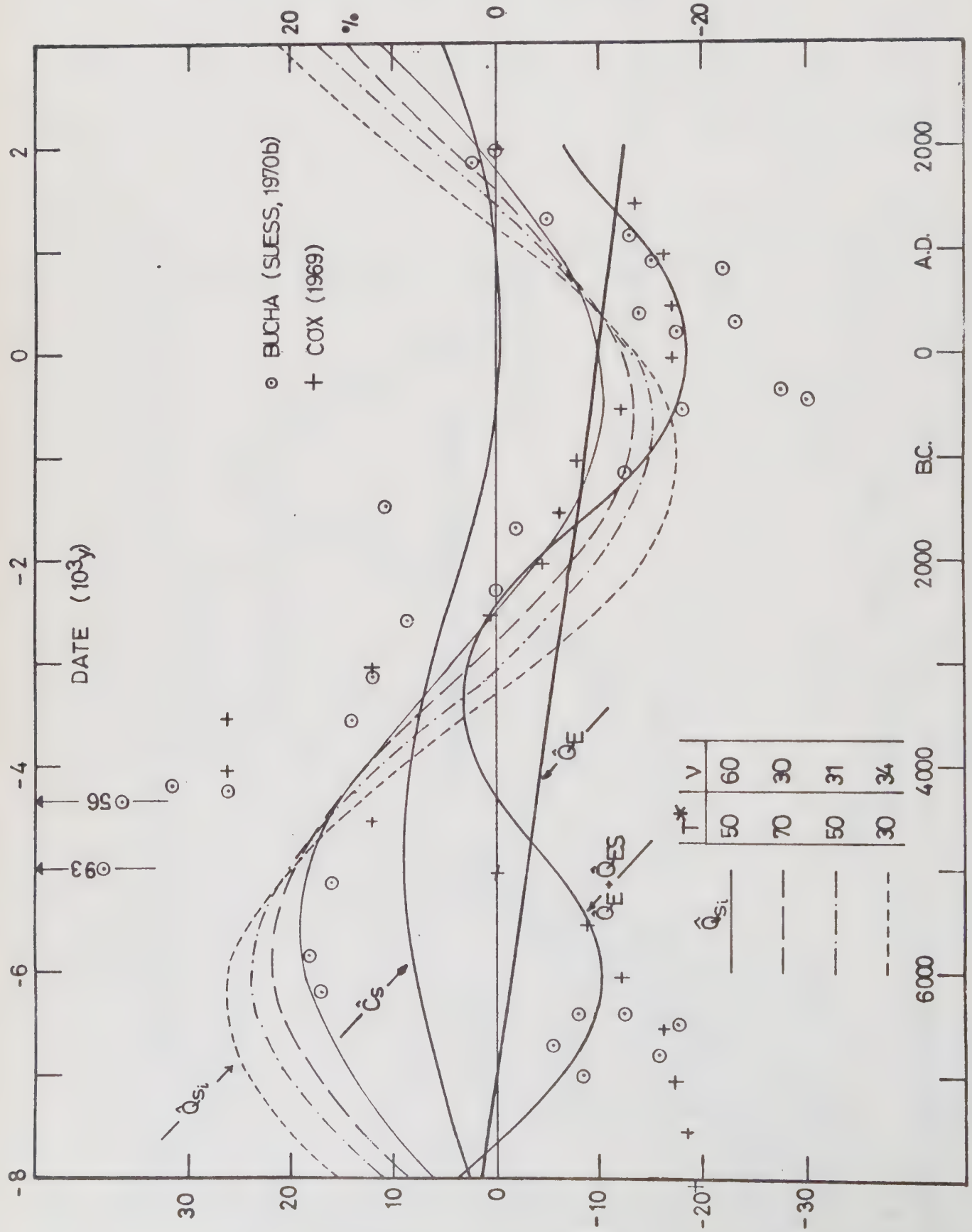

Finding production rates

Whereas the deduction of a theoretical ΔC^{14} function from a given production rate Q(t) may be made by simply integrating Q(t) times a function of the time before t, the reverse deduction of a theoretical production rate from a given $\Delta C^{14}(t)$ function involves solving an integral equation for Q(t). This may be avoided by expressing both functions as harmonic series, because the frequency is not altered by the transformation from Q to ΔC^{14}, or from ΔC^{14} to Q. If the production rate is known as a series of sine and cosine terms of various frequencies, then the C^{14} concentration in a reservoir of the model may be found as a series of the same harmonic terms but with different coefficients, such that the phase is altered, and the amplitude of the C^{14} variation is smaller than that of the production rate. The relationships between the coefficients in one series and those in the other are given in equation B32 of Appendix B. Here these relationships are used to derive the harmonic coefficients of Q(t) from the coefficients of $\Delta C^{14}(t)$ which have been found in the preceeding chapters.

One advantage of proceeding in this direction (from ΔC^{14} to Q), rather than in the reverse direction, is that the ΔC^{14} function is much more accurately known than the production rate. The latter can be deduced only rather roughly from the factors influencing the cosmic-ray flux and the magnetic shielding thereof. These factors include the 200 years of sunspot records; records of super-novae (used by Lingenfelter and Ramaty, 1970); and the earth's magnetic field strength in the past (Bucha, 1970). None of these can as yet approach both the detail of variation and the length of the ΔC^{14} record.

A second advantage in deducing Q(t) from $\Delta C^{14}(t)$ is that the lack of knowledge of the C^{14} concentration before some earliest date is of less importance, than is the lack of knowledge of Q(t) before an earliest date for the reverse deduction. The uncertainty introduced into a theoretical ΔC^{14} curve due to the unknown past portion of the Q(t) record, is expressed by Lingenfelter and Ramaty (1970) in terms of one unknown parameter, the ratio between the present production and decay rates of C^{14} in the total carbon reservoir. If the present production rate were known this uncertainty would disappear. On the other hand, in deducing Q(t) from $\Delta C^{14}(t)$, the same parameter may be introduced, but the fact that it is unknown means only that the absolute value of Q(t) is unknown, while the relative variation of Q(t) is unaffected by this fact. Therefore the theoretical production rate curves may be found

by assuming that the harmonic series approximating the ΔC^{14} data extends to minus infinity, and the error introduced is limited to only the first few hundred years after the earliest data point, during which the transient term (or terms) with the short time constant, equal to the atmospheric residence time, have not yet disappeared.

Large-scale trends in Q

The per mil deviation, $\hat{Q}_S(t)$, of the theoretical production rate which would be necessary to account for the 10,400 y period ΔC^{14} sine wave $\hat{C}_S(t)$ (equation 1, Chapter I), was found by the method described here, and using the equations of Appendix B. The sets of 2-reservoir parameters listed in table 10 were used in a 2-reservoir model, and some of the resulting production rates, $\hat{Q}_S(t)$, are shown in figures 23, 24 and 27, as indicated in the table. As described above, the production rates were essentially the same as those found from a 3-reservoir model by using the corresponding 3-reservoir parameters, also shown in table 10. This table also gives the inverse attenuation factor H, and the relative phase Δt, in years, for a 10,400 y period oscillation; and the amplitude, in per mil, of the production rate variation, which is A = 49.7/H ‰, where 49.7 ‰ is the large-scale ΔC^{14} amplitude. The per mil deviation of the large-scale production rate is given by

$$\hat{Q}_S(t) = 42.7 + A \cdot \sin\left[\frac{2\pi}{10402}(t + 7388 + \Delta t)\right] \text{ ‰} . \qquad (1)$$

Table 10

Parameters of Reservoir Models and of Production Rate Sine Waves

T_{12} (y)	β	T^* (y)	ν	T_{32} (y)	(period = 10,400 y) H	Δt (y)	A (‰)	Figure number
1 -	-	50	60	-	0.330	780	151	23
2 7	0	70	29.8	1735	0.283	1010	175	23
3 7	0	50	31.1	1185	0.253	1190	196	23/24/27
4 7	0	30	34.1	635	0.225	1450	221	23/24
5 7	0.15	30	31.4	1092	0.222	1490	224	--

This table and figure 23 show that the predicted production rates lead the ΔC^{14} sine wave by times between about 800 and 1500 years, and have amplitudes greater than the ΔC^{14} amplitude by factors between about 3 and 4.5. For the cases shown, the production rate's amplitude must be from about 15 % to 22 %, in order to account for the 5 % ΔC^{14} amplitude. The phase difference between Q and ΔC^{14} is smaller for larger deep-sea residence times, T_{32}; for larger atmospheric residence times, T^*; or for larger atmosphere/ocean carbon ratios, ν; although these influences are not unrelated.

The data points shown in the figures, with these theoretical production rate curves, are values of the production rate (in per mil deviations from the present production rate) which are derived from measurements of the earth's past magnetic dipole moment, f(t). Values of the production rate are from (Bucha, 1967), as found in (Suess, 1970b). Additional values were derived from values of f(t) summarized by Cox (1969), as found in (Lingenfelter and Ramaty, 1970). The points shown are $[(f/f_0)^{-0.52}-1]\cdot 1000$, where f_0 is the present value of the dipole moment ($8.0\cdot 10^{25}$ gauss cm^3); and the exponent (-0.52) is from the relation found by Elsasser and co-workers (1956) between the dipole moment and the world average production rate (see also Kigoshi and Hasegawa, 1966; and Ramaty, 1967).

The agreement between the magnetic production rate data and the production rate curves derived from the ΔC^{14} sine wave is in general quite good, as has been shown before by others (Bucha and Neustupny, 1967; Suess, 1970b; Damon, 1970; Lingenfelter and Ramaty, 1970). There is some question of the accuracy of the dates of the magnetic data, especially of the older ones, since these dates are themselves sometimes uncorrected C^{14}-dates. Suess, however, has applied the necessary corrections based on his C^{14} calibration curve.

Damon [1970; see also the discussion in (Suess, 1970b)] maintains that the relative phase between the measured ΔC^{14} and the theoretical ΔC^{14}, derived through reservoir models which use a production rate found from the magnetic data, is of the order of 10^3 y (as is confirmed here); and that this is larger by a factor of 10 than the observed relative phase between the ΔC^{14} data and the magnetic dipole production rate data. Bucha (1970) observes a relative phase of zero between his data and the ΔC^{14} data. Suess (1970b) finds no phase discrepancy. He uses the production rate data derived from the magnetic data (Buch, 1967), which is shown here; finds a sine wave fitting this data best, and having an 8000 y period; and then transforms this sine wave to a ΔC^{14} sine wave of the same period, with a 700 y phase shift (Houtermans, 1966).

By proceeding in the reverse deductive direction in the present work, a minimum phase shift is found of about 800 y, which corresponds to the probably unrealistically large value of $\nu = 60$ (see the above discussion limiting ν to less than about 40). The minimum in the 8000 y sine wave of Suess occurs at 300 B.C. This is later than the minima of the production rate curves shown in figure 23, by only 10 y for case 1 of table 10, and by as much as 790 y for case 5. A smaller phase difference between production rate and C^{14} concentration would require either larger atmospheric or deep-sea residence times, or a smaller effective atmospheric reservoir.

Figure 23 also shows theoretical production rate curves derived from the exponential function and from the exponential plus sine wave (6077 y period) which, in Chapter I, were found to be possible alternative fits to the large scale trend of the ΔC^{14} data (see equations 3 and 5, page 14). The original ΔC^{14} data can be approximated by the sum of these two functions to within about the same standard error of estimate (10 ‰) as is achieved by the 10,400 y period sine wave. The ΔC^{14} function is (t is in A.D. years):

$$\Delta C^{14}(t) = \hat{C}_E(t) + \hat{C}_{ES}(t) \text{ , where} \qquad (2)$$

$$\hat{C}_E(t) = (1.0091 \cdot e^{-t/66915} - 1) \cdot 1000 \quad ‰$$

$$\hat{C}_{ES}(t) = 1.301 + 17.89 \cdot \sin[\frac{2\pi}{6077}(t - 796.4)] \quad ‰ \text{ .}$$

The production rate derived from this ΔC^{14} function by using the 2-reservoir model with $T^* = 50$ y and $\nu = 31.1$ (case 3, table 10) is:

$$\Delta Q(t) = \hat{Q}_E(t) + \hat{Q}_{ES}(t) \text{ , where} \qquad (3)$$

$$\hat{Q}_E(t) = (0.9020 \cdot e^{-t/66915} - 1) \cdot 1000 \quad ‰ \qquad (4)$$

$$\hat{Q}_{ES}(t) = 1.301 + 89.77 \cdot \sin[\frac{2\pi}{6077}(t - 1335)] \quad ‰ \text{ .}$$

Both $\hat{Q}_E$ and $\hat{Q}_E + \hat{Q}_{ES}$ are shown in figure 23. The agreement is good between the latter production rate curve and the magnetic dipole production rate data, except for the region between 3000 and 5000 B.C., where the data are higher than the curve. Near the

year 0, the curve is closer to the data points than are the 10,400 y period production rate sine waves. The agreement extends to the year 7000 B.C., 2000 years before the earliest ΔC^{14} data point, and this may of course be only fortuitous. The case mentioned by Suess (1970b) of an 8270 y mean lived exponential, instead of this one with 67,000 y mean life, has not yet been investigated.

Residual Q

The residual ΔC^{14} approximation functions from Chapter III, with cut-off degrees N = 13, 24 and 43, were transformed to give residual production rate functions with the corresponding cut-off degrees and frequencies. These residual ΔC^{14} functions, and the corresponding total ΔC^{14} functions, have been shown for N = 24 and 43 in figures 15 to 18, and are also shown here in figures 26 and 27. The residual ΔC^{14} function for N = 13 is shown only in figure 25. The total ΔC^{14} approximation function for N = 13, i.e. the residual function plus the 10,400 y period sine wave, is shown in figure 24.

Residual production rates for the N=13, ΔC^{14} function were found by using the 2-reservoir model with T_{12}= 7 y, β= 0, and T^*= 30 y and 50 y (cases 4 and 3, table 10). These two residual production rate curves are shown in figure 25, with the ΔC^{14}, N=13 curve. [Note that for the production rate curves shown in figures 24 to 28, the scale numbers in ‰ must be multiplied by 2, since Q/2 is actually plotted!] These residual production rate curves are added to their corresponding 10,400 y period sine waves to give the two total production rate curves shown in figure 24.

For the cases N = 24 and 43, only the value of 50 y was used for the 2-reservoir parameter T^*, since the higher frequencies involved in these ΔC^{14} functions require rather larger attenuation factors for T^*= 30 y, than they require for T^*= 50 y. The larger uncertainties of the ΔC^{14} amplitudes for these higher frequencies would otherwise be amplified even more for the production rates. The two residual production rates for N = 24 and 43, both for the same choice of model parameters, are shown in figure 26, and the total production rates in figure 27.

FIGURE CAPTIONS

Figures 24 and 27 — TOTAL PRODUCTION RATES (1 and 2) — pages 99, 101

Production rates are shown, which are found from the ΔC^{14} approximation functions with cut-off degrees N, by adding the 10,400 y period sine wave $\hat{Q}_S(t)$, and the residual production rate (figures 25 and 26). Note that Q/2 is plotted, not Q itself. The corresponding ΔC^{14} sine and approximation functions are also shown. Figure 24 shows two production rates, both from the same ΔC^{14}, with N=13. They are from a 2-reservoir model having T^*= 30 y and 50 y; and ratios, ν, as given in table 10. Figure 27 shows one production rate sine wave, and two total production rates, from the two ΔC^{14} functions with N=24 and 43. These are found using only the one value, T^*= 50 y. The magnetic production rate data has been described in the text and in the caption to figure 23.

Figures 25 and 26 — RESIDUAL PRODUCTION RATES (1 and 2) — page 100

Figure 25 shows the ΔC^{14} residual approximation function with cut-off degree N=13; and the two residual production rates derived from it by the two choices of T^*= 30 y and 50 y in a 2-reservoir model. Figure 26 shows the two residual production rates, using only T^*= 50 y, derived from the two residual ΔC^{14} functions with N=24 and 43, which are also shown.

Figure 24

Total Production Rates (1)

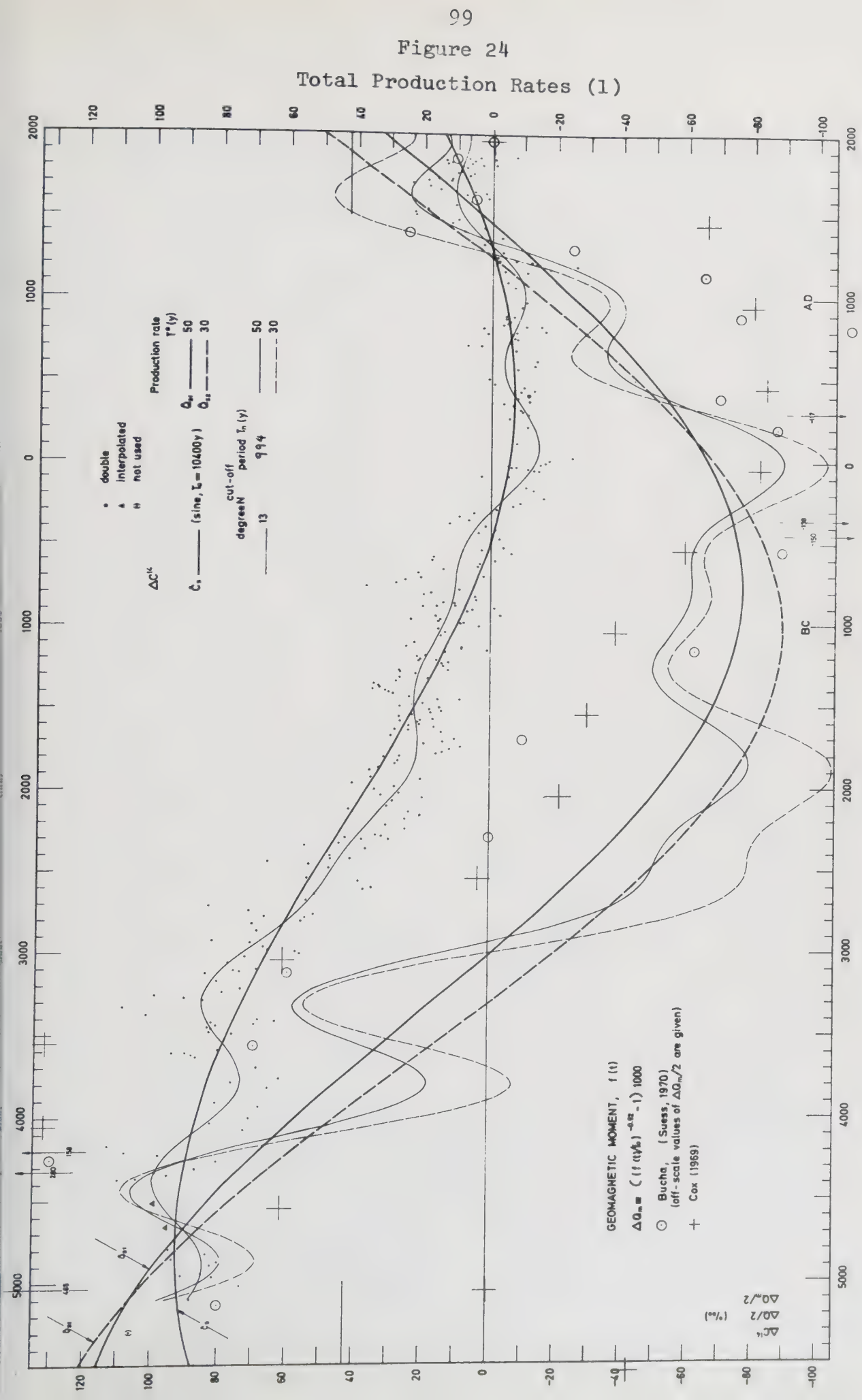

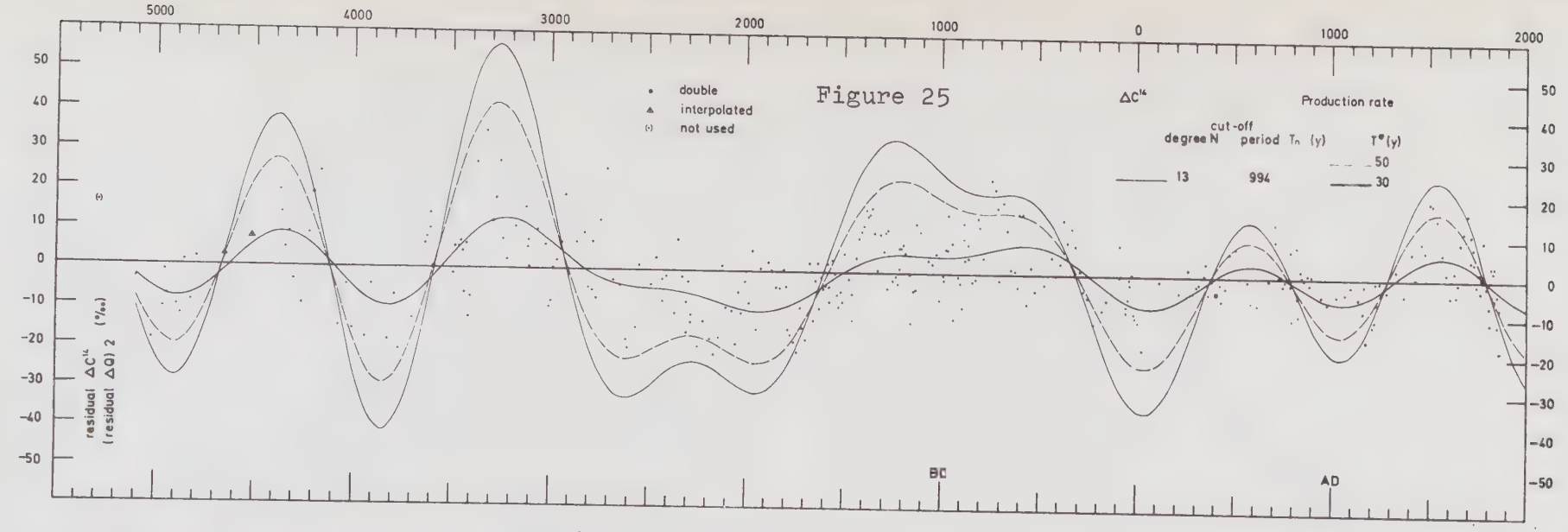

Residual Production Rates (1 + 2)

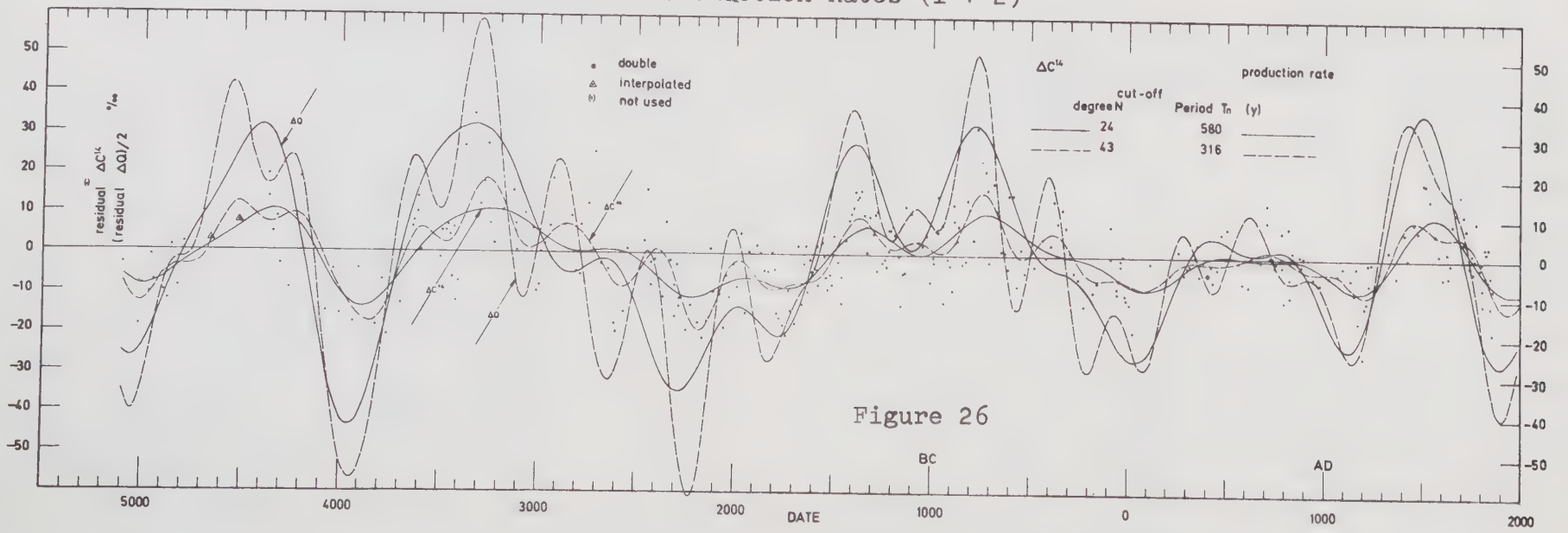

Figure 26

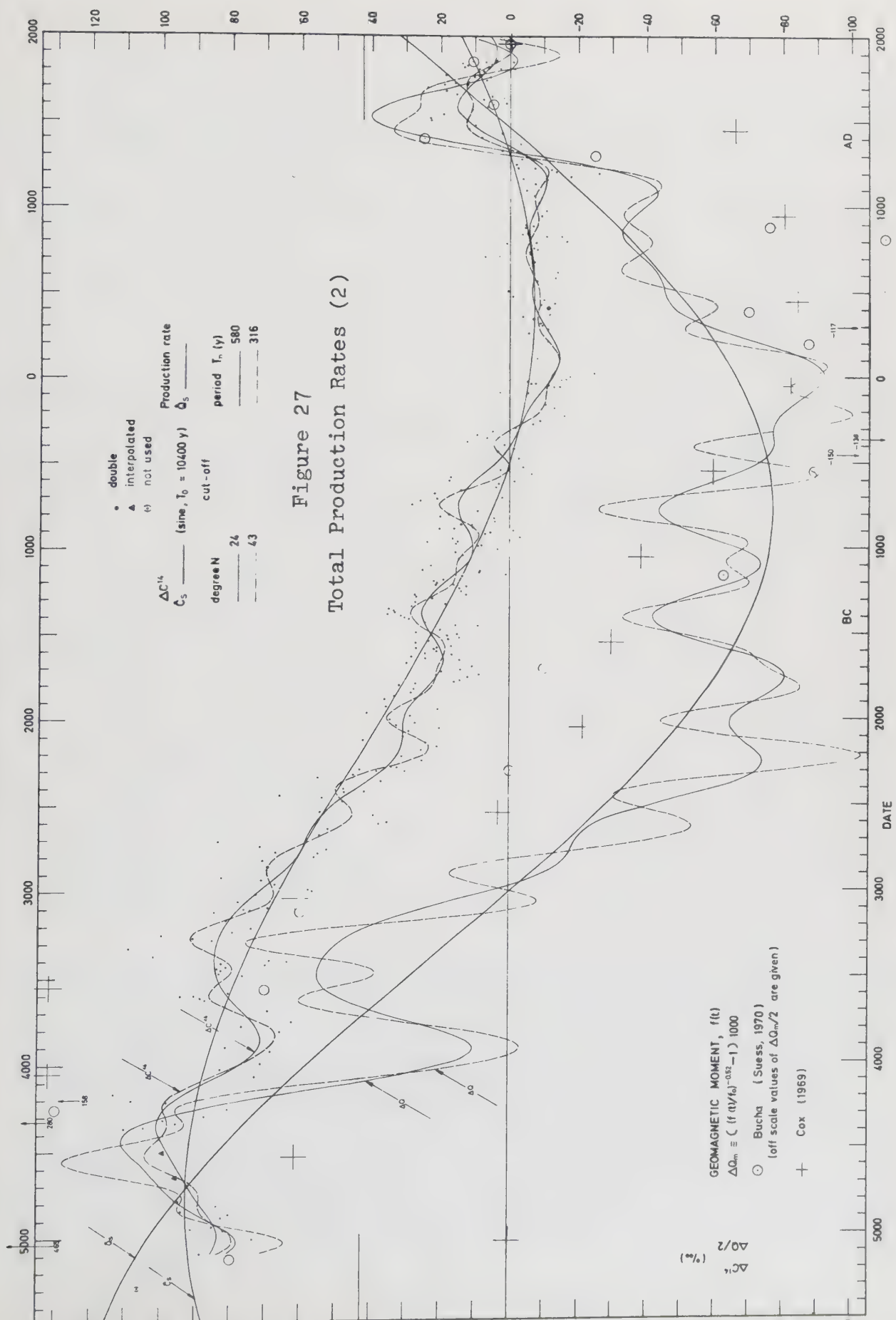
Figure 27
Total Production Rates (2)
• double
▲ interpolated
(•) not used
ΔC14 Cs ——— (sine, T0 = 10400 y)
Production rate Qs ———
degree N
cut-off
period Tn (y)
24 ——— 580
43 - - - - 316
GEOMAGNETIC MOMENT, f(t)
ΔQm ≡ ((f (t)/f0)^-0.52 − 1) 1000
Bucha (Suess, 1970)
(off scale values of ΔQm/2 are given)
Cox (1969)
ΔC14/2 (‰)
ΔQ/2
DATE
BC
AD

The production rate curves for N=13 have cut-off periods of about 1000 y, and thus show little of the detail seen in the curves for N=24 and 43 (the latter includes the important ~400 y cycle). As shown in figure 25, the maximum amplitude of the residual, N=13 production rate curves for T^*= 30 y, is about 10 %, and the rough average amplitude is about 5 %. For T^*= 50 y, these amplitudes are about 30 % smaller. The residual production rate curves with higher frequency cut-offs have somewhat larger amplitudes, up to about 12 %. A 5 % production rate increase would account for the sudden rise in C^{14} concentration after about 1800 B.C.

The larger oscillations occur when the production rate's 10,400 y period sine wave is high, and where the earth's magnetic field intensity is low. When the field intensity is low, the additional cosmic-ray flux in the atmosphere consists of the low energy particles which were previously unable to penetrate the earth's field. In periods of high solar activity, the increased primary flux of low-energy solar particles (less than 100 MeV or 1 GeV, say) will therefore contribute to the C^{14} production rate only when the terrestial field is low. One may therefore expect a positive correlation of C^{14} production rate with solar activity for periods of low terrestial magnetic field, to the extent that this effect of increased solar particle flux is not completely dominated by the competing solar effect, namely that of an increased magnetic shielding by the solar wind during times of increased solar activity. This latter effect will be the only solar effect when the terrestial field is high, and in such times it can cause a negative correlation between solar activity and C^{14} production rate, as has been observed in recent times (Stuiver, 1961; Suess, 1965). For a low terrestial field, the solar shielding effect will be greater. This may be the reason for the higher amplitudes of the 400 y period oscillation, for low terrestial field, seen in figure 26.

The 180° phase shift, expected (by Suess) to result from a change between negative and positive correlation with solar activity, was found between runs IV and III (the data prior to and since about 200 B.C.), although the 400 y period is weak in the modern data. There is some indication in figure 27 for two such phase shifts, one at about 1700 B.C., and the other at about the year zero. These dates straddle the minimum of the production rate sine wave. This would indicate that the solar flux is an important part of the overall solar effect, except when the terrestial field is near its maximum. And this conclusion may be in contradiction to the negative correlations with solar activity observed in modern times.

Appendix A

RECURSIVE FOURIER ANALYSIS OF UNEQUALLY SPACED DATA

Approximation function $Z_N(t)$

In order to approximate the M+1 data points $[t_i, w_i \equiv w(t_i), i=0,1,2,\ldots,m]$, by an analytical function $Z_N(t)$ of degree N, and having N+1 coefficients, we consider three different expansions in terms of three different sets of harmonic basis functions. The data times t_i are assumed normalized to the interval ($t_0=0$, $t_m=2\pi$). They may be irregularly spaced in this interval, there being $M \leqslant m$ independent t_i (M+1 unequal t_i). The data w_i may have been prepared to advantage by the subtraction of a trend from an original data set. The analysis is independent of the value w_m, so the choice $w_0 = w_m$, equal to the mean of corresponding earlier values, is also advantageous. All the data here are given equal weight.

The three expansions of $Z_N(t)$ are

$$Z_N(t) = \frac{1}{2} d_{N0} + \sum_{k=1}^{n} (c_{Nk} \sin kt + d_{Nk} \cos kt) \tag{1}$$

$$Z_N(t) = \sum_{K=0}^{N} G_K P_K(t) \qquad 0 \leqslant N \leqslant M \tag{2}$$

$$Z_N(t) = \sum_{K=0}^{N} G'_K P'_K(t) \tag{3}$$

with $$P_K(t) = \frac{1}{2} b_{K0} + \sum_{j=1}^{k} (a_{Kj} \sin jt + b_{Kj} \cos jt) \tag{4}$$

$$P'_K(t) = \frac{1}{2} b'_{K0} + \sum_{j=1}^{k} (a'_{Kj} \sin jt + b'_{Kj} \cos jt) \tag{5}$$

where $$n = \begin{cases} N/2, & N \text{ even} \\ (N+1)/2, & N \text{ odd} \end{cases}, \quad k = \begin{cases} K/2, & K \text{ even} \\ (K+1)/2, & K \text{ odd} \end{cases}$$

$$d_{2n-1,n} = b_{2k-1,k} = b'_{2k-1,k} = 0, \quad (0 < n,\ 0 < k)$$

$$a'_{2k-1,k} = b'_{2k,k} = 1, \quad (0 < n,\ 0 \leqslant k) \tag{6}$$

The basis functions in the first expansion are the ordinary harmonic functions up to the highest frequency n (cosnt appears only for even N). The basis functions in the two other expansions are linear combinations of these harmonic functions. The latter two are related by the constant ratio

$$\Gamma_K = \frac{P'_K(t)}{P_K(t)} = \frac{a'_{Kj}}{a_{Kj}} = \frac{b'_{Kj}}{b_{Kj}} \quad . \tag{7}$$

Orthogonal basis functions, $P_K(t)$ and $P'_K(t)$

These new basis functions are determined by the condition that they be "orthogonal" over the set of m arbitrarily spaced discreet arguments t_i. Two functions are defined here as being orthogonal over the set of m arguments t_i if they satisfy the condition

$$\sum_{i=0}^{m-1} f_K(t_i) f_J(t_i) \equiv [f_K, f_J] = C\delta_{KJ} \quad , \tag{8}$$

where C is a normalization constant, and the brackets and comma, [,], are a short-hand notation for the summation over i. The symetrical and linear properties:

$$[h, xf+yg] = [xf+yg, h] = x[f, h] + y[g,h] \quad ,$$

for functions f, g and h of t_i, and constants x and y, will be used below. The functions sinkt and coskt are orthogonal in the above sense only over equally spaced arguments $t_i = 2\pi i/m$, in which case $C = m/2$, with the possible exception of k=0 or k=m.

Thus the basis functions $P_K(t)$ and their K+1 coefficients can be determined by the K+1 orthogonality relations

$$[P_K, P_J] = \frac{m}{2}\delta_{KJ} \quad , \qquad 0 \leqslant J \leqslant K, \tag{9}$$

and are normalized to m/2 in analogy with the equal interval case. The basis functions $P'_K(t)$ and their K coefficients are determined by the K relations

$$[P'_K, P'_J] = 0 \quad , \qquad 0 \leqslant J < K, \tag{10}$$

and have been "normalized" already by equation 6, which requires

the last term in $P_K(t)$ to have a coefficient of 1. The two normalizations are related by

$$[P'_K, P'_K] = \Gamma_K^2 [P_K, P_K] = \frac{m}{2} \Gamma_K^2 \quad . \tag{11}$$

By equating the two expansions of $Z_N(t)$, equations 2 and 3, and using the independence of the $P_K(t)$, one finds that $G_K = \Gamma_K G'_K$:

$$\Gamma_K = \frac{P'_K(t)}{P_K(t)} = \frac{G_K}{G'_K} \quad . \tag{12}$$

The basis functions $P_K(t)$ and $P'_K(t)$ are completely determined by the set of arguments t_i. It will be shown below that $P'_K(t)$ may be found recursively.

Coefficients in the expansions of $Z_N(t)$

The Fourier coefficients, c_{Nk} and d_{Nk}, in $Z_N(t)$ (equation 1) can be found by the minimization of the total square deviation $\mathcal{E}_N^2$ of the function from the data:

$$\mathcal{E}_N^2 = \sum_{i=0}^{m-1} [w_i - Z_N(t_i)]^2 \tag{13}$$

Partial differentiation of $\mathcal{E}_N^2$ with respect to the Fourier coefficients leads to N+1 simultaneous linear equations in these coefficients, which cannot be reduced to separate equations, each for only one unknown, because of the failure of orthogonality over the t_i for the ordinary harmonic functions. Rather than solving the set of simultaneous equations (for each desired degree of expansion), an alternative method is used.

The coefficients G_K and G'_K in the alternative expansion (equations 2 and 3) may easily be determined:

$$\frac{\partial}{\partial G_K} \mathcal{E}_N^2 = \frac{\partial}{\partial G_K} \sum_{i=0}^{m-1} [w_i - \sum_{K=0}^{N} G_K P_K(t_i)]^2 = 0$$

$$\sum_{i=0}^{m-1}[w_i - Z_N(t_i)]P_K(t_i) = 0$$

$$[\sum_{K=0}^{N} G_K P_K, P_K] = [w, P_K]$$

$$G_K[P_K, P_K] = [w, P_K]$$

$$G_K = \frac{2}{m}[w,P_K] = \frac{2}{m}\sum_{i=0}^{m-1} w_i P_K(t_i) \tag{14}$$

$$G'_K = \frac{G_K}{\Gamma_K} \tag{15}$$

$$\Gamma_K^2 = \frac{2}{m}[P'_K, P'_K] = \frac{2}{m}\sum_{i=0}^{m-1} P'^2_K(t_i) \tag{16}$$

The Fourier coefficients, c_{Nk} and d_{Nk}, may now be found by identifying like terms in the two expressions for $Z_N(t)$ given by equations 1 and 2, after substituting from equation 4 for $P_K(t)$. One finds the result:

$$\begin{aligned} c_{Nk} &= \sum_{\substack{J=\\ 2k-1}}^{N} G_J a_{Jk} \quad , \quad 1 \leqslant k \leqslant n, \\ d_{Nk} &= \sum_{J=2k}^{N} G_J b_{Jk} \quad , \quad 0 \leqslant k \leqslant n. \end{aligned} \tag{17}$$

(Primes could have been used under the summation, since $G_J a_{Jk} = G'_J a'_{Jk}$, for example.)

Total square deviation $\mathcal{E}_N^2$

The total square deviation may be found easily as follows:

$$\mathcal{E}_N^2 = \sum_{i=0}^{m-1}[w_i^2 - 2w_i Z_N(t_i) + Z_N^2(t_i)]$$

$$= [w, w] - 2[w, Z_N] + [Z_N, Z_N].$$

But
$$[Z_N, Z_N] = \left[\sum_{K=0}^{N} G_K P_K , \sum_{J=0}^{N} G_J P_J \right]$$
$$= \sum_K \sum_J G_K G_J [P_K, P_J]$$
$$= \sum_K G_K^2 [P_K, P_K] = \sum_K G_K [w, P_K]$$
$$= [w, Z_N] = \frac{m}{2} \sum_{K=0}^{N} G_K^2 ,$$

so that
$$\mathcal{E}_N^2 = [w, w] - [w, Z_N]$$
$$= [w, w] - \frac{m}{2} \sum_K G_K^2$$
$$\mathcal{E}_N^2 = \mathcal{E}_{N-1}^2 - \frac{m}{2} G_N^2 , \quad 0 < N$$
$$\mathcal{E}_0^2 = [w, w] - \frac{m}{2} G_0^2 .$$

Defining $\mathcal{E}_{-1}^2 \equiv [w, w]$, we have the recursive relation

$$\mathcal{E}_N^2 = \mathcal{E}_{N-1}^2 - \frac{m}{2} G_N^2 , \quad 0 \leqslant N . \tag{18}$$

Recursion formulae for $P_K(t_i)$

The values at the m arguments t_i of the orthogonal basis functions $P'_K(t)$ can be found recursively from the 4 sets of m values of $P'_{K-v}(t)$, v=1,2,3,4. A recursive definition of functions called $Q_K(t)$ is given below, and it is then shown (A.) that the $Q_K(t)$ have the same form and normalization as the $P'_K(t)$ (equations 5 and 6), and therefore are basis functions for $Z_N(t)$; and (B.) that the $Q_K(t)$ are orthogonal over the t_i (equation 10), and therefore are indeed identical to $P'_K(t)$. (P'_{-2} and P'_{-1} are introduced for convenience.)

We define $Q_K(t)$ for K = -2, -1, 0 and 1 as:

$$Q_{-2} = Q_{-1} = 0 = P_{-1} = P_{-2}$$

$$Q_0 = \frac{1}{2} = P_0$$

$$Q_1(t) = -\frac{1}{m}\sum_{i=0}^{m-1}\sin t_i + \sin t = P_1(t) \qquad (19)$$

$$\left(\text{taking } b'_{10} = -\frac{2}{m}\sum_{i=0}^{m-1}\sin t_i\right) .$$

And we define $Q_K(t)$ for K = 2,3,..., as:

$$Q_K(t) = 2\cos t \cdot Q_{K-2}(t) - \sum_{v=1}^{4}\alpha_{Kv}Q_{K-v}(t) , \qquad (20)$$

where $\alpha_{23} = \alpha_{24} = 1$

$$\alpha_{Kv} = \frac{[Q_{K-v},\ 2\cos t \cdot Q_{K-2}]}{[Q_{K-v},\ Q_{K-v}]} , \begin{cases} K = 2, \text{ and } v = 1 \text{ or } 2 \\ K = 3,4,\ldots, \text{ and} \\ \quad v = 1,2,3,4 \end{cases} \qquad (21)$$

A. The $Q_K(t)$ and $P'_K(t)$ have the same form.

1. Identically true for K = -2, -1, 0 and 1.

2. Since the α_{Kv} are only constants, all harmonic terms appearing in the 4 previous $Q_{K-v}(t)$, but no other ones, will also appear in $Q_K(t)$ (usually with different coefficients), due to the summation term in equation 20.

3. Due to the identities

$$2\cos t \cdot \sin kt = \sin(k-1)t + \sin(k+1)t$$
$$2\cos t \cdot \cos kt = \cos(k-1)t + \cos(k+1)t ,$$

the first term in equation 20 contributes two harmonic terms to $Q_K(t)$, for each harmonic term in $Q_{K-2}(t)$, the two new terms having frequencies one unit lower and one

unit higher than the frequency of the old term. If we consider coskt to be a "higher" harmonic than sinkt (since it is always introduced after sinkt), then we may say that the highest harmonic term in $Q_K(t)$ stems from that of $Q_{K-2}(t)$; that it has the same coefficient (unity if that was the case in Q_{K-2}); that it has the same form (sine or cosine); and that it has a frequency raised by one unit. But these are precisely the properties given in equations 5 and 6 for $P'_K(t)$.

B. The $Q_K(t)$ satisfy: $[Q_K, Q_J] = 0$, for $K \neq J$.

1. K = 1

$$[Q_0, Q_1] = [Q_0, \tfrac{1}{2} b_{10}] + [Q_0, \text{sint}]$$

$$= \frac{m}{4} b_{10} + \frac{1}{2} \sum_{i=0}^{m-1} \text{sint}_i = 0 .$$

2. K = 2

a. $$[Q_0, Q_2] = [Q_0, 2\text{cost}\cdot Q_0] - \alpha_{21}[Q_0, Q_1] - \alpha_{22}[Q_0, Q_0]$$

$$= [Q_0, 2\text{cost}\cdot Q_0] - \frac{[Q_0, 2\text{cost}\cdot Q_0]}{[Q_0, Q_0]} [Q_0, Q_0] = 0 ;$$

b. $$[Q_1, Q_2] = [Q_1, 2\text{cost}\cdot Q_0] - \alpha_{21}[Q_1, Q_1] - \alpha_{22}[Q_1, Q_0]$$

$$= [Q_1, 2\text{cost}\cdot Q_0] - \frac{[Q_1, 2\text{cost}\cdot Q_0]}{[Q_1, Q_1]} [Q_1, Q_1] = 0 .$$

3. K = 3, 4, 5, ...

Assume that $[Q_J, Q_L] = 0$, $J \neq L$, for $J < K$, and $L < K$ (i.e. that the Q_J form an orthogonal set for $J < K$).

Show that $[Q_K, Q_J] = 0$, for $J < K$ (i.e. that Q_K is orthogonal to each member of an orthogonal set).

The premise is true for K = 3.

$$[Q_K, Q_J] = [2\cos t \cdot Q_{K-2}, Q_J] - \sum_{v=1}^{4} \alpha_{Kv} [Q_{K-v}, Q_J]$$

a. If $K-4 \leq J < K$:

$$[Q_K, Q_J] = [2\cos t \cdot Q_{K-2}, Q_J] - \alpha_{K,K-J} [Q_J, Q_J]$$

$$= [2\cos t \cdot Q_{K-2}, Q_J] - \frac{[Q_J, 2\cos t \cdot Q_{K-2}]}{[Q_J, Q_J]} [Q_J, Q_J]$$

$$= 0 .$$

b. If $J < K-4$

$$[Q_K, Q_J] = [2\cos t \cdot Q_{K-2}, Q_J] .$$

Since $J+2 < K-2$, we have

$$0 = [Q_{J+2}, Q_{K-2}]$$

$$= [2\cos t \cdot Q_J, Q_{K-2}] - \sum_{v=1}^{4} \alpha_{J+2,v} [Q_{J+2-v}, Q_{K-2}]$$

$$= [2\cos t \cdot Q_J, Q_{K-2}] \text{ , since } J+2-v < J+2 < K-2$$

$$= [2\cos t \cdot Q_{K-2}, Q_J]$$

$$= [Q_K, Q_J] \qquad \text{Q.E.D.}$$

Therefore the recursively defined $Q_K(t)$ are identical to the $P'_K(t)$ of equations 5, 6 and 10.

$$Q_K(t) = P'_K(t) \tag{22}$$

$P'_K(t)$ need be evaluated only at the arguments t_i, in order to calculate the various functions of interest in the Fourier analysis. The values $P'_{K-4}(t_i)$ are not needed after the values $P'_K(t_i)$ have been found. However, all the α_{K-v} should be retained for the subsequent calculation of the Fourier coefficients, c_{Nk} and d_{Nk}.

Recursive formulae for a'_{Nk} and b'_{Nk}

An examination of the recursive equations for $P'_K(t)$ leads to the following recursive scheme for finding the harmonic coefficients, a'_{Nk} and b'_{Nk}, in $P'_K(t)$. A matrix of these coefficients is of assistance in visualizing the six different contributions to a harmonic term in $P'_K(t)$, from harmonic terms in the four previous P'_{K-v}.

So that the following scheme can apply to all frequencies k, which are of interest for a given N (n or n+1 frequencies), these non-zero coefficients must be preceded by one artificial zero value, and succeeded by two artificial zero values.

As usual we let $n = \left\lceil \begin{matrix} N/2 \text{ for even } N \\ (N+1)/2 \text{ for odd } N \end{matrix} \right\rceil$.

1. Initialization, for $N \geq -2$:

$$a'_{N0} = a'_{N,n+1} = a'_{N,n+2} = 0$$
$$a'_{11} = 1$$

$$b'_{N,-1} = b'_{N,n+1} = b'_{N,n+2} = 0$$
$$b'_{-1,0} = 0$$
$$b'_{00} = 0$$
$$b'_{10} = -\frac{2}{m}\sum_{i=0}^{m-1}\sin t_i \quad ; \quad b'_{11} = 0$$

2. Recursive calculation, for $N = 2, 3, 4, \ldots$:

$$a'_{Nk} = a'_{N-2,k-1} + a'_{N-2,k+1} - \sum_{v=1}^{4}\alpha_{Nv}a'_{N-v,k};k = 1,2,3,\ldots, n$$
$$b'_{Nk} = b'_{N-2,k-1} + b'_{N-2,k+1} - \sum_{v=1}^{4}\alpha_{Nv}b'_{N-v,k};k = 0,1,2,\ldots, n \qquad (23)$$

These coefficients need not be found explicitly, but the recursion formulae, in combination with equation 17 enables the direct recursive calculation of the Fourier coefficients c_{Nk} and d_{Nk}.

APPENDIX B

TWO- AND THREE-RESERVOIR MODELS OF THE ATMOSPHERE AND OCEANS

The equations of the 3-reservoir model and their general solutions are given below. The particular case of harmonic production rates and atmospheric C^{14} concentrations are treated, and relationships between the parameters of the 3-reservoir model and those of the 2-reservoir model are found.

Three-reservoir model

The three reservoirs are the atmosphere (i=1), the upper "mixed" layer of the oceans (i=2), and the deep oceans (i=3). Their C^{12} and C^{14} contents, in atoms/cm_e^2, are Y_i and X_i, respectively. Each reservoir is assumed to be well-mixed, i.e. to have a homogeneous C^{14} concentration $R_i = X_i/Y_i$. Radiocarbon is introduced into the atmosphere at the variable rate Q(t), and may leave the deep sea at the constant sedimentation rate S, both rates being in C^{14} atoms/(sec·cm_e^2). The reservoir sizes Y_i are assumed to be constant (the C^{12} being in equilibrium in spite of sedimentation). The radiocarbon decays with mean-life $\tau = 1/\lambda = 8267$ y. It is assumed that C^{12} and C^{14} are transfered from reservoir i to reservoir j at rates that are proportional to the same rate constant $k_{ij} = 1/T_{ij}$, where T_{ij} is the residence time in reservoir i with respect to transfer to reservoir j. The rate of C^{12} transfer is assumed the same from i to j as from j to i. Furthermore, it is assumed that the transfer rate from atmosphere to deep sea is a constant fraction, β, of the transfer rate from atmosphere to mixed layer. The residence times, rate constants, and reservoir size ratios are related by

$$\frac{T_{21}}{T_{12}} = \frac{k_{12}}{k_{21}} = \frac{Y_2}{Y_1} = \nu_2 \quad ; \quad \frac{T_{12}}{T_{13}} = \frac{k_{13}}{k_{12}} = \beta$$

$$\frac{T_{31}}{T_{13}} = \frac{k_{13}}{k_{31}} = \frac{Y_3}{Y_1} = \nu_3 \qquad (1)$$

$$\frac{T_{32}}{T_{23}} = \frac{k_{23}}{k_{32}} = \frac{Y_3}{Y_2} = \frac{\nu_3}{\nu_2}$$

Here ν_2 and ν_3 are defined as the ratios of the C^{12} in reservoirs 2 and 3, respectively, to the C^{12} in the atmosphere; the total amount of C^{12} is $Y = Y_1 + Y_2 + Y_3 = Y_1(1 + \nu_2 + \nu_3)$.

The model has 6 parameters, which may be taken to be

$$\nu_2 \ , \ \nu_3 \ , \ \beta \ , \ T_{12} \ , \ T_{32} \ , \text{ and } S \ .$$

Equations and first integral

The differential equations describing the equilibrium of C^{14} are:

$$\begin{aligned} \dot{X}_1 &= Q - (\lambda+k_{12}+k_{13})X_1 + k_{21}X_2 + k_{31}X_3 \\ \dot{X}_2 &= k_{12}X_1 - (\lambda+k_{21}+k_{23})X_2 + k_{32}X_3 \\ \dot{X}_3 &= -S + k_{13}X_1 + k_{23}X_2 - (\lambda+k_{31}+k_{32})X_3 \end{aligned} \tag{2}$$

The total C^{14} is

$$X(t) = X_1(t) + X_2(t) + X_3(t) = -S + e^{-\lambda t}\int_{-\infty}^{t} Q(t')e^{\lambda t'}dt' \ . \tag{3}$$

By eliminating $X_2(t)$, say, from equations 2 one finds:

$$\begin{aligned} \dot{X}_1 &= Q_1 - (\lambda+\phi_{11})X_1 + \phi_{13}X_3 \\ \dot{X}_3 &= Q_3 + \phi_{31}X_1 - (\lambda+\phi_{33})X_3 \end{aligned} \tag{4}$$

where

$$\begin{aligned} Q_1(t) &= Q(t) + k_{21}X(t); \ \phi_{11} = k_{12}+k_{13}+k_{21}; \ \phi_{13} = k_{31} - k_{21} \\ Q_3(t) &= -S + k_{23}X(t); \ \phi_{31} = k_{13} - k_{23} \ ; \ \phi_{33} = k_{31}+k_{32}+k_{23} \end{aligned} \tag{5}$$

Method of solution

We assume that the solutions of equations 4 have the form

$$X_1(t) = e^{-\lambda_1 t}\int_{-\infty}^{t} p_{11}(t')e^{\lambda_1 t'}dt' + e^{-\lambda_3 t}\int_{-\infty}^{t} p_{13}(t')e^{\lambda_3 t'}dt'$$

$$X_3(t) = e^{-\lambda_1 t}\int_{-\infty}^{t} p_{31}(t')e^{\lambda_1 t'}dt' + e^{-\lambda_3 t}\int_{-\infty}^{t} p_{33}(t')e^{\lambda_3 t'}dt' \qquad (6)$$

where $p_{ij}(t)$ are some functions of t, and λ_1 and λ_3 are constants. Putting these forms for $X_1(t)$ and $X_3(t)$ into equations 4, and separately equating the coefficients of the various terms (which are independent functional forms) one finds that

$$p_{11}(t) + p_{13}(t) = Q_1(t) \qquad p_{31}(t) = r_1 p_{11}(t)$$

$$p_{31}(t) + p_{33}(t) = Q_3(t) \qquad p_{33}(t) = r_3 p_{13}(t) \qquad (7)$$

where
$$r_1 = \frac{\lambda + \phi_{11} - \lambda_1}{\phi_{13}} = \frac{\phi_{31}}{\lambda + \phi_{33} - \lambda_1}$$

$$r_3 = \frac{\lambda + \phi_{11} - \lambda_3}{\phi_{13}} = \frac{\phi_{31}}{\lambda + \phi_{33} - \lambda_3} \; . \qquad (8)$$

Both of equations 8 are the same quadratic equation for $\lambda - \lambda_i$:

$$(\lambda-\lambda_i)^2 + (\phi_{11}+\phi_{33})(\lambda-\lambda_i) + (\phi_{11}\phi_{33}-\phi_{13}\phi_{31}) = 0 \; ,$$

which has the solutions

$$\left.\begin{aligned} \lambda_1 &= \lambda + \lambda_0 + \alpha \\ \lambda_3 &= \lambda + \lambda_0 - \alpha \end{aligned}\right\} = \frac{\lambda+\lambda'}{2} \pm \alpha \qquad (9)$$

where $\lambda_0 = \frac{1}{2}(\phi_{11} + \phi_{33}) = \frac{1}{2}\Sigma k_{ij}$ (9)

$$\alpha = \frac{1}{2}[(\phi_{11} - \phi_{33})^2 + 4\phi_{13}\phi_{31}]^{1/2} .$$

$$\lambda' = \lambda + \Sigma k_{ij} .$$

Thus if the solutions to equations 4 are required to have the form of equations 6, $\lambda_1 = 1/T_1$ and $\lambda_3 = 1/T_3$ must take these values. The characteristic times T_1 and T_3 (and $T' = 1/\lambda'$) are the 3-reservoir equivalents of the characteristic time $T^* = 1/\lambda^*$ in the 2-reservoir model, where $\lambda^* = \lambda + k_{as} + k_{sa}$.

The functions $p_{ij}(t)$, found from equations 7, 8 and 9, are then

$$p_{11}(t) = \frac{\phi_{13}}{2\alpha}[r_3 Q_1(t) - Q_3(t)]; \quad p_{13}(t) = \frac{\phi_{13}}{2\alpha}[-r_1 Q_1(t) + Q_3(t)]$$

$$p_{31}(t) = r_1 p_{11}(t) \qquad ; p_{33}(t) = r_3 p_{13}(t) \tag{10}$$

Thus the integrands in equations 6 for $X_1(t)$ and $X_3(t)$ contain linear combinations of $Q_1(t)$ and $Q_3(t)$ (equations 10), or linear combinations of S, Q(t) and X(t) (equations 5). The terms in $X_1(t)$ and $X_3(t)$ which contain X(t) may be integrated by parts, using equation 3 for X(t). The solutions for $X_1(t)$ and $X_3(t)$ will then be linear combinations of a constant and three integrals whose integrands are

$$Q(t)e^{\lambda t}, \quad Q(t)e^{\lambda_1 t} \text{ , and } \quad Q(t)e^{\lambda_3 t} .$$

Finally, $X_2(t)$ may be found from X, X_1 and X_3.

3-reservoir solution

The solution for the C^{14} content in the three reservoirs is

$$X_i(t) = -A_i \tau S + B_i e^{-\lambda t} \int_{-\infty}^{t} Q(t')e^{\lambda t'} dt'$$

$$+ C_i e^{-\lambda_1 t} \int_{-\infty}^{t} Q(t')e^{\lambda_1 t'} dt' \tag{11}$$

$$+ D_i e^{-\lambda_3 t} \int_{-\infty}^{t} Q(t')e^{\lambda_3 t'} dt'$$

The rate constants λ_1 and λ_3 have been given in equation 9, but are repeated here in terms of 5 of the problem's 6 independent parameters (see equation 1).

$$T_1 = 1/\lambda_1 \ , \ T_3 = 1/\lambda_3$$

$$\binom{\lambda_1}{\lambda_3} = \lambda + \lambda_0 \pm \alpha = \lambda + \frac{\phi_{11}+\phi_{33}}{2} \pm \alpha = \frac{\lambda+\lambda'}{2} \pm \alpha \qquad (12)$$

$$2\lambda_0 = \phi_{11} + \phi_{33} = \Sigma k_{ij} = \lambda' - \lambda$$

$$4\alpha^2 = (\phi_{11}-\phi_{33})^2 + 4\phi_{13}\phi_{31} \qquad (13)$$

$$\lambda' = \lambda_1 + \lambda_3 - \lambda$$

$$\phi_{11} = (1 + \beta + 1/\nu_2)k_{12} \ , \quad \phi_{13} = (\beta/\nu_3 - 1/\nu_2)k_{12}$$

$$\phi_{31} = \beta k_{12} - (\nu_3/\nu_2)k_{32}, \quad \phi_{33} = (\beta/\nu_3)k_{12} + (1 + \nu_3/\nu_2)k_{32}. \qquad (14)$$

The coefficients in equation 11 are given by

$$B_i = Y_i/Y \ , \ i=1,2,3 \ ; \ B_1 = \frac{1}{1+\nu_2+\nu_3} ; \ B_j = \nu_j B_1 \ , \ j=2,3 \ ;$$

$$\binom{C_1}{D_1} = \frac{1-B_1}{2} \pm \frac{1}{2\alpha}\left[(1+\beta)k_{12} - (1-B_1)\lambda_0\right]$$

$$\binom{C_2}{D_2} = -\frac{B_2}{2} \mp \frac{1}{2\alpha}\left[k_{12} - B_2\lambda_0\right] \qquad (15)$$

$$\binom{C_3}{D_3} = -\frac{B_3}{2} \mp \frac{1}{2\alpha}\left[\beta k_{12} - B_3\lambda_0\right];$$

$$A_i/B_i = 1 + \frac{1}{\tau}\frac{\gamma_i}{B_i}\left[C_{4-i}T_1 + D_{4-i}T_3\right] \ ;$$

where

$$\gamma_1 = B_1/B_3 = Y_1/Y_3 = 1/\nu_3$$

$$\gamma_2 = \frac{B_2\lambda' - k_{32}}{B_2\lambda' - k_{12}}$$

$$\gamma_3 = \frac{(1-B_1)\lambda' - [(\beta/\nu_3)k_{12}+k_{32}]}{(1-B_1)\lambda' - (1+\beta)k_{12}} \ .$$

The following relations hold between these coefficients

$$\Sigma A_i = \Sigma B_i = B_1 + C_1 + D_1 = 1$$

$$\Sigma C_i = \Sigma D_i = B_2 + C_2 + D_2 = B_3 + C_3 + D_3 = 0 \ .$$

The steady state C^{14} content, X_{i0}, for an arbitrary constant production rate Q_0 is

$$X_{i0} = X'_{i0} - A_i\tau S,$$

where

$$X'_{i0} = (B_i\tau + C_iT_1 + D_iT_3)Q_0 \ ,$$

and is the steady state C^{14} content for the case of no sedimentation. The deviation, $x_i(t) = X_i(t) - X_{i0}$, of the C^{14} content from the steady state value, X_{i0}, is due to a production rate deviation, $q(t) = Q(t) - Q_0$, from the steady state value Q_0.

The C^{14} concentration is

$$R_i(t) = \frac{X_i(t)}{Y_i} = \frac{X_{i0}+x_i(t)}{Y_i}$$

$$= R_{i0} + r_i(t)$$

$$= R_{i0}[1 + \Delta C_i(t)] \ ;$$

where $\Delta C_i(t)$ is the fractional deviation of the C^{14} concentration (or content) in reservoir i, from its steady state value:

$$\Delta C_i(t) = \frac{r_i(t)}{R_{i0}} = \frac{x_i(t)}{X_{i0}} \quad .$$

It is a function of the production rate's fractional deviation:

$$\Delta Q(t) = \frac{q(t)}{Q_0} = \frac{Q(t) - Q_0}{Q_0} \quad .$$

Rewriting equation 11 in terms of fractional deviations, we have

$$\Delta C_i(t) = b_i e^{-\lambda t} \int_{-\infty}^{t} \Delta Q(t') e^{\lambda t'} dt' + c_i e^{-\lambda_1 t} \int_{-\infty}^{t} \Delta Q(t') e^{\lambda_1 t'} dt'$$

$$+ d_i e^{-\lambda_3 t} \int_{-\infty}^{t} \Delta Q(t') e^{\lambda_3 t'} dt' \quad . \qquad (16)$$

The new coefficients are given by

$$\frac{B_i}{b_i} = \frac{C_i}{c_i} = \frac{D_i}{d_i} = \frac{X_{i0}}{Q_0} = \frac{R_{i0}}{Q_0} Y_i$$

$$= \left[1 - \frac{A_i \tau}{X'_{i0}/Q_0} \cdot \frac{S}{Q_0} \right] \frac{X'_{i0}}{Q_0}$$

$$= (1 - a_i \frac{S}{Q_0}) \frac{X'_{i0}}{Q_0} ,$$

where $a_i = A_i\tau/(X'_{i0}/Q_0)$ is independent of S, and is a rather insensitive function of the other 5 parameters, being of the order of unity.

If the C^{14} concentration's fractional deviation from R_{i0}, in the case of no sedimentation, is called $\Delta C'_i(t)$, we have:

$$\Delta C'_i(t) = (1 - a_i \frac{S}{Q_0}) \Delta C_i(t) \quad . \tag{17}$$

Thus the effect of sedimentation is to increase the fractional deviation of the concentration by the factor $1/(1-a_iS/Q_0)$, because the absolute deviation $x_i(t)$ is independent of S, whereas sedimentation decreases the steady state C^{14} content by the above factor.

In the subsequent work the sedimentation rate S will be assumed zero, and a correction can be applied at any point in the argument. Dropping the primes for zero sedimentation, $\Delta C_i(t)$ is given by equation 16, with

$$b_i = Q_0 B_i / X_{i0} , \quad c_i = Q_0 C_i / X_{i0}, \quad \text{and } d_i = Q_0 D_i / X_{i0} . \tag{18}$$

For example, for the atmosphere one has

$$b_1 = B_1/(B_1\tau + C_1 T_1 + D_1 T_3) .$$

2-reservoir model

The 2-reservoir model has two "effective" reservoirs, called "atmosphere" (j=a), and "ocean" (j=s), each of which, to some unknown extent, shares the carbon in the upper mixed layer of the ocean (i=2). One of the model's two parameters is the "effective" ratio ν, between the C^{12} contents of "ocean" and "atmosphere". The model includes the essential feature of a "hold-up time", which is an average delay between the production of a C^{14} atom (after which it is quickly mixed throughout the upper reservoir) and its transfer to the "ocean". The second "effective" parameter is this "atmospheric" residence time, T_{as}.

The same assumptions as were made above regarding well mixed reservoirs and transfer of carbon between reservoirs are made here. The index j is used for 2-reservoir quantities (j=a and s, for atmosphere and sea), while the index i is used for 3-reservoir quantities (i=1,2,3).

The basic model equations are

$$\nu = Y_s/Y_a = T_{sa}/T_{as} = k_{as}/k_{sa} \tag{19}$$

$$\begin{aligned} \dot{X}_a(t) &= Q(t) - (\lambda + k_{as})X_a(t) + k_{sa} X_s(t) \\ \dot{X}_s(t) &= -S + k_{as} X_a(t) - (\lambda + k_{sa})X_s(t) . \end{aligned} \tag{20}$$

The total C^{12} is $X(t)=X_a + X_s = -S + e^{-\lambda t} \int_{-\infty}^{t} Q(t')e^{\lambda t'} dt'$; and the solution of equations 20 is:

$$X_j(t) = -A_j \tau S + B_j e^{-\lambda t} \int_{-\infty}^{t} Q(t')e^{\lambda t'} dt' + C_j e^{-\lambda^* t} \int_{-\infty}^{t} Q(t')e^{\lambda^* t'} dt' \quad (j=a,s) \tag{21}$$

where $B_a = 1/(\nu+1)$; where $B_s = C_a = -C_s = \nu B_a$; and where T^* is the characteristic time in the 2-reservoir model:

$$T^* = 1/\lambda^* \quad , \quad \lambda^* = \lambda + k_{as} + k_{sa} .$$

The two model parameters may be conveniently taken as ν and T^*, instead of ν and T_{12}. (T^* is a few per cent less than T_{as}.)

The steady state solution, for constant production rate Q_0, is:

$$X_{j0} = X'_{j0} - A_j \tau S \quad ; \quad X'_{j0} = (B_j \tau + C_j T^*) Q_0 \quad ;$$

and the fractional deviation from steady state (in terms of the production rate's fractional deviation ΔQ) is:

$$\Delta C_j(t) = (X_j(t) - X_{j0})/X_{j0} = (R_j(t) - R_{j0})/R_{j0}$$

$$= \Delta C'_j(t)/(1 - a_j \frac{S}{Q_0})$$

$$\Delta C_j(t) = b_j e^{-\lambda t} \int_{-\infty}^{t} \Delta Q(t') e^{\lambda t'} dt' + c_j e^{-\lambda^* t} \int_{-\infty}^{t} \Delta Q(t') e^{\lambda^* t'} dt' \qquad (22)$$

Here, as in the 3-reservoir model, the primes denote S=0; the sedimentation factor is $a_j = A_j \tau Q_0 / X'_{j0}$; and the coefficients are given by:

$$\frac{B_j}{b_j} = \frac{C_j}{c_j} = \frac{X_{j0}}{Q_0} = (1 - a_j \frac{S}{Q_0}) \frac{X'_{j0}}{Q_0} \quad .$$

Treating only the case of zero sedimentation, and dropping the primes, we can then use equation 22 for $\Delta C_j(t)$, with

$$b_j = \frac{Q_0}{X_{j0}} B_j \quad , \quad c_j = \frac{Q_0}{X_{j0}} C_j \quad .$$

In particular,

$$b_a = 1/(\tau + \nu T^*), \; c_a = \nu b_a \quad ,$$

$$b_s = 1/(\tau - T^*) \; , \; c_s = -b_s \quad . \qquad (23)$$

Relations between the two models

The 2-reservoir model is sufficient (at least in comparison with the 3-reservoir model) to adequately describe the variations in the atmospheric C^{14} concentration in terms of the production rate variations.

There remains, however, the question of the best values for the pair of 2-reservoir ("effective") parameters, ν and T^*. They are not amenable to direct measurement, since they are defined as just those values which make the predictions of the model come closest to the truth, which is itself of course the object of the investigation. Nevertheless, limits can be put on these parameters, although reasonable limits for T^* are themselves somewhat open to question.

In addition, the 2-reservoir model parameters may be related individually to the parameters in a 3-reservoir model. Some of the latter, for example ν_2, ν_3, and T_{12}, are more amenable to direct measurement (than are ν and T^*): through oceanographic means; through the behaviour of C^{14} and C^{13} in contexts other than the variation of atmospheric C^{14} concentration (Suess, 1954a; Revelle and Suess, 1957; Arnold and Anderson, 1957; and Craig, 1957b and 1963); or through the behaviour of other isotopes such as tritium, (Bainbridge, 1963; Dockins et al., 1967).

However, until better values for the remaining 3-reservoir parameters, β and T_{32}, (see Craig, 1963), are known, the more complex 3-reservoir model will give no essential improvement over the simpler model, in describing the C^{14} variations, although for other purposes it may indeed be more realistic. The uncertainties in β and T_{32} are attributable, in turn, to the rather unrealistic assumption that the deep oceans constitute a well-mixed reservoir (see Bien et al., 1965).

In spite of these remarks it is interesting to see what the meanings are of the 2-reservoir paramters, ν and T^*, in terms of the well-known 3-reservoir parameters ν_2, ν_3, and T_{12}, and the less well-known parameters β and T_{32}.

The two parameters of the 2-reservoir model (ν and T^*) can be related to the 5 parameters of the 3-reservoir model (ν_2, ν_3, β, T_{12}, and T_{32}) by equating the radiocarbon concentration in corresponding reservoirs for the case of a constant production rate Q_0:

$$\text{("atmosphere")} \quad R_{a0} = R_{10} \quad \text{(atmosphere)}$$

$$\text{("ocean")} \quad R_{s0} = R_{30} \quad \text{(deep ocean)} \quad .$$

Using the expressions found above (equations 12 to 15, and 21), and equating coefficients of Q_0, one finds the following two relations between the two sets of parameters (using the coefficients of S, leads to the same equations):

$$\begin{aligned} \nu T^* &= (1 + \nu_2 + \nu_3)(C_1 T_1 + D_1 T_3) \\ \nu_3 T^* &= -(1 + \nu_2 + \nu_3)(C_3 T_1 + D_3 T_3) \quad . \end{aligned} \tag{24}$$

If we define ε as the fraction of the mixed layer (i=2) which is included in the "atmosphere" (j=a), and use the relation $Y = Y_a + Y_s = Y_1 + Y_2 + Y_3$, then we have:

$$Y_a = Y_1 + \varepsilon Y_2 \quad , \quad Y_s = Y_3 + (1-\varepsilon) Y_2$$

$$\nu = \frac{Y_s}{Y_a} = \frac{\nu_3 + (1-\varepsilon)\nu_2}{1 + \varepsilon \nu_2}$$

$$26.5 = \frac{\nu_3}{1+\nu_2} \leqslant \nu \leqslant \nu_3 + \nu_2 = 59.5 \quad ,$$

where the values $\nu_2 = 1.2$ and $\nu_3 = 58.3$ are from Craig (1963).

In terms of the parameters of the particular two sets refered to above, and using the above values for ν_2 and ν_3, equations 24 may be put in the following forms:

$$\varepsilon = [1 + (\nu_2+\nu_3) \frac{T_{12}}{T_{32}}]^{-1} = [1 + 59.5 \frac{T_{12}}{T_{32}}]^{-1} \tag{25}$$

$$\nu = \frac{\nu_3 + (1-\varepsilon)\nu_2}{1 + \varepsilon \nu_2} = \frac{58.3 + 1.2(1-\varepsilon)}{1 + 1.2\varepsilon} \tag{26}$$

$$\frac{T^*}{T_{12}} = (1 - \frac{Y_1}{Y})[1 + \frac{Y_1 + Y_2}{Y_2 + Y_3} \frac{T_{32}}{T_{12}}][1 + \beta(1 + \frac{Y_1}{Y_3} \frac{T_{32}}{T_{12}})]^{-1} \tag{27}$$

$$T^* = T_{12}[0.985 + 36.4 \frac{T_{32}/1000}{T_{12}}][1 + \beta(1 + 17.2 \frac{T_{32}/1000}{T_{12}}]^{-1} \quad . \tag{28}$$

(in years)

The last two equations may be put in the alternative forms:

$$\frac{T_{32}}{T_{12}} = \frac{Y}{Y_1 + Y_2}\left[(1+\beta)\frac{T^*}{T_{12}} - (1 - \frac{Y_1}{Y})\right]\left[1 - \beta\frac{Y/Y_3}{1 + Y_2/Y_1}\frac{T^*}{T_{12}}\right]^{-1} \qquad (29)$$

$$T_{32} = 27.5\ T_{12}\left[(1+\beta)\frac{T^*}{T_{12}} - 0.985\right]\left[1 - 0.47\beta\frac{T^*}{T_{12}}\right]^{-1} \quad (y) \quad . \qquad (30)$$

For $\beta = 0$, one sees that T^* is given by a linear equation in T_{32}:

$$T^* = 0.985\ T_{12} + 36.4\ \frac{T_{32}}{1000} \quad (y) \qquad (31)$$

which says that for every 1000 years of deep ocean residence time, the 2-reservoir model's residence time in the upper reservoir (which is essentially T^*) is increased by 36 y, over the 3-reservoir atmospheric residence time T_{12}.

Harmonic input and output

If the production rate fractional deviation $\Delta Q(t)$ can be expressed as a sum of sines and cosines of various frequencies, then the fractional deviation of the C^{14} concentration in any reservoir will be a sum of the same harmonics, each shifted in phase and attenuated in amplitude, by amounts which depend on the frequency. If, instead, the concentrations are known, then the production rate may be found. If the fractional deviation of the production rate is

$$\Delta Q(t) = D_0 + \sum_{k=1}^{n}(C_k \sin\omega_k t + D_k \cos\omega_k t) \quad ,$$

then the fractional deviation of the C^{14} concentration in reservoir i (here, either i=i,2,3, or i=a,s) is

$$\Delta C_i(t) = D_{i0} + \sum_{k=1}^{n}(C_{ik} \sin\omega_k t + D_{ik} \cos\omega_k t) \quad ,$$

where $D_{i0} = D_0$; and where, for k=1,2,...,n, the new coefficients are given by

$$C_{ik} = \Theta_{ik}C_k + \Phi_{ik}D_k \ , \quad C_k = [\Theta_{ik}C_{ik} - \Phi_{ik}D_{ik}]/H_i \ ,$$
$$D_{ik} = -\Phi_{ik}C_k + \Theta_{ik}D_k \ , \quad D_k = [\Phi_{ik}C_{ik} + \Theta_{ik}D_{ik}]/H_i \ ; \tag{32}$$

with

$$\Theta_{ik} = \frac{b_i\lambda}{\lambda^2 + \omega_k^2} + \frac{c_i\lambda_1}{\lambda_1^2 + \omega_k^2} + \frac{d_i\lambda_3}{\lambda_3^2 + \omega_k^2}$$

$$\Phi_{ik} = \left[\frac{b_i}{\lambda^2 + \omega_k^2} + \frac{c_i}{\lambda_1^2 + \omega_k^2} + \frac{d_i}{\lambda_3^2 + \omega_k^2}\right] \omega_k \ ;$$

the inverse attenuation factor is $H_i(\omega_k)$, where

$$H_i^2(\omega_k) = \Theta_{ik}^2 + \Phi_{ik}^2 = \frac{C_{ik}^2 + D_{ik}^2}{C_k^2 + D_k^2} = \frac{k^{th}\text{power of } C^{14}}{k^{th}\text{power of } Q} \leqslant 1 \tag{33}$$

When using these formulae with the 2-reservoir model, with i=a or s, one must let $d_i = 0$, and substitute λ^* for λ_1 in the above.

An alternative form of the above statements is:
if $\Delta Q(t) = C_k \sin\omega_k t$, then $\Delta C_i(t) = Cik(\omega_k)\sin[\omega_k t - \delta(\omega_k)]$.
The output coefficient, $C_{ik}(\omega_k) = H_i(\omega_k)C_k$ is a factor $(1/H_i)$ smaller than the input coefficient C_k; and the phase lag $\delta(\omega_k)$ is given by $\tan\delta(\omega_k) = \Phi_k/\Theta_k$.

SAMPLE NUMBER LJ:	TREE RING DATE (-:BC,+:AD)	C14 DATE (T = 5730Y)	ΔC14 (‰)	C= ΔC14-$\hat{C}_S$ (‰)	SAMPLE NUMBER LJ:	TREE RING DATE (-:BC,+:AD)	C14 DATE (T = 5730Y)	ΔC14 (‰)	C= ΔC14-$\hat{C}_S$ (‰)
1921	-5290	-4457	106.0	15.9	1497	-3065	-2446	77.7	9.9
1535	-5100	-4401	88.2	-3.3	1494	-3025	-2444	72.8	6.0
1712	-5020	-4435	73.3	-18.6	1704	-3005	-2550	56.6	-9.7
1734	-4966	-4318	81.5	-10.6	1268	-2995	-2530	57.9	-8.1
1536	-4955	-4237	90.8	-1.3	1496	-2985	-2457	65.9	.2
1732	-4946	-4274	84.7	-7.5	1662	-2965	-2426	67.4	2.2
1739	-4896	-4_{243}	$8_{2\cdot2}$	-10.1	1498	$-_{2}940$	$-_{23}71$	$71._{2}$	6.7
1740	-4876	-4239	80.1	-12.2	1663	-2925	-2267	82.8	18.7
1691	-4856	-4116	93.6	1.2	1509	-2865	-2311	69.3	6.8
1738	-4825	-4162	83.5	-8.9	1511	-2825	-2260	70.7	9.3
1539	-4795	-4049	94.5	2.1	1510	-2805	-2353	56.2	-4.6
1543	-4370	-3507	110.0	19.2	1692	-2785	-2342	55.0	-5.3
1552	-4365	-3544	104.4	13.6	1270	-2780	-2242	67.2	7.1
1540	-4345	-3_{592}	95.4	4.8	1518	-2765	-2342	52.5	-7.2
1503	-4325	-3544	99.1	8.6	1589	-2745	-2173	71.7	12.6
1506	-4305	-3615	87.1	-3.2	1519	-2715	-2050	83.8	25.5
1505	-4265	-3623	80.7	-9.2	1269	-2680	-2240	54.7	-2.6
1504	-4225	-3452	98.0	8.4	1313	-2645	-2224	52.3	-4.0
1553	-4205	-3357	108.0	18.6	1319	-2612	-2307	37.6	-17.7
1542	-4170	-3285	113.0	24.0	1318	-2605	-2318	35.3	-19.8
1302	-40_{77}	-3495	72.9	-15.0	1320	-25_{65}	-224_{6}	39.3	$-14._{6}$
1307	-4035	-3377	82.8	-4.6	1321	-2545	-2106	54.5	1.1
1305	-4005	-3436	71.3	-15.6	1327	-2485	-2097	48.0	-3.6
1306	-3938	-3392	68.3	-17.7	1326	-2460	-2025	54.0	3.1
1308	-3910	-3265	81.2	-4.4	1333	-2445	-1914	66.4	16.0
1304	-3822	-3295	65.8	-18.4	1332	-2425	-2041	47.6	-2.2
1299	-3790	-3180	76.6	-7.0	1325	-2425	-2086	41.9	-7.9
1301	-376_{5}	-326_{5}	$62._{4}$	-20.8	1328	-2405	-2020	47.7	-1.5
1300	-3700	-3147	69.2	-12.9	1185	-2362	-2061	37.1	-10.8
1298	-3635	-2945	87.1	6.3	1187	-2346	-1900	55.4	7.9
1340	-3625	-2924	88.5	7.9	1196	-2328	-1963	45.2	-1.7
1312	-3610	-2866	94.2	13.9	1198	-2307	-1996	38.3	-8.0
1341	-3610	-2895	90.4	10.1	1197	-2302	-2055	30.3	-15.9
1295	-3595	-2955	80.5	.4	1193	-2297	-1947	43.3	-2.7
128_{6}	-3495	-2_{886}	76.5	-1.5	118_{6}	-228_{3}	-2019	32.5	-13.1
1705	-3485	-2824	83.2	5.4	1194	-2281	-2003	34.2	-11.3
1288	-3465	-2807	82.9	5.5	1204	-2247	-2040	25.3	-19.2
1294	-3455	-2789	83.9	6.8	1203	-2220	-1968	31.0	-12.7
1342	-3445	-2800	81.2	4.3	1180	-2185	-1978	25.4	-17.2
1290	-3435	-2876	70.0	-6.7	1177	-2162	-1993	20.7	-21.3
1344	-3425	-2769	82.6	6.1	1174	-2141	-1942	24.4	-16.9
1322	-3415	-2_{903}	$63._{9}$	-12.4	1176	-2121	-177_{9}	42.2	1.5
1289	-3405	-2855	68.8	-7.3	1199	-2105	-1854	30.8	-9.4
1523	-3375	-257_{1}	102.2	26.8	1181	-2074	-1836	29.2	-10.1
1585	-3325	-2470	109.0	34.8	1192	-2058	-1892	20.3	-18.5
1287	-3290	-2613	85.4	12.0	1188	-2040	-1773	32.8	-5.5
1529	-3275	-2557	90.8	17.7	1183	-2025	-1804	27.1	-10.7
1526	-3255	-2469	99.8	27.2	1483	-2005	-1724	34.6	-2.7
152_{8}	-3240	-260_{8}	$79._{5}$	7.3	14_{80}	-198_{5}	-1752	$28._{6}$	$-_{8}1.1$
1276	-3220	-2630	74.0	2.3	1588	-1965	-1630	41.3	5.2
1524	-3175	-2530	81.2	10.6	1694	-1945	-1775	20.8	-14.7
1489	-3125	-2452	84.8	15.4	1475	-1925	-1636	35.6	.7
1699	-3115	-2521	74.5	5.4	1476	-1885	-1593	36.0	2.3
1487	-3110	-2504	76.1	7.1	1592	-1865	-1594	33.3	.2
1275	-3105	-2550	69.4	.5	1472	-1845	-1613	28.5	-4.0

SAMPLE NUMBER LJ:	TREE RING DATE (-:BC, +:AD)	C14 DATE (T = 5730Y)	ΔC14 (‰)	C= ΔC14-$\hat{C}_S$ (‰)	SAMPLE NUMBER LJ:	TREE RING DATE (-:BC, +:AD)	C14 DATE (T = 5730Y)	ΔC14 (‰)	C= ΔC14-$\hat{C}_S$ (‰)
1596	-1825	-1600	27.6	-4.3	1858	-1155	-1146	1.1	-12.6
1473	-1806	-1546	31.9	.5	1873	-1145	-1072	8.9	-4.6
1849	-1795	-1572	27.3	-3.7	1877	-1135	-1063	8.8	-4.4
1467	-1785	-1653	16.1	-14.7	1249	-1130	-923	25.4	12.3
1853	-1775	-1656	14.5	-16.0	1875	-1105	-917	23.0	10.5
1850	-1755	-1656	12.1	-17.8	1550	-1065	-943	14.9	3.4
1468	-1740	-1666	9.0	-20.4	1547	-1045	-933	13.6	2.5
1474	-1725	-1562	19.9	-9.1	1556	-1025	-897	15.6	5.0
1851	-1715	-1597	14.4	-14.3	1549	-1005	-975	3.6	-6.6
1857	-1695	-1606	10.8	-17.4	1209	-988	-911	9.4	-.4
1855	-1675	-1432	29.8	2.2	1554	-985	-918	8.1	-1.6
1839	-1655	-1535	14.6	-12.4	1695	-975	-847	15.6	6.1
1465	-1645	-1445	24.5	-2.2	1555	-965	-839	15.3	6.0
1844	-1635	-1402	28.6	2.2	1250	-963	-766	24.1	14.9
1537	-1625	-1488	16.7	-9.5	1562	-945	-810	16.5	7.7
1845	-1615	-1415	24.5	-1.4	1208	-938	-962	-2.9	-11.6
1457	-1605	-1432	21.2	-4.4	1247	-912	-852	7.3	-.8
1847	-1595	-1417	21.8	-3.5	1564	-905	-859	5.6	-2.4
1693	-1585	-1364	27.1	2.1	1557	-895	-902	-.9	-9.6
1258	-1580	-1408	21.0	-3.9	1210	-888	-720	20.5	12.9
1840	-1575	-1434	17.2	-7.6	1566	-885	-751	16.3	8.8
1846	-1555	-1333	27.2	3.0	1559	-880	-792	10.7	3.3
1466	-1545	-1353	23.5	-.4	1696	-865	-775	11.0	3.9
1831	-1535	-1388	17.9	-5.7	1248	-852	-744	14.4	7.4
1456	-1525	-1405	14.6	-8.8	1590	-845	-807	4.6	-2.1
1838	-1515	-1367	18.1	-5.0	1591	-825	-785	4.9	-1.4
1828	-1505	-1380	15.2	-7.6	1565	-815	-650	20.1	14.0
1833	-1495	-1273	27.2	4.7	1567	-805	-660	17.7	11.8
1837	-1475	-1310	20.2	-1.8	1570	-785	-707	9.5	4.0
1834	-1455	-1379	9.2	-12.2	1569	-765	-462	37.3	32.2
1257	-1455	-1325	15.8	-5.6	1594	-745	-513	28.5	23.8
1836	-1435	-1235	24.5	3.6	1572	-725	-514	25.8	21.5
1827	-1415	-1177	29.2	8.8	1213	-712	-540	21.0	16.9
1703	-1405	-1157	30.5	10.4	1595	-705	-686	2.3	-1.6
1903	-1395	-1138	31.6	11.8	1573	-685	-507	21.8	18.2
1885	-1385	-1097	35.4	15.8	1697	-665	-548	14.3	11.1
1882	-1375	-1103	33.4	14.1	1571	-645	-612	4.0	1.2
1894	-1365	-1091	33.7	14.7	1574	-625	-597	3.4	.9
1884	-1355	-1071	35.0	16.2	1284	-610	-620	-1.2	-3.4
1168	-1340	-1108	28.4	10.0	1577	-605	-462	17.5	15.4
1893	-1325	-1173	18.6	.6	1575	-585	-445	17.1	15.3
1881	-1315	-1092	27.3	9.6	1702	-565	-616	-6.1	-7.5
1879	-1295	-1111	22.5	5.3	1578	-545	-522	2.8	1.7
1870	-1285	-1064	27.1	10.1	1576	-525	-555	-3.6	-4.4
1252	-1276	-1053	27.4	10.7	1669	-475	-496	-2.5	-2.5
1864	-1275	-1171	12.7	-4.0	1668	-435	-403	3.9	4.5
1345	-1250	-1134	14.1	-2.0	1670	-415	-423	-1.0	-.1
1872	-1235	-1114	14.7	-1.0	1678	-395	-381	1.7	2.9
1871	-1225	-1121	12.6	-2.8	1682	-375	-272	12.5	14.0
1869	-1215	-1081	16.3	1.1	1679	-355	-300	6.7	8.4
1254	-1215	-1039	21.5	6.3	1687	-335	-255	9.7	11.7
1865	-1205	-1032	21.2	6.3	1680	-315	-272	5.2	7.4
1876	-1195	-1015	22.0	7.3	1686	-295	-307	-1.5	1.0
1205	-1185	-1025	19.5	5.1	1681	-275	-331	-6.7	-4.0
1878	-1165	-1053	13.7	-.2	1685	-255	-326	-8.6	-5.6

SAMPLE NUMBER LJ:	TREE RING DATE (-:BC,+:AD)	C14 DATE (T = 5730Y)	ΔC14 (‰)	C= ΔC14-$\hat{C}_S$ (‰)	SAMPLE NUMBER LJ:	TREE RING DATE (-:BC,+:AD)	C14 DATE (T = 5730Y)	ΔC14 (‰)	C= ΔC14-$\hat{C}_S$ (‰)
1232	-225	-356	-15.7	-12.4	828	943	867	-9.1	-4.6
1233	-180	-286	-12.7	-8.9	802	978	892	-10.4	-6.3
1230	-160	-246	-10.4	-6.4	801	1023	956	-8.1	-4.5
1229	-90	-131	-5.0	-.3	720	1068	1011	-6.9	-3.8
843	-90	-65	3.0	7.7	800	1096	1056	-4.8	-2.0
1215	-55	-174	-14.3	-9.3	722	1131	1070	-7.4	-5.0
1216	-55	-162	-12.9	-7.9	1072	1153	1065	-10.6	-8.5
844	-45	-136	-11.0	-5.9	799	1160	1128	-3.9	-1.9
1221	-35	-85	-6.0	-.8	1075	1173	1027	-17.5	-15.7
1228	-35	-96	-7.4	-2.2	716	1199	980	-26.1	-24.6
1220	-25	-66	-5.0	.2	1074	1203	1091	-13.4	-12.0
845	-17	-141	-14.9	-9.6	1077	1213	1113	-12.0	-10.7
1214	-10	-144	-16.1	-10.7	798	1222	1204	-2.2	-1.0
846	2	-142	-17.3	-11.8	1073	1227	1166	-7.3	-6.2
847	24	-181	-24.5	-18.9	797	1241	1228	-1.6	-.7
841	112	49	-7.6	-1.4	795	1279	1252	-3.3	-3.0
1171	213	124	-10.7	-4.1	780	1323	1343	2.4	2.1
840	260	217	-5.2	1.6	794	1368	1343	-3.0	-4.1
1746	285	194	-10.9	-4.1	721	1405	1474	8.4	6.7
1759	305	227	-9.4	-2.5	783	1428	1446	2.2	.1
1752	315	242	-8.8	-1.9	793	1458	1557	12.0	9.4
1747	345	290	-6.6	.3	784	1476	1559	10.1	7.2
1756	355	325	-3.6	3.3	723	1505	1692	22.9	19.5
819	368	273	-11.4	-4.4	785	1518	1706	23.0	19.3
1751	385	319	-7.9	-.9	777	1538	1697	19.4	15.3
823	405	314	-11.0	-4.0	774	1563	1653	11.0	6.5
1758	405	314	-11.0	-4.0	786	1583	1637	6.5	1.6
1748	425	351	-8.9	-1.9	719	1605	1614	1.1	-4.2
834	433	326	-12.8	-5.8	775	1623	1686	7.7	2.0
1757	455	374	-9.7	-2.7	792	1632	1648	1.9	-4.0
1750	475	468	-.8	6.1	787	1643	1687	5.3	-.8
1740	505	510	.6	7.5	772	1655	1782	15.5	9.1
821	568	504	-7.7	-.9	776	1673	1827	18.8	12.1
830	583	475	-13.0	-6.3	771	1695	1889	23.8	16.6
829	615	502	-13.6	-7.0	715	1710	1866	19.0	11.5
824	677	619	-7.0	-.7	791	1710	1812	12.4	4.9
1718	705	766	7.4	13.6	770	1723	1853	15.9	8.1
825	709	735	3.1	9.3	812	1725	1825	12.2	4.4
1744	725	676	-5.9	.2	717	1740	1796	6.8	-1.3
1715	735	687	-5.8	.2	768	1755	1839	10.2	1.7
835	748	683	-7.8	-1.8	811	1759	1807	5.8	-2.8
1722	755	699	-6.8	-.9	743	1765	1840	9.1	.4
1724	775	726	-5.9	-.1	765	1771	1923	18.6	9.8
1811	785	794	1.1	6.8	763	1791	1854	7.6	-1.7
826	786	724	-7.5	-1.8	762	1800	1874	9.0	-.5
1714	795	658	-16.4	-10.7	773	1806	1829	2.8	-6.8
1721	815	835	2.4	7.9	813	1808	1798	-1.2	-10.8
1743	821	734	-10.5	-5.0	761	1814	1923	13.3	3.5
827	825	700	-15.0	-9.6	767	1818	1870	6.3	-3.6
1723	835	806	-3.5	1.9	760	1824	1926	12.4	2.4
1731	845	804	-4.9	.4	810	1830	1874	5.3	-4.8
1720	855	810	-5.4	-.2	759	1832	1944	13.7	3.5
1716	875	839	-4.3	.8	741	1845	1901	6.8	-3.7
1812	885	830	-6.6	-1.6	742	1845	1837	-1.0	-11.5
1719	895	859	-4.4	.5	713	1855	1793	-7.5	-18.2
					809	1855	1885	3.6	-7.1

Table 12

FOURIER COEFFICIENTS

$$Z_N(t) = \frac{1}{2}d_{N0} + \sum_{k=1}^{n}(c_{Nk}\sin kt + d_{Nk}\cos kt),\ N = \begin{cases} 2n-1 \\ 2n \end{cases}$$

	N = 76		N = 54		N = 43		N = 24		N = 13	
k	d_{Nk}	c_{Nk}	d_{Nk}	c_{Nk}	d_{Nk}	c_{Nk}	d_{Nk}	c_{Nk}	d_{Nk}	c_{Nk}
0	0.075		-0.064		-0.305		-0.378		-0.429	
1	0.705	0.757	0.766	0.751	0.407	0.382	0.240	0.289	0.109	0.173
2	-1.067	2.511	-0.729	2.929	-0.966	2.532	-0.914	2.217	-1.363	2.412
3	2.276	-3.350	1.958	-3.346	2.228	-3.769	2.510	-3.562	2.2[illegible]	-3.773
4	-0.773	3.808	-0.828	3.724	-0.652	3.450	-0.634	3.104	-0.77[illegible]	2.835
5	-2.286	0.661	-2.020	.884	-2.232	0.801	-1.721	0.684	-1.63[illegible]	0.438
6	-2.082	-3.286	-1.848	-3.535	-1.717	-3.293	-1.112	-2.926	-0.78[illegible]	-3.300
7	-1.777	-4.112	-1.097	-4.493	-1.435	-4.537	-1.158	-4.538	0.000	-4.641
8	0.595	-1.792	0.774	-1.535	0.466	-1.790	0.528	-1.589		
9	0.548	-0.392	0.564	-0.444	0.336	-0.741	0.277	-0.725		
10	-2.099	0.583	-1.839	0.286	-1.512	0.416	-1.403	0.453		
11	-0.570	-0.883	-0.775	-0.446	-0.325	-0.443	0.044	-0.417		
12	-1.964	-0.241	-2.300	0.465	-2.063	0.128	-2.350	0.396		
13	1.524	0.150	1.084	0.491	1.185	-0.022				
14	-1.427	-0.722	-1.406	-0.850	-0.811	-0.729				
15	0.922	-0.612	0.767	-0.486	1.406	-0.050				
16	0.418	1.462	0.104	1.496	0.359	2.086				
17	-1.651	-1.236	-1.148	-1.699	-1.732	-1.024				
18	0.417	-0.506	0.901	-0.859	0.697	-0.474				
19	0.711	-0.413	0.781	-1.038	0.492	-0.416				
20	-0.344	-0.977	-0.128	-1.374	-0.861	-1.228				
21	0.466	0.254	0.964	0.582	-0.663	0.443				
22	1.187	-1.762	1.884	-1.310	0.000	-1.752				
23	0.075	-0.210	0.290	0.460						
24	0.630	2.957	0.491	3.378						
25	-1.771	.440	-2.107	0.890						
26	-0.706	-1.566	-1.226	-1.267						
27	-1.850	-1.438	-2.400	-1.523						
28	0.702	-0.652								
29	0.165	-0.668								
30	-0.613	-0.197								
31	-0.515	0.114								
32	1.432	1.087								
33	-2.559	0.999								
34	-1.421	-0.136								
35	1.391	0.484								
36	1.572	0.623								
37	1.096	-1.476								
38	1.609	-0.607								

Table 13

FOURIER POWER

$$P_{Nk}^2 = c_{Nk}^2 + d_{Nk}^2$$

k	N = 76	N = 54	N = 43	N = 24	N = 13
0	0.006	0.004	0.09	0.14	0.18
1	1.07	1.15	0.31	0.14	0.04
2	7.44	9.11	7.34	5.75	7.67
3	16.40	15.03	19.17	18.99	18.84
4	15.10	14.55	12.33	10.04	8.64
5	5.66	4.86	5.62	3.43	2.87
6	15.14	15.91	13.79	9.80	11.50
7	20.07	21.39	22.64	21.94	21.54
8	3.56	2.96	3.42	2.80	
9	0.45	0.52	0.66	0.60	
10	4.74	3.46	2.46	2.17	
11	1.10	0.80	0.30	0.18	
12	3.92	5.51	4.27	5.68	
13	2.34	1.42	1.40		
14	2.56	2.70	1.19		
15	1.22	0.82	1.98		
16	2.31	2.25	4.48		
17	4.25	4.20	4.05		
18	0.43	1.55	0.71		
19	0.68	1.68	0.42		
20	1.07	1.90	2.25		
21	0.28	1.27	0.64		
22	4.51	5.26	3.07		
23	0.05	0.30			
24	9.14	11.65			
25	3.33	5.25			
26	2.95	3.11			
27	5.49	8.08			
28	0.92				
29	0.47				
30	0.41				
31	0.28				
32	3.23				
33	7.55				
34	2.04				
35	2.17				
36	0.41				
37	3.38				
38	2.96				

B I B L I O G R A P H Y

[Abbreviation: RVAC: Radiocarbon Variations and Absolute Chronology, see Olsson (1970).]

Anderson, E.C., and W.F. Libby, 1951, Phys. Rev., 81, 64-69.

Anderson, E.C., Libby, W.F., Weinhouse, S., Reid, A.F., Kirschenbaum, A.D., and A.V. Grosse, 1947, Phys. Rev., 72, 931-936.

Arnold, J.A., and E.C. Anderson, 1957, Tellus 9, 28-32.

Bainbridge, A.E., 1963, J. Geophys. Res., 68, 3785-3789.

Bien, G.S., Rakestraw, N.W., and H.E. Suess, 1963, Radioactive Dating, I.A.E.A., Vienna, pp. 159-173.

Broecker, W.S., and E.A. Olson, 1959, Am. J. Sci. Radiocarbon Suppl., 1, 111-132.

Broecker, W.S., and E.A. Olson, 1961, Radiocarbon, 3, 176-204.

Bucha, V., 1967, Archaeometry, 10, 12-22.

Bucha, V., 1970, in RVAC, Olsson, I.U., ed., pp. 501-511.

Bucha, V., and E. Neustupny, 1967, Pamatky Archeologické, 58, 599-612.

Cox, A., 1969, Science, 163, 237-245.

Craig, H., 1957a, Geochim. Cosmochim. Acta, 12, 133-149.

Craig, H., 1957b, Tellus, 9, 1-17.

Craig, H., 1963, in Earth Science and Meteorites, Geiss, J., and E.D. Goldberg, eds., New York Interscience, pp. 103-114.

Damon, P.E., 1968, Meteorological Monographs, 8, 151-154.

Damon, P.E., 1970, in RVAC, Olsson, I.U., ed., pp. 571-593.

Damon, P.E., Long, A., and D.C. Grey, 1966, J. Geophys. Res., 71, 1055-1063.

Damon, P.E., Long A., and D.C. Grey, 1970, in RVAC, Olsson, I.U., ed., pp. 615-618.

Dockins, K.O., Bainbridge, A.E., Houtermans, J.C., and H.E. Suess, 1967, in Radioactive Dating and Methods of Low-level Counting, I.A.E.A., Vienna, pp. 129-141.

Elsasser, W., Ney, E.P., and J.R. Winkler, 1956, Nature, 178, 1226-1227.

Ferguson, C.W., 1968, Science, 159, 839-846.

Ferguson, C.W., 1970, in RVAC, Olsson, I.U., ed., pp. 237-259.

Godwin, H., 1962, Nature, 195, p. 984.

Grey, D.C., 1969, J. Geophys. Res., 74, 6333.

Grey, D.C., Damon, P.E., and A. Long, 1966, American Geophysical Union, 6th Western National Meeting, University of California at Los Angeles, September, Trans. A.G.U., 47, p. 495 (abstract).

Hartree, D.R., 1952, Numerical Analysis, Oxford Univ., Press, p. 245.

Houtermans, F.G., and H. Oeschger, 1958, Helv. Phys. Acta., 31, 117-126.

Houtermans, J., 1966, Z. für Physik, 193, 1-12.

Houtermans, J., Suess, H.E., and W.H. Munk, 1967, in Radioactive Dating and Methods of Low-level Counting, I.A.E.A., Vienna, pp. 57-68.

Hüsser, R., 1957, Orthogonale Polynome mehrerer Veränderlichen und ihre Anwendung in der ein- und zweidimensionalen Ausgleichsrechnung, Inaugural Dissertation, Universität Bern.

Hüsser, R., 1968, Ausgleichung mit Orthogonalen Polynomen, Universität Bern, Ref. Nr. CH 03.35.089 D.

Johnsen, S.J., Dansgaard, W., Clausen, H.B., and C.C. Langway, 1970, Nature, 227, 482-483.

Kigoshi, K., and H. Hasegawa, 1966, J. Geophys. Res., 71, 1065-1071.

Lal, D., and V.S. Venkatavaradan, 1970, in RVAC, Olsson, I.U., ed. pp. 549-569.

Lerman, J.C., Mook, W.G., and J.C. Vogel, 1970, in RVAC, Olsson, I.U., ed., pp. 275-301.

Libby, W.F., 1967, in Radioactive Dating and Methods of Low-level Counting, I.A.E.A., Vienna, pp. 3-25.

Lingenfelter, R.E., 1963, Rev. Geophys., 1, 35-55.

Lingenfelter, R.E., and R. Ramaty, 1970, in RVAC, Olsson, I.U., ed., pp. 513-537.

Loosli, H., and H. Oeschger, 1968, Earth and Planetary Science Letters, 5, 191-198.

Milne, W.E., 1949, Numerical Calculus, Princeton Univ. Press, pp. 255-280.

Oeschger, H., Houtermans, J., Loosli, H., and M. Wahlen, 1970, in RVAC, Olsson, I.U., ed., pp. 471-498.

Olsson, I.U., 1968, Earth-Science Reviews, 4, 203-218.

Olsson, I.U., 1970, ed., Radiocarbon Variations and Absolute Chronology, Twelfth Nobel Symposium, Uppsala, Aug. 11-15, 1969, Almqvist and Wiksell, Stockholm and John Wiley and Sons, New York.

Ralph, E.K., and H.N. Michael, 1967, Archaeometry, 10, 3-11.

Ralph, E.K., and H.N. Michael, 1970, in RVAC, Olsson, I.U., ed., pp. 619-623.

Ramaty, R., 1967, in Magnetism and the Cosmos, Runcorn, S.K., ed., NATO Advanced Study Institute on Planetary and Stellar Magnetism, 1965, Newcastle-upon-Tyne, Oliver and Boyd, Edinburgh, pp. 66-78.

Revelle, R., and H.E. Suess, 1957, Tellus, 9, 18.

Stuiver, M., 1961, J. Geophys. Res., 66, 273-276.

Stuiver, M., 1965, Science, 149, 533-534.

Stuiver, M., and H.E. Suess, 1966, Radiocarbon, 8, 534-540.

Suess, H.E., 1954a, Proc. Williams Bay Conf., September, 1953, NAS-NSF Publ., p. 52.

Suess, H.E., 1954b, Science, 120, 1-3.

Suess, H.E., 1960, Proc. Highland Park, Ill., Conf., Publ. 845, NAS-NRC, pp. 90-95., Washington, D.C.

Suess, H.E., 1965, J. Geophys. Res., 70, 5937-5952.

Suess, H.E., 1967, in Radioactive Dating and Methods of Low-Level Counting, I.A.E.A., Vienna, pp. 143-151.

Suess, H.E., 1968, Meteorological Monographs, 8, 146-150.

Suess, H.E., 1970a, in RVAC, Olsson, I.U., ed., pp. 303-311.

Suess, H.E., 1970b, in RVAC, Olsson, I.U., ed., pp. 595-605.

Vries, Hl. de, 1958, Koninkl. Ned. Akad. Wetenshap. Proc., Ser. B. 61, no. 2, 94-102.

Whittaker, E.T., and G. Robinson, 1940, The Calculus of Observations, Blackie and Son, London and Glasgow, pp. 282-283.

Willis, E.H., Tauber, H., and K.O. Münnich, 1960, Am. J. Science, Radiocarbon Suppl., 2, 1-4.

Wood, L., and W.F. Libby, 1964, in Isotopic and Cosmic Chemistry, Craig, H., Miller, S.L., and G.J. Wasserberg, eds., North Holland Publishing Co., Amsterdam, pp. 205-210.

L E B E N S L A U F

Name:	Houtermans, Jan Cornelius
Geburtsdatum:	4. November 1935
Geburtsort:	Charkov, USSR
Staatsangehörigkeit:	USA
Wohnort:	vor 1939 : USSR und England 1939 - 1967: USA seit 1967 : Bern, Schweiz
Bildung:	1953 - 1955: University of Rochester Rochester, N.Y.
	1956 - 1958: New York University New York, N.Y.
	1958 - 1959: Universität München
	1961 - 1964: University of Wisconsin Madison, Wisconsin
	1967 - 1971: Universität Bern
Bildungsstufen:	1958 : Bachelor of Arts New York University (Mathematik, Physik, Philosophie)
	1966 : Master of Arts University of Wisconsin (Physik)
Arbeit:	1960 - 1961: Lamont Geological Observatory Columbia University Pallisades, N.Y.
	Oceanographische Arbeit auf dem Forschungsschiff VEMA, unter Leitung von Dr. J. Worzel
	1964 - 1967: University of California at San Diego La Jolla, California
	Forschung über Tritium und Radiocarbon, unter Leitung von Professor H.E. Suess

Publikationen:

Houtermans, Jan, 1965, Tritium in the Surface Water of the North Pacific Ocean, in Proceedings of the Sixth International Conference of Radiocarbon and Tritium Dating, Pullman, Washington, pp. 565-576.

Houtermans, Jan, 1966, On the Quantitative Relationships between Geophysical Parameters and the Natural C^{14} Inventory, Zeitschrift für Physik, 193, 1-12.

Houtermans, J., Suess, H.E., and Munk, W., 1967, Effect of Industrial Fuel Consumption on the Carbon-14 Level of Atmospheric CO_2, in Radioactive Dating and Methods of Low-Level Counting, I.A.E.A., Vienna, pp. 57-68.

Dockins, K.O., Bainbridge, A.E., Houtermans, J.C., and Suess, H.E., 1967, Tritium in the Mixed Layer of the North Pacific Ocean, in Radioactive Dating and Methods of Low-Level Counting, I.A.E.A., Vienna, pp. 129-141.

Oeschger, H., Houtermans, J., Loosli, H., and Wahlen, M., 1970, The Constancy of Cosmic Radiation from Isotope Studies in Meteorites and on the Earth, in Nobel Symposium 21, Radiocarbon Variations and Absolute Chronology, Almqvist and Wiksell, Uppsala, pp. 471-498.

ACKNOWLEDGMENTS

I thank Professor J. Geiss and Professor H. Oeschger for the opportunity to work on this project at the "Institut für exakte Wissenschaften der Universität Bern". I have profited greatly from many discussions with Professor Oeschger, whom I thank for his great help and understanding, and for the encouragement which he has given me. The ΔC^{14} data analysed here was measured in the laboratory of H.E. Suess, in La Jolla, California. I am grateful to Professor Suess for the opportunity to use these measurements and for valuable discussions and advice. Professor H. Carnal helped me to develop a recursive definition of orthogonal basis functions for the Fourier analysis of unequally spaced data, and I thank him for our fruitful conversations. I thank my colleagues in the radiocarbon and low-level counting group, especially Dr. Ulrich Siegenthaler, Dr. Martin Wahlen and Dr. Heinz Loosli, for many discussions about the subjects of this dissertation.

I thank Claire Houtermans for plotting; Violette Pini for drawing; and Balthasar Burkhard for photographing the ΔC^{14} functions. I am grateful to Urs Stooss, Ralph Gentner, Henry Rufli and Kurt Hänni for drawing many of the figures. I especially thank Erika Rohrer for her typing of the thesis.

The calculations were done using the Bull Gamma-30 computer of the "Rechenzentrum der Universität und der Finanzdirektion des Kantons Bern", for the use of which I thank Professor W. Nef of the "Institut für angewandte Mathematik der Universität Bern". I thank Mrs. T. Riesen of the radiocarbon group for administrative help.

I am grateful to the Swiss National Science Foundation from which I have received financial support during the time of my work on this project. The research in this field was also supported through a grant for solar-terrestial relationships to H.E. Suess by the U.S. National Science Foundation.

Thanks to Jean-Frédéric Schnyder for the piece at the front.

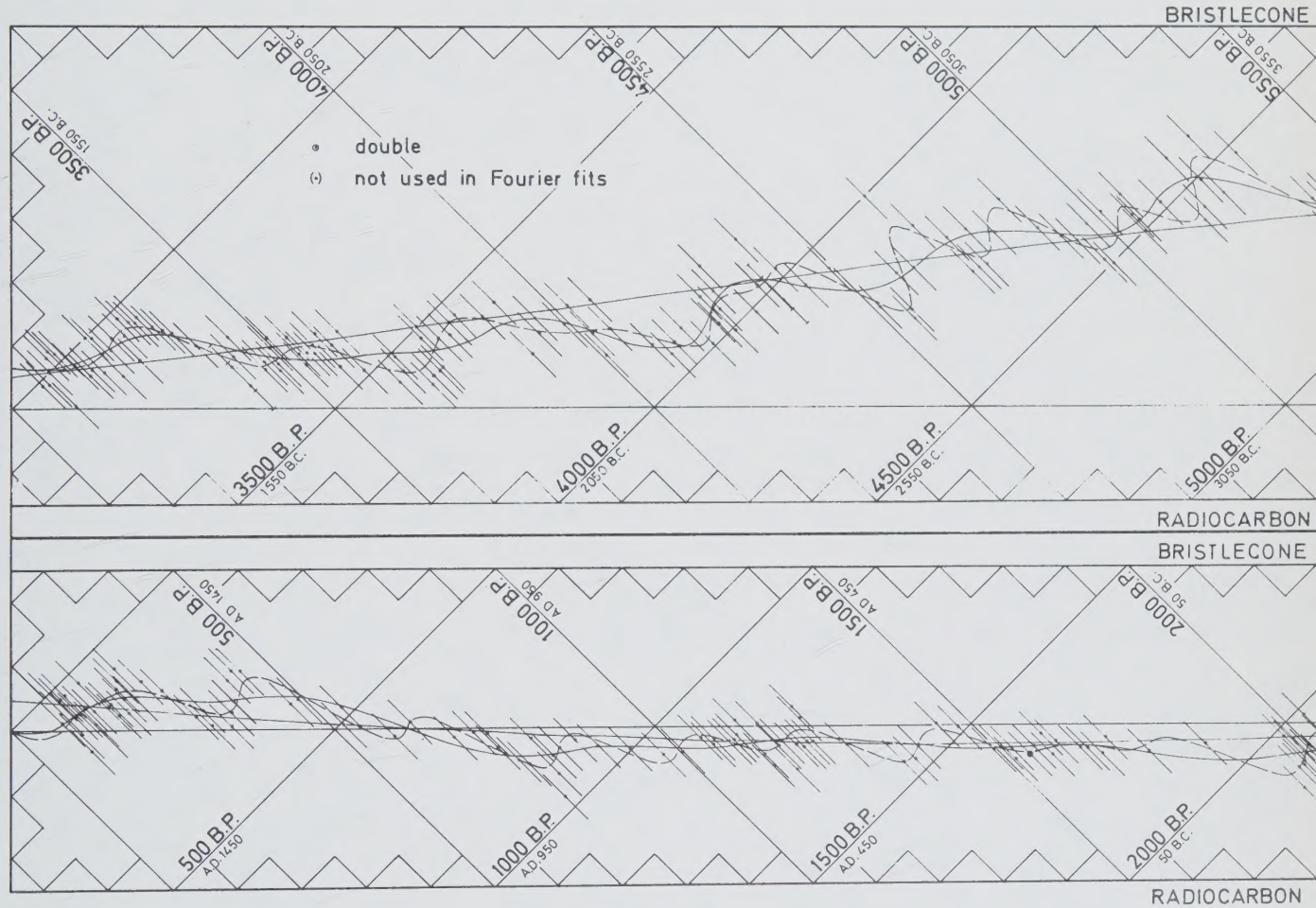
BRISTLECONE
3500 B.P.
1550 B.C.
4000 B.P.
2050 B.C.
4500 B.P.
2550 B.C.
5000 B.P.
3050 B.C.
5500 B.P.
3550 B.C.
double
not used in Fourier fits
RADIOCARBON
BRISTLECONE
500 B.P.
A.D. 1450
1000 B.P.
A.D. 950
1500 B.P.
A.D. 450
2000 B.P.
50 B.C.
RADIOCARBON